

Title	The development of a computer model to optimize the performance of a 50kWp photovoltaic system
Authors	McCarthy, Sean
Publication date	1986
Original Citation	McCarthy, S. 1986. The development of a computer model to optimize the performance of a 50kWp photovoltaic system. PhD Thesis, University College Cork.
Type of publication	Doctoral thesis
Link to publisher's version	http://library.ucc.ie/record=b1134039~S0
Rights	© 1986, Sean McCarthy - http://creativecommons.org/licenses/by-nc-nd/3.0/
Download date	2025-07-31 22:37:25
Item downloaded from	https://hdl.handle.net/10468/1657

*Presented to the National University
of Ireland for the Degree of Ph.D.*

THE DEVELOPMENT OF A COMPUTER MODEL TO OPTIMIZE
THE PERFORMANCE OF A 50kWp PHOTOVOLTAIC SYSTEM

Sean McCarthy, B.E., M.Eng.Sc.

June 1986

*Department of Electrical Engineering and Microelectronics
University College, Cork*

Professor G.T. Wrixon Thesis Supervisor



C O N T E N T S

	Page
ABSTRACT	
ACKNOWLEDGEMENTS	
CHAPTER 1 INTRODUCTION	
1.1 Introduction	1
1.2 Description of the Computer Model	2
1.3 Fotavoltaic Project	4
1.4 Layout of the Computer Model	7
1.5 Modelling Techniques	7
CHAPTER 2 PV ARRAY MODEL	
2.1 Introduction	21
2.2 Model of Planar Insolation	21
2.3 Model of Module Temperature	29
2.4 Model of PV Array	35
2.5 Conclusion	43
CHAPTER 3 BATTERY AND INVERTER MODELS	
3.1 Introduction	44
3.2 Battery Model	44
3.3 Model of Self-Commutated Inverters	56
3.4 Model of Line-Commutated Inverters	58
3.5 Conclusion	69

	Page
CHAPTER 4	MODEL OF POWER MANAGEMENT
4.1	Introduction 70
4.2	Power Management of the Fotavoltaic Project 70
4.3	Modelling Techniques for the Power Management Model 81
4.3.1	Model Concepts 81
4.3.2	Model Implementation 82
4.3.3	Model Verification 83
4.4	Conclusion 89
CHAPTER 5	OPTIMIZATION TECHNIQUES
5.1	Introduction 90
5.2	Optimization Parameters 93
5.3	Modelling of Changes to the Hardware Design and Power Management 96
5.4	Optimization of Component Size 106
5.4.1	Minimum Size of the Battery 106
5.4.2	Optimum Size of the Line-Commutated Inverter 108
5.5	Optimum System Design 110
5.5.1	Optimum Tilt of the PV Array 110
5.5.2	Optimum PV Array/Battery Combination 114
5.6	PV System Design as a Function of the Load Profile 118
5.7	Summary 125
5.8	Conclusion 127

CHAPTER 6 SUMMARY AND CONCLUSION

6.1	Summary	128
6.1.1	The Development of the Computer Model	128
6.1.2	The Results of the Optimization	131
6.1.3	Further Applications of the Computer Model	132
6.2	Conclusion	135

REFERENCES

APPENDICES

APPENDIX A	Photovoltaic Terminology	155
APPENDIX B	Hourly Recorded Data for the Fotavoltaic Project	156
APPENDIX C	Power Management Algorithms	160
APPENDIX D	Variables and Software Flags for each Hourly Simulation	170
APPENDIX E	Calculations for the Ice Producing Unit	174

ABSTRACT

A computer model has been developed to optimize the performance of a 50kWp photovoltaic system which supplies electrical energy to a dairy farm at Fota Island in Cork Harbour. Optimization of the system involves maximising the efficiency and increasing the performance and reliability of each hardware unit. The model accepts horizontal insolation, ambient temperature, wind speed, wind direction and load demand as inputs. An optimization program uses the computer model to simulate the optimum operating conditions. From this analysis, criteria are established which are used to improve the photovoltaic system operation. This thesis describes the model concepts, the model implementation and the model verification procedures used during development. It also describes the techniques which are used during system optimization. The software, which is written in FORTRAN, is structured in modular units to provide logical and efficient programming. These modular units may also be used in the modelling and optimization of other photovoltaic systems.

ACKNOWLEDGEMENTS

The work presented in this thesis was supervised by Professor G.T. Wrixon, to whom I am extremely grateful.

I wish to thank the postgraduate students and staff of the National Microelectronics Research Centre, led by Professor Wrixon and of the Electrical Engineering Department, led by Professor M.C. Sexton, for their assistance during the course of this work. A special word of thanks to Anne Kovach for her patience and valuable comments while reviewing this thesis, and to Janet Murphy for the excellent job in typing this thesis. I wish to thank my family and friends for their encouragement and support.

A special debt of gratitude is owed to my wife, Mary and daughter Sylvia whose encouragement, support and help has been immeasurable.

CHAPTER I

INTRODUCTION

1.1 Introduction

Several computer models [1-5] exist which simulate the performance of photovoltaic systems. These models take into account the load demand, geographical location and climate to determine the optimum component size and component design for any system. The models are designed to simulate any combination of PV array, battery, inverter, load and utility grid. They assume that each component is an individual electrical unit and that the power management is optimized. The computer model described in this thesis was developed to simulate the performance of a system in which the main hardware units are divided into subunits (13 subarrays, 2 batteries, 3 self-commutated inverters, 3 loads) and the power management is not optimized. In addition, the power management, which consists of a complex switching strategy [6], has seven modes of operation.

The motivation for the model development was the optimization of the system, i.e. the attainment of maximum efficiency, performance and reliability. This is achieved by:

- optimizing the power management
- optimizing the hardware design.

In addition to optimizing this system the models can be used to simulate and optimize the performance of other PV systems.

Chapter 1 describes the techniques used during the model development.

Chapters 2 and 3 describe the models which simulate the PV array, battery and inverters.

Chapter 4 describes the simulation of the power management.

Chapter 5 describes the software used to determine the optimum operation.

Chapter 6 discusses the accuracy of the model, its limitations and the success of the optimization. This chapter also discusses further applications of the model especially the modelling of other PV systems.

1.2 Computer Model

The computer model is a collection of programs, written in FORTRAN, which simulate the PV system operation on an hourly basis (see figure 1.1). Its inputs are horizontal insolation, ambient temperature, wind speed, wind direction, load demand and systems status (e.g. hardware faults). The model simulates the performance of the PV array, battery, inverters and power management, and it outputs data in graphical and statistical format.

The model was developed on a VAX 11/780 at the National Microelectronics Research Centre, Cork. The data used during the development was obtained from the Fotavoltaic Project. Twenty months of data were available for the model development.

The software packages, which simulate the operation of the hardware, are designed so that they may be used to simulate and optimize other PV systems. This is especially significant to the CEC projects [6] where the design and control strategies are very similar to those of the Fotavoltaic Project.

In addition to system optimization the computer model is now used as a diagnostic tool. It is used:

- to examine irregularities in the system's operation
- to examine degradation in the PV array and battery.

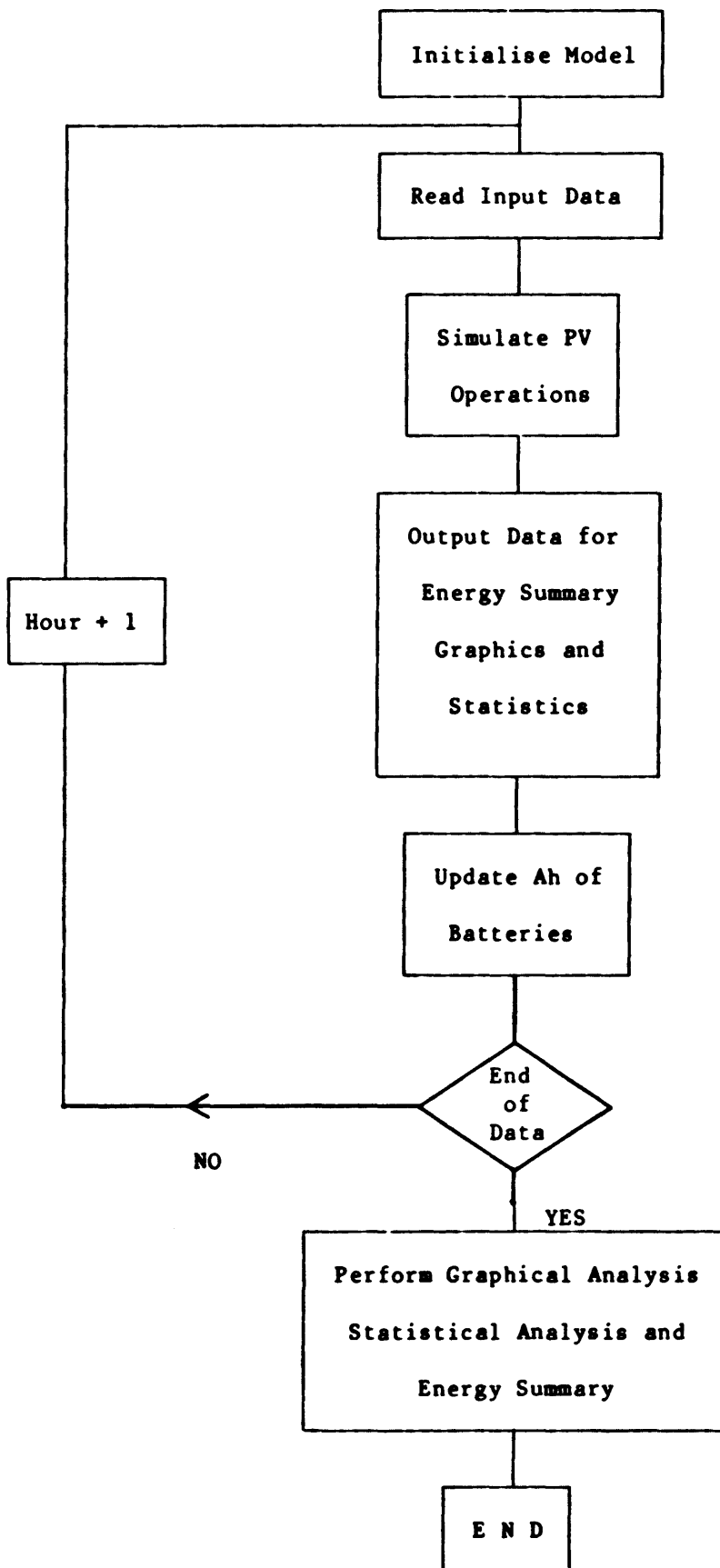


Figure I.1 Hourly Simulation

Irregularities are detected by plotting measured data from the system against data calculated from the computer model. Irregularities, which may be caused by hardware failures or measurement inaccuracies, may be detected as outliers in the plot. Figure 1.2 shows a plot where the actual PV array output is plotted against the simulated output. A linear plot is obtained but a number of outliers exist. When analysed it was found the source of these outliers was a DC fuse failure on the line-commutated inverter. PV array and battery degradation is calculated by testing the models accuracy at regular intervals (annually). The degradation may be further analysed by reviewing the model concepts described in Chapter 2 and 3.

1.3 Fotavoltaic Project

The Fotavoltaic Project [7] is the name given to one of the fifteen photovoltaic projects which have been built throughout Europe under the auspices of the CEC solar energy R&D program. The Fotavoltaic project consists of a 50kWp photovoltaic system which is used to supply electrical energy to a 250 head dairy farm.

The farm, which is located on Fota Island in Cork Harbour, was selected because its seasonal energy requirements are well matched to available insolation. During the summer months peak load demands exist due to the high milk yield, and during the winter months the load demand decreases due to the decrease in milk yield,

Figure 1.3 shows the layout of the complete system and table 1.1 is a summary of the main characteristics of the components.

FIGURE 1.2 SYSTEM ANALYSIS USING MODEL.

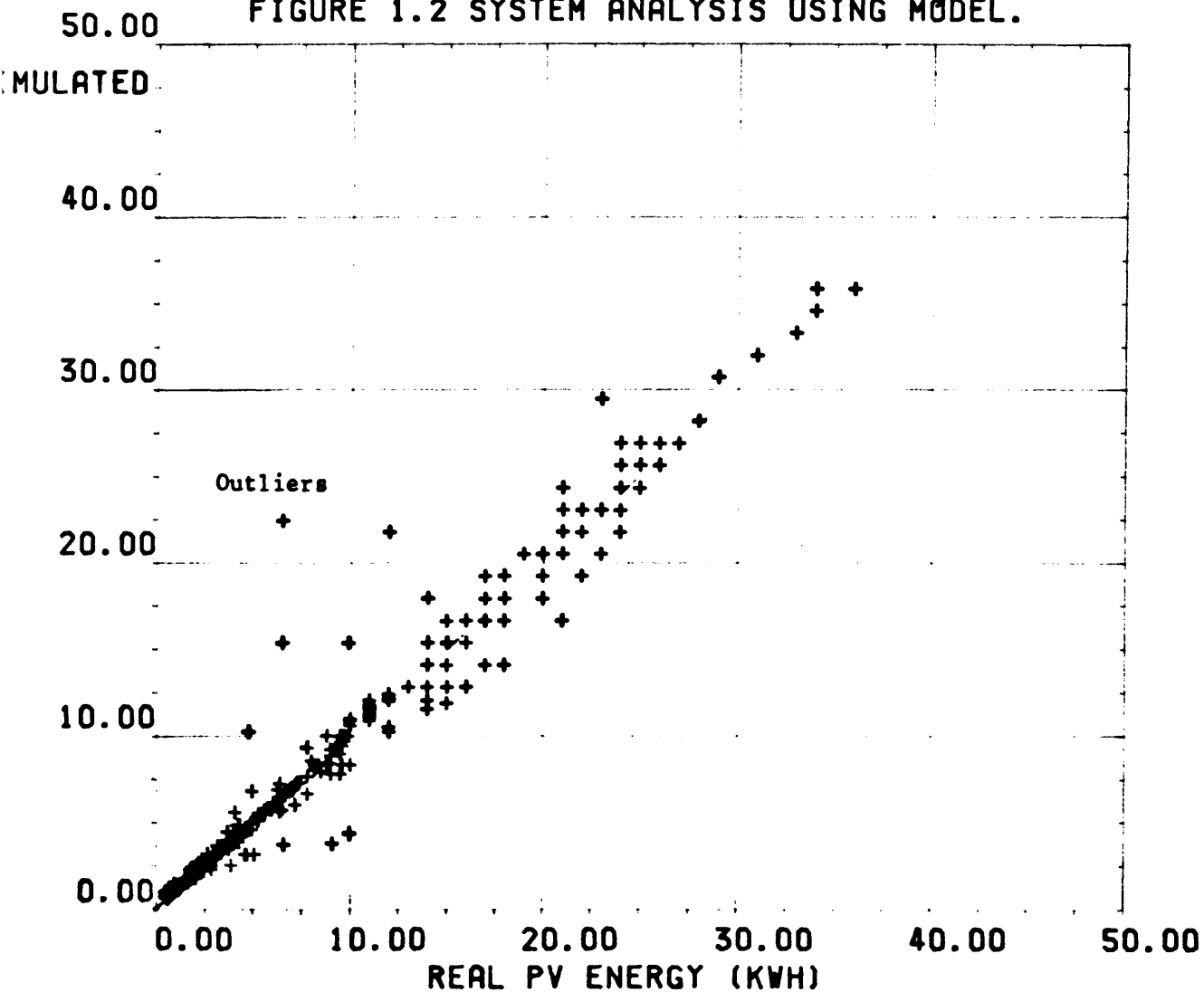


Figure 1.3 Layout of The Fotovoltaic System

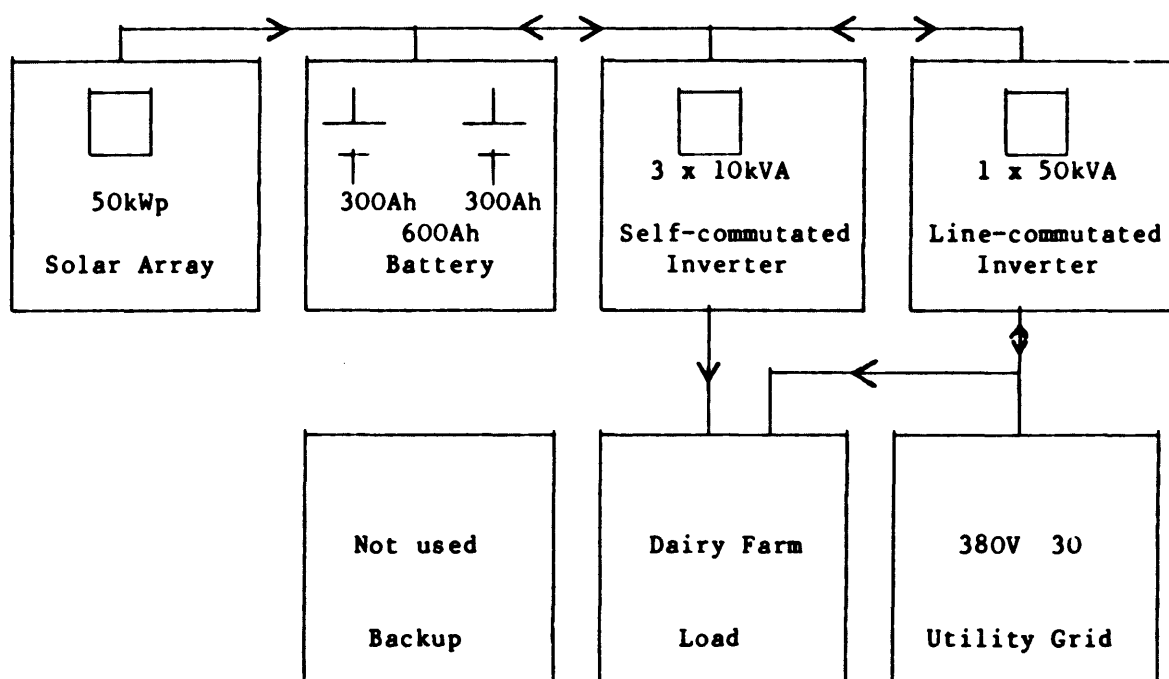


TABLE 1.1 Characteristics of the Main Hardware Components

Solar Generator:	Rated Peak Power	50kWp
	Nominal DC Voltage	268V
	Material	Polycrystalline Si
	Number of Modules	2775 type PQ 10/20/02
Battery:	Type	Lead Acid VARTA Bloc (Vb 2306)
	Capacity	600 Ah
	Nominal Voltage	268V
Inverter:	Self-commutated	3 x 10 kVA
	Output Voltage	380V 30, 50Hz
	THD	Less than 5%
	Efficiency	95% at FL, 86% at 10% FL
	Line Commutated	1 x 50 kVA
	Output Voltage	380V 3 phase 50Hz
	THD	Less than 5%
	DC Nominal Voltage	268V
	Max DC Current	100A
	Efficiency	88% at full load, 75% at 10% full load
Load:	Dairy Farm Motors	
	Max Demand	12kW
	Daily Demand	Summer 115kWh/Day
		Winter 10kWh/Day
Controller:	Motorola 6800 microprocessor system 24k control software.	

The 50kWp PV array consists of 2775 PV modules mounted on the roof of a south facing building (figure 1.4). Two 300Ah lead-acid batteries are used for energy storage and three 10kVA self-commutated inverters are used to supply three independent loads on the dairy farm. The loads are AC induction motors which are used for milking, cooling and washing.

A 50kVA line-commutated inverter is used to deliver excess energy from the PV system to the utility grid. This unit may also be used in a converter mode to recharge the batteries during periods of prolonged low insolation. The complete system operates automatically and is controlled using a Motorola 6800 based microcomputer [8].

A computer link connects the microcomputer to the VAX 11/780 at the NMRC (20km from Fota). The system is checked daily and all events (system shutdown, inverter failure, grid failure etc.) are entered in a log book. This information is supplied as input data to the model during the verification process.

1.4 Layout of Computer Model

Figure 1.5 describes the layout of the overall model and Table 1.2 contains a summary of the characteristics of each individual component model. Each of the individual models are described in the following chapters.

1.5 Modelling Techniques

The techniques [10,11,12,13,14] used during the development of the computer model are summarised in the following order:



FIGURE 1.4 THE FOTAVOLTAIC PROJECT

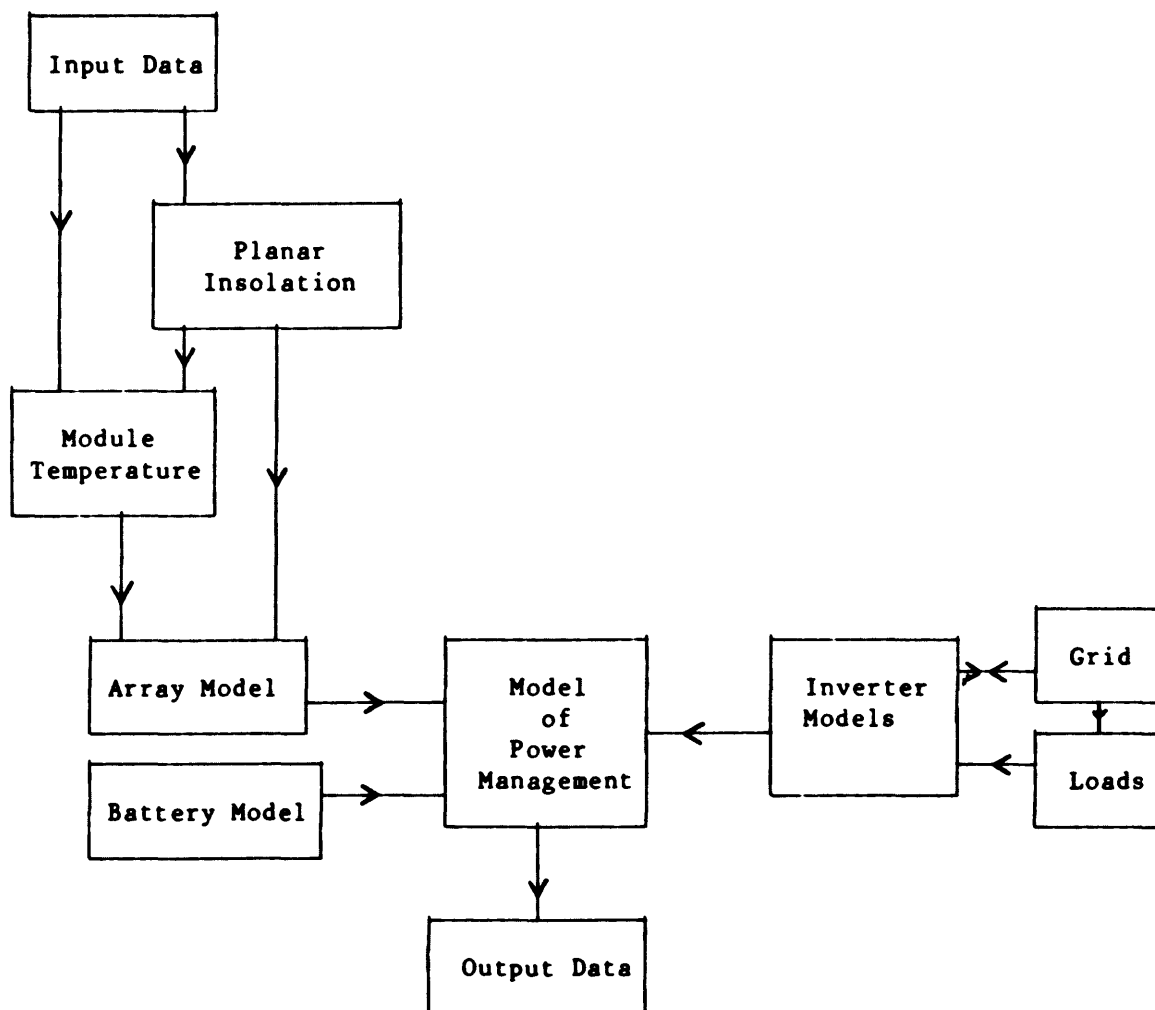


Figure 1.5 Layout of Computer Model

Table I.2: Characteristics of Individual Models

Input Data:	Horizontal insolation, planar insolation, ambient temperature, module temperature, wind speed, wind direction, date, time, load demand, horizontal status
Planar Insolation:	Calculated (if required) using horizontal insolation, day of year and the time of day
Module Temperature:	Calculated (if required) using ambient temperature, planar insolation, wind speed and wind direction.
PV Array Model:	The array output energy is calculated using planar insolation and module temperature
Battery Model:	The battery voltages are expressed as a function of current, Ah and temperature
Inverter Model:	Inverter efficiency is described as a function of the output energy and the mode of operation
Model of Power Management:	Algorithms simulate the different modes of operation
Loads:	This is supplied as input data to the model
Grid:	The availability of the grid is defined as input data i.e. hardware status
Output Data:	The data is output in 4 formats - as an energy summary - in graphical form for visual verification - in a format suitable for statistical analysis - in a format similar to CEC recorded data [9]

- definition of problem
- data collection
- bibliography compilation
- model concepts
- model implementation
- model verification

The development procedure is shown in figure 1.6.

1.5.1 Definition of Problem

In this section the aims of the computer model were defined. The main aims were that the computer model would a) optimize the performance of a 50kWp system; b) operate on an hourly basis; c) be structured in a format suitable for the simulation and optimization of other PV systems.

Following this, the model layout (figure 1.5) was established and the parameters used for modelling were defined (table 1.2). The other tasks defined in this phase were

- a) the model verification procedures (section 1-10)
- b) the data input format (Annex C)
- c) the optimization procedures (Chapter 6)

When the above phase was completed a time schedule was compiled.

1.5.2 Data Collection

In this phase a data recording format was selected. The data is recorded in a format specified by the CEC Pilot Program [9]. The data selected for CEC analysis are:

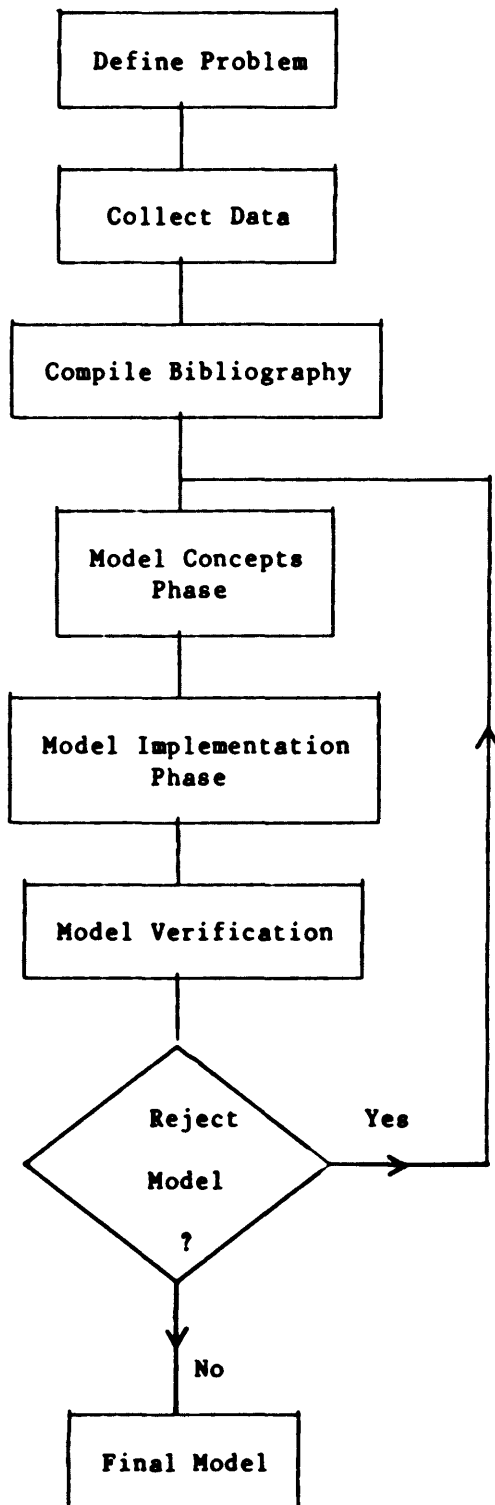


Figure 1.6 Development Procedure for Computer Model

- Meteorological data (horizontal insolation, wind speed, wind direction, ambient temperature)
- System's energies (PV array, battery, inverters, and grid)
- Load energies.

For an analysis in accordance with the CEC pilot program a total of twenty two values are recorded every hour. In order to cover all aspects of the system in the model development supplementary data was required. This supplementary data includes the energies of the subunits, the temperatures of the subarrays and batteries, and the maximum values of some measuring points. The maximum values are recorded to examine and model the system performance during periods of high insolation with varying cloud cover. The recorded values are maximum planar insolation, maximum array output and the maximum battery charging currents. A total of fifty extra values are recorded every hour. An example of an hourly recorded data file is shown in Table 1.3. The significance of each value is documented in Appendix C.

Table 3.1 Layout of Hourly Recorded Data from the Fotavoltaic Project

% Fota % 11-10-85,12.00										
1,	0.28,	0.53,	0.086,	61.,	1.6,	2.1,	1.7			
2,	13.,	32.,	20.,	5.0,	1.9,	14.,	13.,	14.,	0.083	
3,	0.00,	0.00,	.0024,	1.1,						
4,	1.5,	1.6,	1.5,	1.5,	1.4,	1.7,	1.7,	1.5,	1.4,	1.6
5,	1.7,	1.5,	1.1,	34.,	27.,	33.,	13.,	13.,	10.,	4.0
6,	287.,	0.080.,	23.,	17.,	59.,	277.,	0.076.,	20.,	21.,	34
7,	0.43.,	0.89.,	0.40.,	1.0	0.056,	0.29,	16.,	16.,	38.,	36.
8,	1.7,	2.3,	1.8,	948.,	948.,	0.96,	0.92,	4.0,	2.6,	0.55

1.5.3 Bibliography Compilation

When the aims of the model were defined a computer search facility was used to compile information on existing PV computer models and hardware models. The theories described in these reports provided a basis for the development of the model concepts. (Section 1.5.4) The reference section at the end of this thesis contains all reports used during the model development. This compilation should provide a useful reference for future work in this area.

1.5.4 Model Concepts

In this phase the hypotheses and assumptions, which are used to simulate the PV system's performance, are analysed. The model concepts for this PV system is divided into two areas:

- model concepts of the hardware units
- model concepts of the power management.

In both cases the model concepts are tested using data obtained from the Fotovoltaic Project. The concepts described in Chapters 2, 3 and 4, are the most successful from the overall analysis. This phase was very time consuming both in man hours and in computer hours.

To develop the model concepts for the power management all the individual hardware models were linked to simulate the overall system performance. The procedures used to develop the model concepts for the power management are summarised as follows:

- define and describe each mode of operation explicitly
- examine variations of each mode due to variations in operating conditions
- determine the conditions which initiate and terminate each mode.

Seven modes of operation exist. Each mode was defined and described by manually examining each hours data for a number of months. By defining the mode of operation during each hour, it was possible statistically to determine conditions which initiate and terminate each mode.

This analysis provided a better understanding of the control parameter sensitivities and this led to system improvements.

1.5.5 Model Implementation

In this phase the model concepts were translated into logical flow charts and then into software. The computer facilities, programming conventions and software layout were defined at this stage.

FORTRAN 77 was selected as the programming language on the VAX 11/780. A graphics terminal (GIGI) and graphics plotter were selected for the graphical analysis of the results. The programming conventions of the NMRC were selected and an example shown in Appendix D.

A modular software layout was adopted so that the individual models could be used to simulate other PV systems. In addition, a modular structure is easier to implement and revise. The individual models shown in Figure 1.5 are structured as subroutines and the input parameters defined in table 1.2 are defined as subroutine variables, e.g. the subroutine for the estimation of planar insolation is defined as SUBROUTINE PLANAR (HORIZ, MONTH, DAY, HOUR).

HORIZ represents the horizontal insolation in kWh/m².

The flowcharts of the power management were constructed in this phase and are shown in Appendix D. The flowcharts of the individual hardware models are not shown since they are described explicitly in Chapters 2 and 3.

1.5.6 Model Verification

The main aim of the model verification is to assess the accuracy of the model in predicting the actual system performance.

Model verification [10,15,16,17] is performed in the hardware modelling and in the power management modelling. In both cases the objectives are as follows:

- assess the difference between the model prediction and the actual performance.
- explain the difference in terms of physical factors
- recommend changes in the model concepts.

Therefore, the model development is an iterative process involving the concepts, implementation and verification phases. An adequate model is achieved when the error is less than 5%.

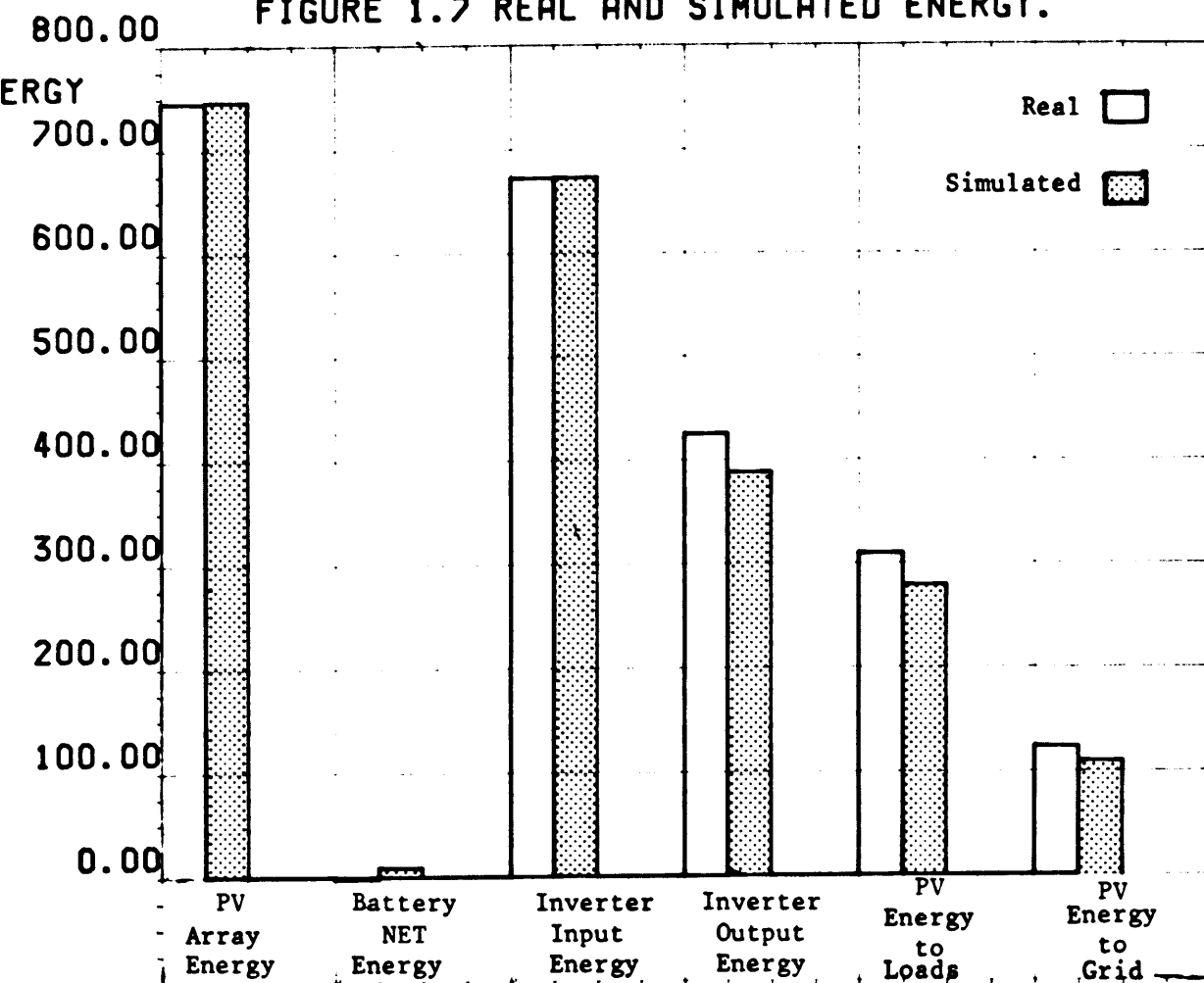
The methods used to verify the model are:

- Graphical Analysis
- Energy Summaries
- Statistical Analysis

The graphical analysis and the energy summaries are mainly used to verify the power management model.

Graphical analysis is used as a visual method of examining the accuracy of the model. Figure 1.7 is an example of a graphical display of the actual energy values and the simulated energy values. It is clear from this histogram that the model is very accurate. This analysis only provides a visual display, however, and it does not quantify the accuracy. The histogram may be plotted on a graphics terminal or on a graphics plotter.

FIGURE 1.7 REAL AND SIMULATED ENERGY.



Energy summaries are used to quantify the accuracy of the simulation. The energy summary for the simulation shown in figure 1.7 is listed in table 1.4.

Table 1.4 Energy Summary of Simulation			
	Measured	Simulated	Error %
PV Array (kWh)	744.91	746.61	0.2
Battery Net Energy (kWh)	-1.75	9.03	3.5
Inverter Input Energy (kWh)	672.54	673.18	0.1
Inverter Output Energy (kWh)	424.92	388.37	-8
Energy to Load (kWh)	309.77	278.85	-7
Energy to Utility Grid (kWh)	123.82	109.52	-4.5
Grid energy to load (kWh)	207.68	221.97	6
Inverter Efficiency	0.63	0.58	7.9
	* Error/300Ah		
	** Error/Total AC Energy		

Statistical analysis is performed using the statistical package SPSS [18]. Scatter plots are used to compare the hourly measured values, with the hourly simulated values and regression analysis techniques are used to quantify the accuracy of the simulation. Figure 1.8 is an example of a scatter plot of the actual PV array output energy versus the simulated PV array output energy. A one-to-one relationship exists between the real and simulated values if the points are on the 45° diagonal. In this plot it is clear that the simulation is very accurate. Table 1.5 is a statistical summary of the scatter plot shown in figure 1.8. The regression line associated with the plot has a slope of 1.01 and it intersects the origin i.e. the regression line is the 45° diagonal. The statistical parameter R^2 is a measure of the accuracy of the regression line. R^2 varies from 0 to 1

FIGURE 1.8 VERIFICATION OF ARRAY MODEL

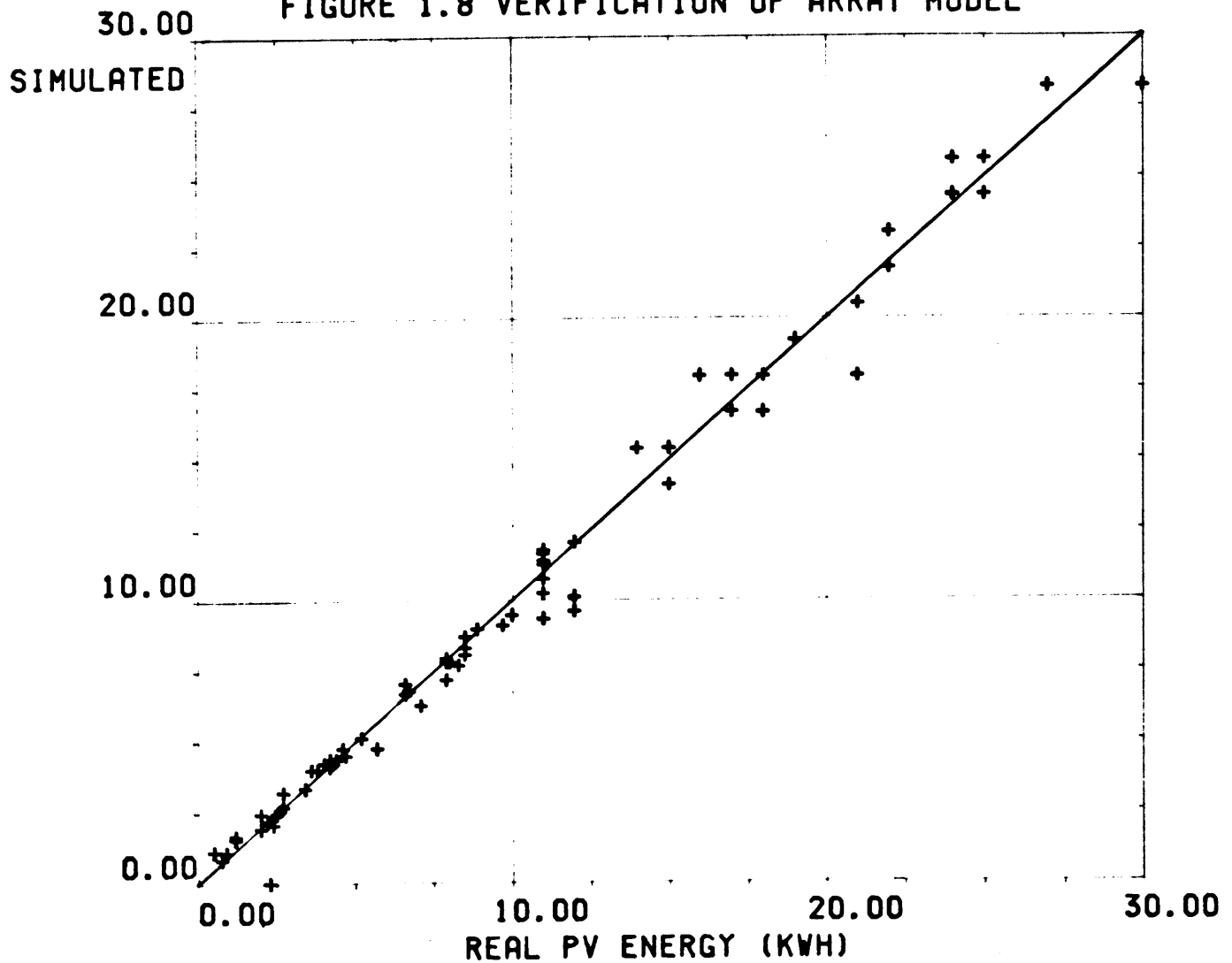


TABLE 1.5 Statistical Summary of Figure 1.8

R Squared	=	0.96
Slope of Regression Line	=	1.01
Intercept on Y Axis	=	0.09
Standard Error or Estimate	=	0.86
Number of Plotted Points	=	72

with the value 1 representing a perfect fit. In the plot of figure 1.8 the R^2 value is 0.96 i.e. the regression line explains 96% of the variation about the mean value. Therefore, the simulation explains 96% of the real performance.

Other examples of scatter plots are included in Chapters 2 and 3.

The overall verification procedure may be summarised as follows: The graphical analysis is first used to visually examine the overall simulation. The energy summary is then used to quantify its accuracy. The scatter plots are used to visually examine the hourly simulations, and the regression analysis is used to quantify their accuracy.

The verification methods described in this section provide a fast and efficient method of measuring the models accuracy. Similar techniques have been developed to successfully analyse the recorded data. These analysis techniques [19] have aided in the system analysis and led to an improved and more efficient system.

CHAPTER 2

MODEL OF PHOTOVOLTAIC ARRAY

2.0 Introduction

The energy produced by a PV array is dependent on the level of planar insolation, the temperature of the modules and the operating current and voltage of the array. In this model, the PV array output is calculated from standard meteorological data, i.e. horizontal insolation, ambient temperature, wind speed and wind direction. Other parameters such as array tilt and latitude, are supplied as constants.

This chapter describes the models of: the planar insolation, the module temperature and the thirteen subarrays. Though these parameters are measured in the Fotovoltaic system the models may be used to examine the performance of a PV array at any geographical location and for any climate.

2.1 Model of Planar Insolation

The insolation on the plane of the array is calculated as a function of the direct and diffuse components of the horizontal insolation. The generalized equation [29] is summarized as:

$$I_t = R I$$

$$R = (1 - I_d) R_b + K_h(1 + \cos b)/2$$

where

I_t = Insolation on the plane of the array

I = Total hourly horizontal insolation

R = Ratio of planar insolation to horizontal insolation

K_h = Diffuse insolation factor i.e. the ratio of the diffuse horizontal insolation to the total horizontal insolation.

$I - I_d$ = Direct horizontal insolation.

R_b = Ratio of the hourly extraterrestrial insolation on a tilted surface to the insolation on a horizontal surface.

b = PV array tilt angle to the horizontal

This section describes the hypotheses used to calculate these parameters. The procedures followed in calculating the insolation on any plane is then outlined and some sample calculations are given. Several authors [19,33,34,35,37,38] have developed models to calculate the monthly and daily insolation on the plane of an array. The most notable of these authors were Liu and Jordan [29,30,31] whose theories are a basis to any work in this area. Only a few authors [36,37,39] have developed hourly models mainly due to the unavailability of hourly data. The hourly models which have been developed are very accurate but are also very site specific due to their dependancy on local climatic conditions. All existing hourly models were tested in the development of the model for the Fotavoltaic system. The final model, which has an error of less than 5%, uses the most accurate equations to calculate the parameters outlined in the previous equation.

Calculation of Diffuse and Direct Components of the Horizontal Insolation

In the Fotavoltaic system the total horizontal insolation is measured. Its direct and diffuse components are determined analytically. The clearness index, K_t , is a measure of the amount of cloud cover during a sampled hour and is defined as:

$$K_t = \frac{I}{I_0}$$

where

I = total horizontal insolation

S_0 = The extraterrestrial horizontal insolation i.e. the radiation which would be incident on the same horizontal surface in the absence of any atmosphere.

Previous authors [36,37,39] have developed models relating K_t and K_h . These were tested using data from the Fotavoltaic system, and the most accurate was selected [37]. This relationship is summarised as:

$$\begin{array}{ll} K_h = 1 - 0.249 * K_t & 0 < K_t < 0.35 \\ & = 1.557 - 1.84 * K_t & 0.35 < K_t < 0.75 \\ & = 0.177 & K_t > 0.75 \end{array}$$

$K_t < 0.35$ represents overcast periods with little direct insolation

$K_t > 0.75$ represents high insolation periods with little cloud cover

$0.35 < K_t < 0.75$ represents periods of variable insolation and variable cloud cover.

From this equation the diffuse and direct components of the horizontal insolation are calculated as:

$$\begin{array}{ll} I_d = K_h * I & \text{diffuse} \\ I_b = I - I_d & \text{direct.} \end{array}$$

The accuracy of this model is discussed at the end of this section.

Calculation of Rb, the ratio of the hourly extraterrestrial insolation

The parameter Rb is calculated geometrically using an equation described by Liu and Jordan [29].

$$R_b = \frac{\cos(\Phi - b) \cos d \cos W + \sin(\Phi - b) \sin d}{\cos \Phi \cos d \cos W + \sin \Phi \sin d}$$

where:

Φ = latitude = 51.45°

b = PV array tilt angle = 45°

d = angle of declination (calculated)

W = hour angle.

The hour angle, W, is measured as follows.

At noon $W=0^\circ$, 11:00 $W=-15^\circ$, 13:00 $W=+15^\circ$.

During a sampled hour the value of Rb is evaluated at the half hour point i.e. 10:30 etc.

Procedures to Calculate the Insolation on the Plane of an Array

This section describes the procedures involved in calculating the insolation on an array plane. The procedures are based on the theories outlined in the previous sections.

(a) Define the following parameters

- Latitude = Φ = 51.45°
- Day of Year = DAY January 1 = 1
- Array Tilt Angle = b 45°
- Hour Angle = W

- (b) Calculate the solar declination angle.

$$\sin d = \sin (23.45) \sin \left(\left(\frac{284 + \text{DAY}}{365} \right) * 360 \right)$$

This is a standard astronomical equation.

- (c) Compute the extraterrestrial insolation on a plane held normal to the sun's rays [34].

$$S_0 = S \left(\left(1 + 0.0167 \cos \left(\frac{\text{DAY}}{365} * 360 \right) \right)^2 \right)$$

$$S = 1.356 \text{ kw/m}^2 = \text{solar constant.}$$

- (d) Calculate the extraterrestrial insolation on the horizontal for the sampled hour [29]:

$$S_{oh} = S_0 (\cos \Phi \cos d \cos W + \sin \Phi \sin d)$$

This is a standard astronomical equation.

- (e) Calculate the clearness index K_t .

$$K_t = \frac{I}{S_{oh}}$$

I = total horizontal insolation.

- (f) Calculate the diffuse insolation factor K_h .

$$\begin{aligned} K_h &= 1 - 0.249 * K_t & 0 < K_t < 0.35 \\ &= 1.557 - 1.84 * K_t & 0.35 < K_t < 0.75 \\ &= 0.177 & K_t > 0.75 \end{aligned}$$

- (g) Calculate R_b

$$R_b = \frac{\cos (\Phi - b) \cos d \cos W + \sin (\Phi - b) \sin d}{\cos \Phi \cos W \cos d + \sin \Phi \sin d}$$

(h) Calculate R

$$R = (I - I_d)R_b + K_h(1 + \cos B)/2$$

(i) Calculate the insolation on the plane of the array.

$$I_t = R \cdot I$$

Table 2.1 contains three sample calculations using these procedures. In all cases the error of the calculated planar insolation is less than 2%.

The overall model is verified by plotting the real planar insolation against the simulated planar insolation and by examining its statistical summary. The model is verified for November 1985. Figure 2.1 shows the plot and table 2.2 contains its statistical summary.

The R^2 is 0.96 indicating that the simulation explains 96% of the real insolation. This accuracy is sufficient for the overall system model.

Table 2.1 Sample Calculations of Hourly Insolation
on the plane of the array $\Phi = 51.45^\circ$, $b = 45^\circ$

Step	Parameter	Sample 1	Sample 2	Sample 3
(a)	Day	234	235	235
	W	15	15	-15
	In	0.779	0.589	0.369
(b)	d	10.8	10.8	10.8
(c)	So	1.328	1.328	1.328
(d)	Soh	0.979	0.979	0.898
(e)	Kt	0.795	0.6	0.41
(f)	Kh	0.205	0.305	0.484
(g)	Rb	1.316	1.316	1.28
(h)	R	1.21	1.17	1.05
(i)	It	0.944	0.684	0.389
	Measured	0.94	0.67	0.39
	Error	0.4%	2%	0.25%

FIGURE 2.1 MODEL OF PLANAR INSULATION.

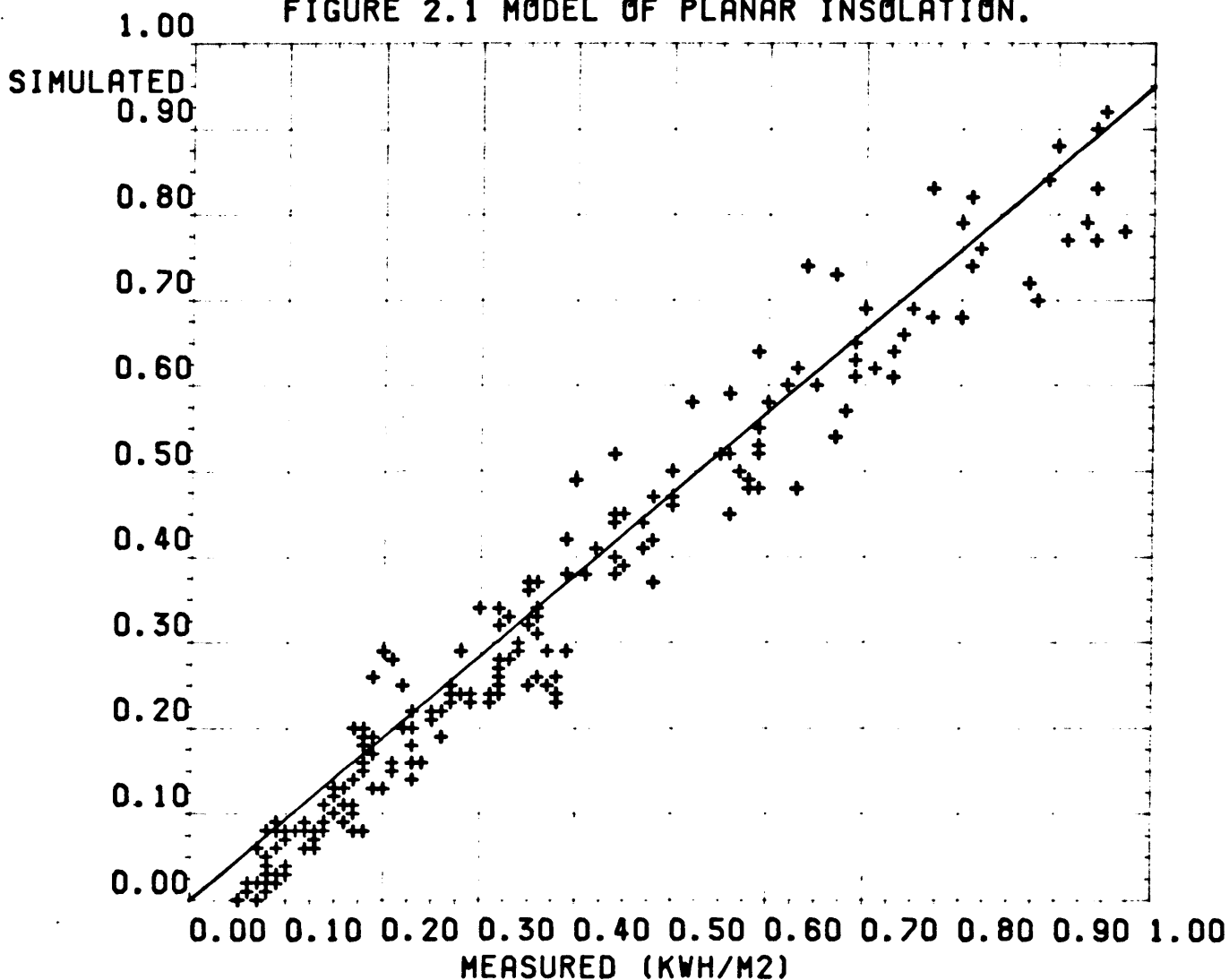


TABLE 2.2 Statistical Summary of Figure 2.1

R Squared	=	0.96
Slope of Regression Line	=	0.95
Intercept on Y Axis	=	0.02
Standard Error or Estimate	=	0.047
Number of Plotted Points	=	200

2.3 Model of Module Temperature

The temperature of a PV module is an important parameter in the calculation of the PV array efficiency. Typically, the maximum available power output decreases 0.5% for every degree centigrade rise in temperature. In this model the module temperature is expressed as a function of planar insolation, ambient temperature and wind speed. Some authors [33,35] have included extra parameters such as: IR radiation, radiation reflected from the cover glass and albedo. These parameters are not measured in the Fotovoltaic system and are therefore omitted.

The model is verified by comparing the results with the data from temperature sensors in the PV array. The three sensors (PT100) are mounted directly onto the cells to provide accurate cell temperatures.

The main source of error in this model is due to the fact that the modules are not in thermal equilibrium with the environment. In the Irish climate where the planar insolation and the wind speed are constantly varying thermal equilibrium is seldom reached. The final model predicts the module temperature with an error of less than 5°C.

The model was developed by examining the effects of the following parameters on the module temperature:

- planar insolation
- wind speed
- wind direction
- ambient temperature

Planar Insolation

The insolation on the plane of a PV module is divided as follows:

- it produces electrical energy (10%)
- it generates heat within the module (85%)
- a small factor is reflected.

The amount of radiation reflected depends on its angle of incidence to the array plane. In this system the reflected energy is only significant in the early morning and in the late afternoon. During these periods the array output is low (<2kw) and the effects of module temperature are small. In this analysis the reflected energy during these periods is neglected.

When electrical energy is generated in a PV module the temperature of the module decreases. The decrease is proportional to the electrical energy generated, which in turn is proportional to the planar insolation. Consequently, the net increase in temperature is proportional to the level of planar insolation, i.e.

$$T_m - T_a = K I_n$$

where:

T_m = module temperature °C

T_a = ambient temperature °C

I_n = planar insolation kwh/m²

K = constant of proportionality.

A scatter plot of the increase in module temperature versus the planar insolation at a fixed wind speed is shown in figure 2.2. The slope of the regression line describing this plot is equal to the constant K . From the statistical analysis $K = 25.62$.

Figure 2.2 Module temperature increase as a function of the Planar Insolation at zero wind speed.

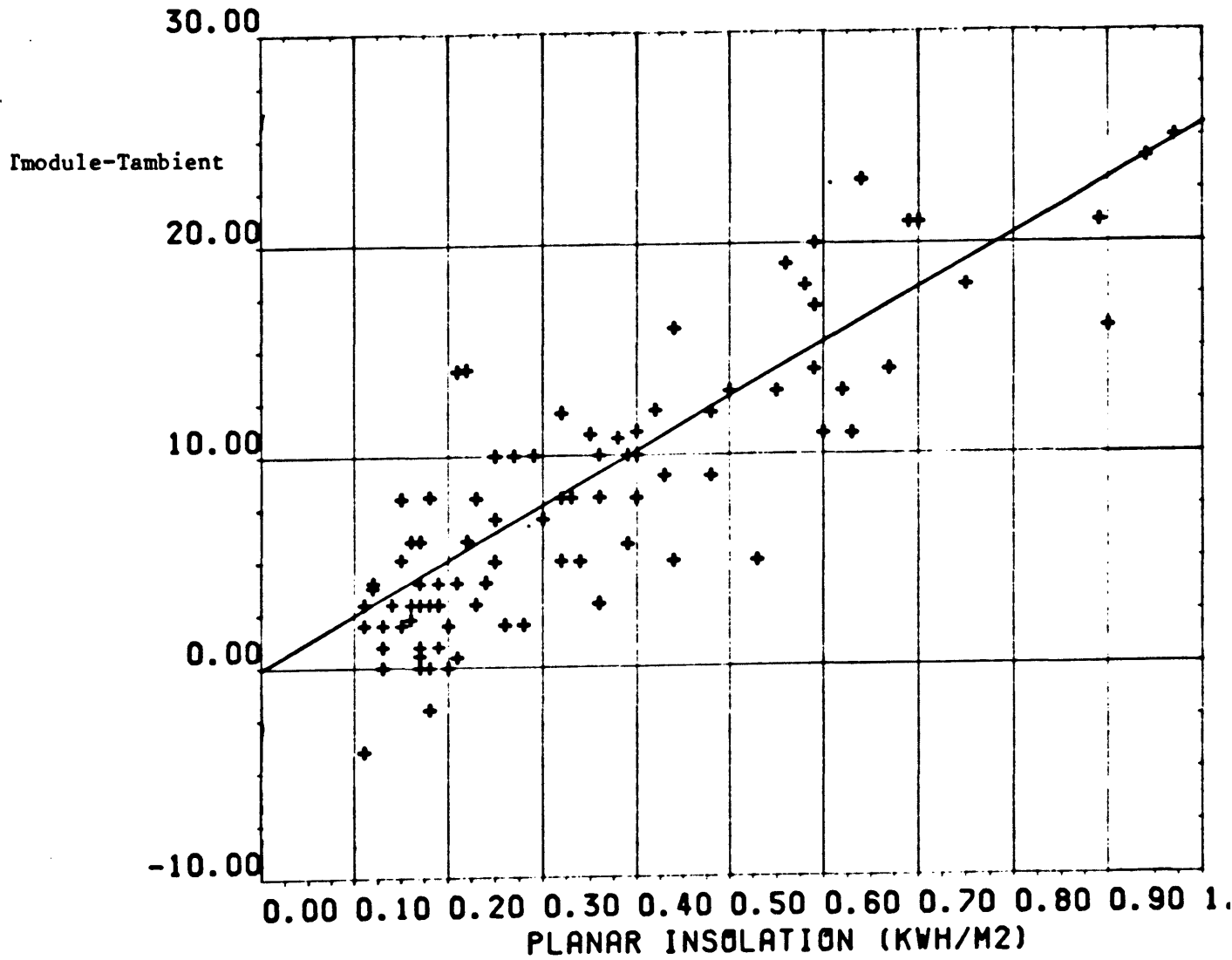


TABLE 2.3 Statistical Summary of Figure 2.2

R Squared	=	0.6
Slope of Regression Line	=	25.62
Intercept on Y Axis	=	-0.31
Standard Error or Estimate	=	4.6
Number of Plotted Points	=	94

Wind Speed

The cooling effects of the wind speed are analysed using the theories outlined by Schott [32]. In this analysis a linear relationship is assumed to exist between the rate of cooling and the wind speed. The previous equation is thus improved to:

$$T_m - T_a = \frac{25.62 \ln}{a + b V_W}$$

where

V_W = wind speed ms^{-1}

a, b = constants.

The constants a, b are determined by plotting $\frac{25.62}{T_m - T_a}$ versus V_W .

A regression analysis of this plot gives $a = 0.68$ and $b = 0.11$

$$T_m - T_a = \frac{25.62 \ln}{0.68 + 0.11 V_W}$$

The main source of error in this calculation is due to the uncertainties of the forced and free convection on the plane of the array.

Wind Direction

The effect of wind direction is very dependent on the shape of the building and on the immediate surroundings [35]. The solar building at Fota is situated on the highest point of the island, and its front and rear are sheltered by trees. The building has a south facing roof, tilted at 45° to the horizontal. The back of the building is closed and consequently the modules are not cooled from the rear. The effect of wind direction on the plane of the array is difficult to determine due to eddy currents. In this model, as in other models [11,12,15] the wind direction is neglected.

Ambient Temperature

The heat-loss coefficient of convection varies with ambient temperature [35]. Schott [32] suggests that the coefficient varies linearly with ambient temperature and that the constants may be positive or negative. The previous equation is improved to:

$$T_m - T_a = \frac{22.26 \ln + d T_a}{0.68 + 0.11 VW}$$

where d is a constant.

Due to the high correlation between planar insolation and ambient temperature a regression analysis is not used with both parameters. Instead, the residuals (Real-simulated) from the previous equation are analysed as a function of T_a . A regression analysis between the residuals and the ambient temperature gives a value of $d = 0.16$. The final model is therefore summarised as:

$$T_m - T_a = \frac{22.36 \ln + 0.12 T_a}{0.68 + 0.11 VW}$$

This equation is verified by examining the plot of the real temperature versus the simulated temperature. Figure 2.3 shows the plot and table 2.4 is the statistical summary for this analysis. The low R^2 value of 0.8 is mainly due to the problems of thermal equilibrium. The standard error is 3.17°C and this is sufficiently accurate for the overall system model.

FIGURE 2.3 MODULE TEMPERATURE MODEL.

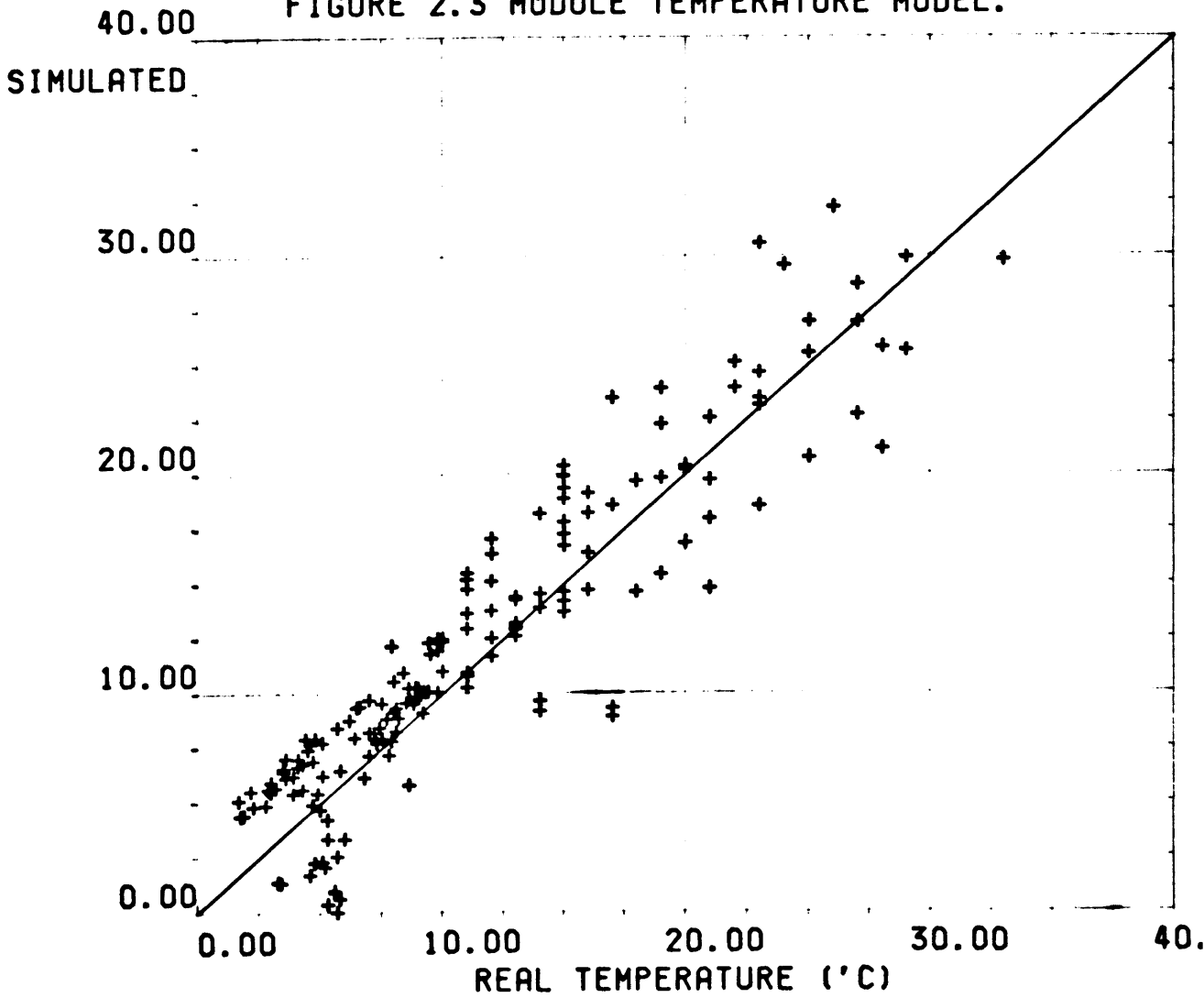


TABLE 2.4 Statistical Summary of Figure 2.3

R Squared	=	0.8
Slope of Regression Line	=	0.96
Intercept on Y Axis	=	0.03
Standard Error or Estimate	=	3.17
Number of Plotted Points	=	170

2.4 Model of PV Array

The 50kWp PV array is divided into thirteen subarrays. Each subarray can be connected to either battery 1 or battery 2 or they can be open-circuited. This section describes the modelling of subarray 1. Similar techniques are then used to model the remaining twelve subarrays. The distribution of the subarrays between the batteries and their disconnection from the batteries is described in the power management model (Chapter 4).

The subarray model was developed both analytically and statistically. The analytical model is less accurate than the statistical model but it only requires three parameters to develop. It is therefore very suitable for the modelling of systems which have no operating data. The statistical model is very accurate but it requires a large amount of data. The development of both models is described in the following sections.

2.4.1 Analytical Model of Subarray

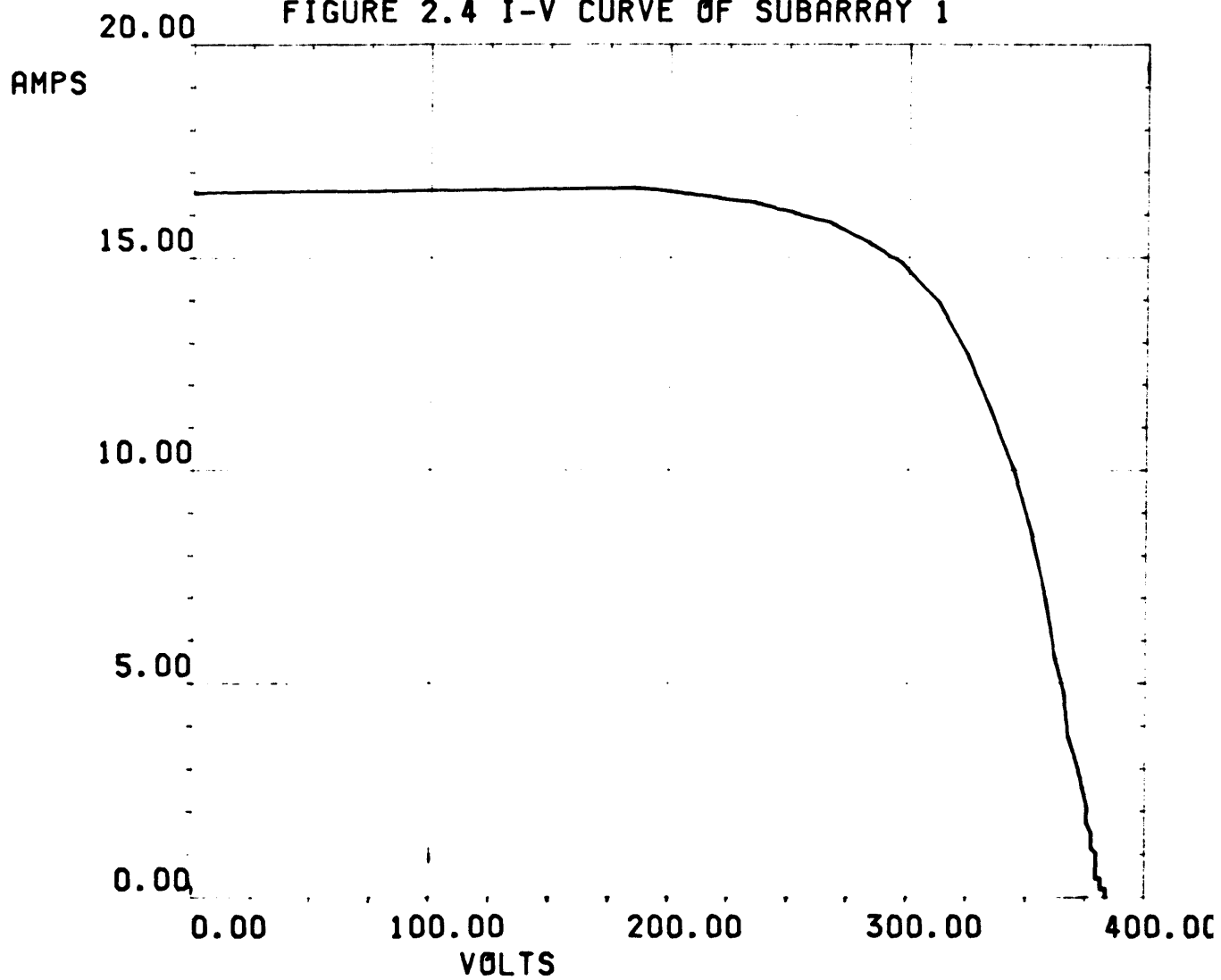
The current-voltage characteristic of the subarray was obtained using equipment [47] developed at the National Microelectronics Research Centre. The curve shown in figure 2.4 is corrected to STC. The equation describing this curve is the standard solar cell equation:

$$I = I_{sc} - I_0 \left(\exp \frac{qV}{kT} (V + IR_s) \right)$$

where:

- I, V = current, voltage
- I_{sc} = short circuit current
- I_0 = reverse saturation current
- q = electronic charge
- k = Boltzmanns constant

FIGURE 2.4 I-V CURVE OF SUBARRAY 1



T = temperature (°K)

Rs = series resistance of subarray.

Several methods [37-40] have been developed to solve this equation. All were tested and the most accurate and applicable method was that suggested by Singer [39]. In this analysis three points are selected on the curve and the exponential equation is fitted. The selected points are: the open-circuit voltage, the short-circuit current and the current and voltage at the maximum power point.

Using this method subarray 1 is modelled as

$$I = 16.39 - 2.08 \times 10^{-7} [\exp (0.047 (V + I * 79))]$$

This equation is only applicable at STC i.e. at 1000 w/m² and at a temperature of 25°C. The curve is translated to any other insolation and temperature using the following relationships [37].

$$V_{\text{new}} = V_{\text{stc}} + dV$$

$$I_{\text{new}} = I_{\text{stc}} + dI$$

$$dV = -BdT + R_s dI$$

$$dI = a \left(\frac{L}{L_{\text{stc}}} \right) dT + \left(\frac{L}{L_{\text{stc}}} - 1 \right) I_{\text{stc}}$$

where

L = Planar insolation

L_{stc} = Insolation at STC

a = Temperature coefficient of current (2.5 mA/°C/cell)

B = Temperature coefficient of voltage (2 mV/°C/cell)

Rs = Series resistance of subarray = 7.9Ω

The maximum power produced at any insolation and temperature is:

$$P_{\max} = I_{\text{MPPT}} * V_{\text{MPPT}} \\ = (I_m + dI) * (V_m + dV)$$

where

$$V_m = V_{\text{MPPT}} \text{ at STC}$$

$$I_m = I_{\text{MPPT}} \text{ at STC}$$

The equation is expanded and the least significant values are neglected to give:

$$P_m = \left(\frac{V_m I_m - R_s I_m^2}{L_{\text{stc}}} \right) L + \left(\frac{V_r B I_r}{L_{\text{stc}}} \right) dTL$$

The values of I_m , V_m , I_{sc} , a , B are substituted to give:

$$P_m = 2.668L + 0.0279 dTL$$

This equation can be used to calculate the subarray output for any level of planar insolation and for any module temperature. The equation was verified by plotting the real subarray energy against the simulated subarray output and by analysing its statistical summary. The plot is shown in figure 2.5 and the statistical summary is presented in table 2.5. The R^2 is 0.96 but the slope of the regression line is 1.12. These figures indicate that the error is proportional to the subarray output energy.

The main sources of error in this analysis are due to the assumption that:

- (a) The fill factor is constant. This assumption is made in the calculation of dV and dI .
- (b) The subarray always operates at MPP. This assumption is made in the calculation of P_{\max} .
- (c) The model was developed for a solar cell. The performance of the subarray is identical to the performance of a solar cell and this assumption accounts for some errors in dV .

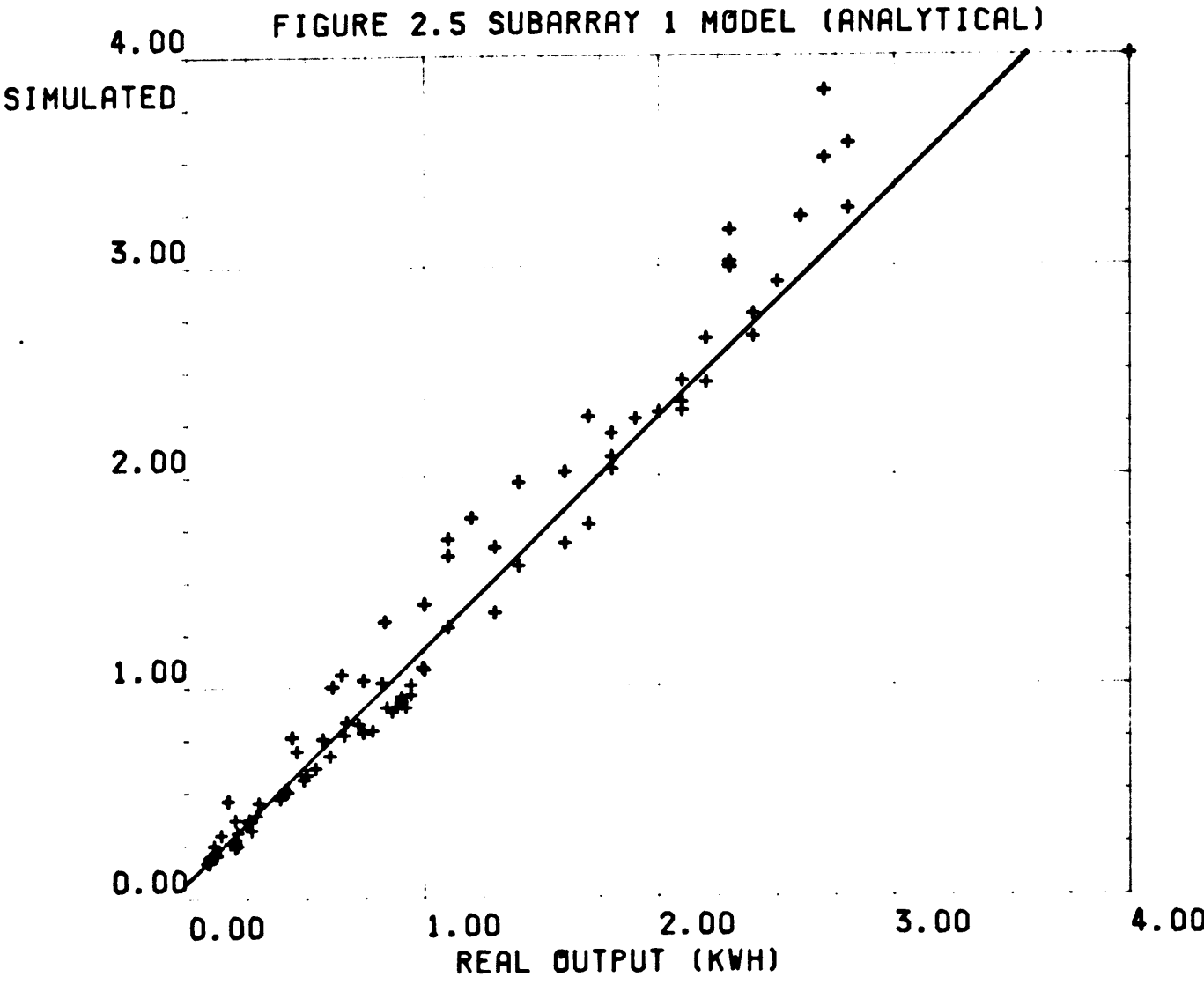


TABLE 2.5 Statistical Summary of Figure 2.5

R Squared	=	0.96
Slope of Regression Line	=	1.13
Intercept on Y Axis	=	0.08
Standard Error or Estimate	=	0.155
Number of Plotted Points	=	70

2.4.2 Statistical Model of Subarray

The statistical model is based on the equation developed in the previous section.

$$P_m = \left(\frac{V_m I_m - R_s I_m^2}{L_{stc}} \right) xL + \left(\frac{V_m + I_m}{L_{stc}} \right) dT L$$
$$= A L + C dT, L$$

where A, C, are constants.

The constants are determined statistically using step-wise regression [18] between the subarray output and the planar insolation, and the temperature * insolation value. The model was developed using data for the months March, April, and May 1985 and the resulting equation was:

$$P_m = 2.528 * L + 0.0279 dT * L$$

This model is verified by plotting the real subarray energy against the simulated subarray energy. The plot is shown in figure 2.6 and the statistical summary is presented in table 2.6. The overall regression has an R^2 of 0.97 i.e. the simulation explains 97% of the real data.

The step-wise regression which is used during the development of this model is summarised in table 2.7. The increase in R^2 caused by the addition of different parameters is shown.

The R^2 value increases from 0.96 to 0.972 by including the temperature value. Therefore, the contribution by the temperature value is small but significant. This accounts for the accepted error of 5°C in the thermal model.

This regression analysis also shows that a simple relationship between the subarray output and the planar insolation will provide an accurate result.

Based on the high accuracy of the statistical model it is reasonable to suggest that this model could be developed with a small amount of data.

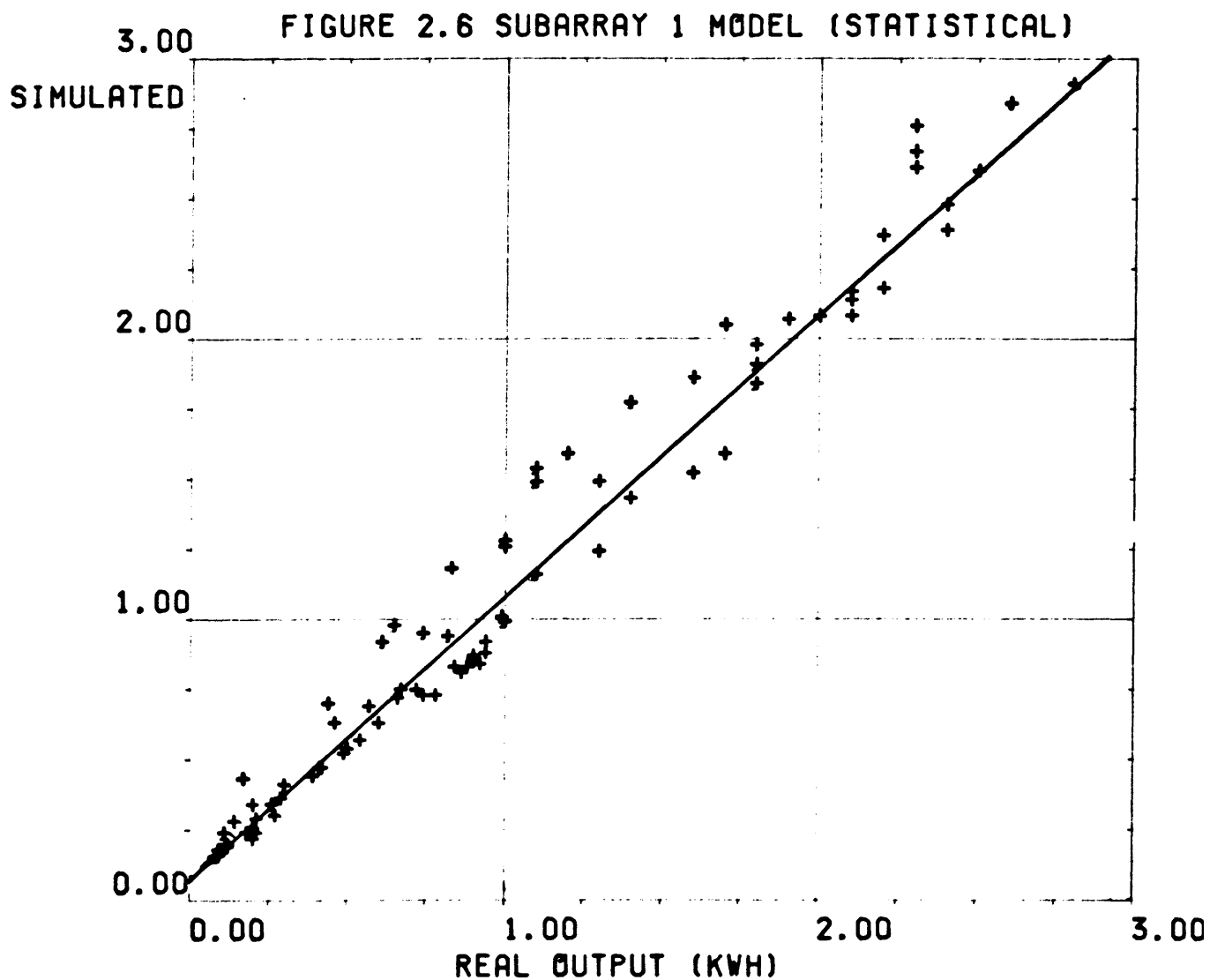


TABLE 2.6 Statistical Summary of Figure 2.6

R Squared	=	0.97
Slope of Regression Line	=	1.02
Intercept on Y Axis	=	0.12
Standard Error or Estimate	=	0.12
Number of Plotted Points	=	86

TABLE 2.7 Step-wise Regression of Subarray 1 Energy
with Planar Insolation and
Insolation * Temperature Value.

$$\begin{aligned} \text{Subarray 1 Energy} = & A * \text{Planar insolation} + \\ & B * \text{Planar insolation} * \text{module} \\ & \text{temperature increase} + \\ & C \end{aligned}$$

where A, B, C are constants.

STEP 1 Regression with Planar Insolation Only

R SQUARED = 0.96

STEP 2 Regression with Planar Insolation and Insolation * Temperature

R SQUARED = 0.972

Variable	Coefficient	Symbol
Planar	2.528	A
Planar * Temperature	0.019	B
Constant	0.004	C

2.5 Conclusion

The models described in this chapter represent the basis for the modelling of any PV system. The high accuracy attained suggests that these simple modelling techniques could be used for other systems. This is especially significant to the CEC Pilot Program as the models are designed based on the data recorded from these systems.

In addition to system modelling, the three models are used to test the meteorological equipment in the Fotavoltaic System [47]. Interruptions or calibration errors are detected by examining the verification plots shown in this Chapter. This is now a standard analysis procedure for the system. Similar analysis techniques can be applied to other PV systems.

CHAPTER 3

Battery and Inverter Models

3.1 Introduction

The Fotavoltaic Project has two battery groups, three self-commutated inverters and a line-commutated inverter. This chapter describes the models of: one battery group, one self-commutated inverter and the line commutated inverter. Chapter 4 links these individual models to simulate the overall power management of the system. The battery model describes the battery voltage as a function of the stage of charge, the charge/discharge current and the temperature. The inverter models describe the inverters efficiencies as a function of their input and output energies.

3.2 Battery Model

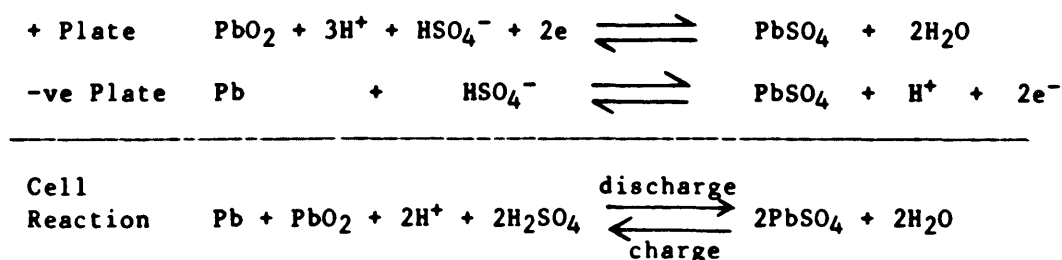
The battery model is the most difficult component to model due to its many dependent variables. Battery operation is a complex function of charge/discharge current, temperature, state of charge and the number and depth of charge/discharge cycles. In this model the battery history is not included. The model is reduced to analysing the battery voltage as a function of charge/discharge current, state of charge and temperature.

In the Fotavoltaic Project the battery state of charge is not measured. The Logistronic, a unit provided by Varta and designed to measure the state of charge, failed to operate. In the model the battery state of charge is estimated from the summation of battery input/output current measurements. Without a direct way to measure the state of charge the long term performance predictions of the model are limited.

A considerable amount of literature [48-68] is available describing the chemical reactions of charging and discharging. The computer models, developed by battery manufacturers [51,61,62,63] are used to optimise the battery design and are not suitable for PV system modelling. In addition, Voss [63] says that 'even though important improvements have been made in the understanding of lead acid batteries the work on modelling of cells is still performed in a more or less empirical basis'.

3.2.1 Battery Theory of Operation

Lead acid batteries consist of positive and negative electrodes of lead oxide and lead respectively. These react chemically with the electrolyte (sulphuric acid). The reaction is summarised as follows:



The characteristics of the different materials will be discussed in the following sections.

3.2.2 Battery Management in Fotovoltaic System

The Fotovoltaic Project is designed to operate automatically in a remote location. Software control algorithms have been developed which provided proper charging characteristics and prevent deep-discharging and overcharging.

Battery Charging Between Deep-Discharge and Over-Charge

Normal battery charging (between deep-discharge and over-charge) follows the characteristic shown in figure 3.1, and figure 3.2.

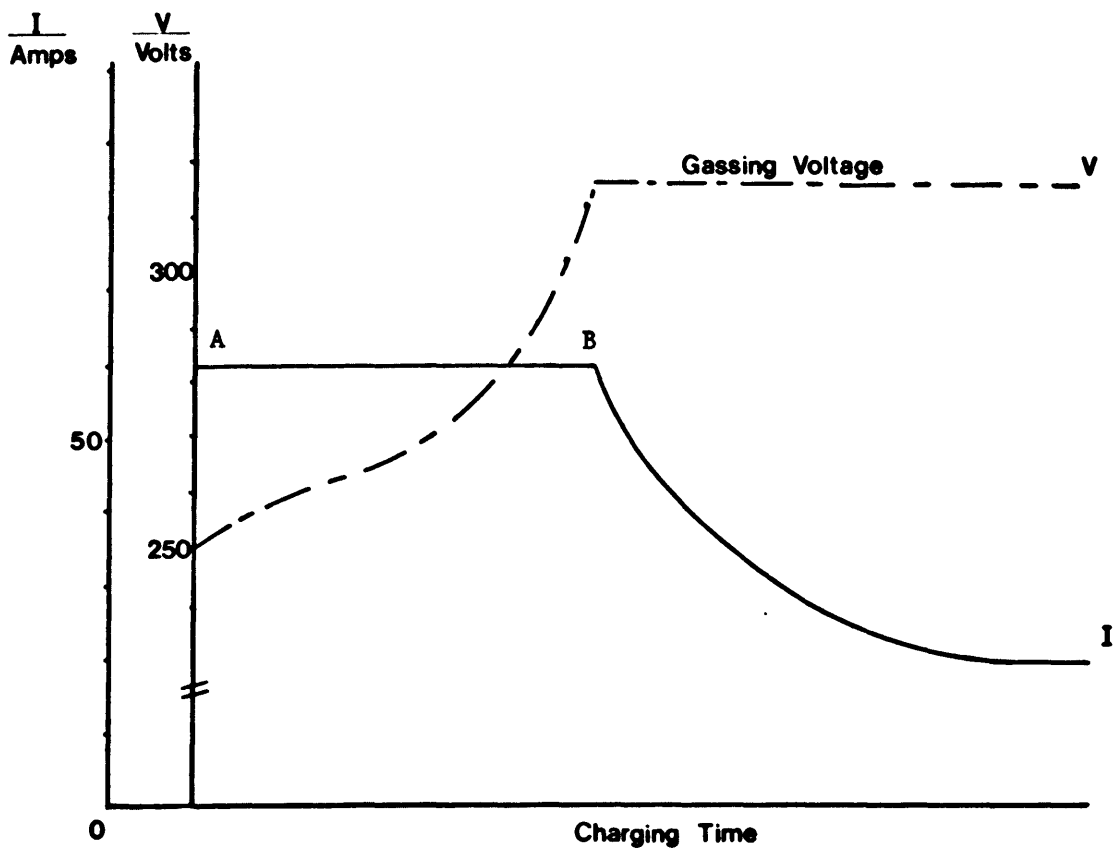


Figure 3.1 Recommended Charging Characteristics

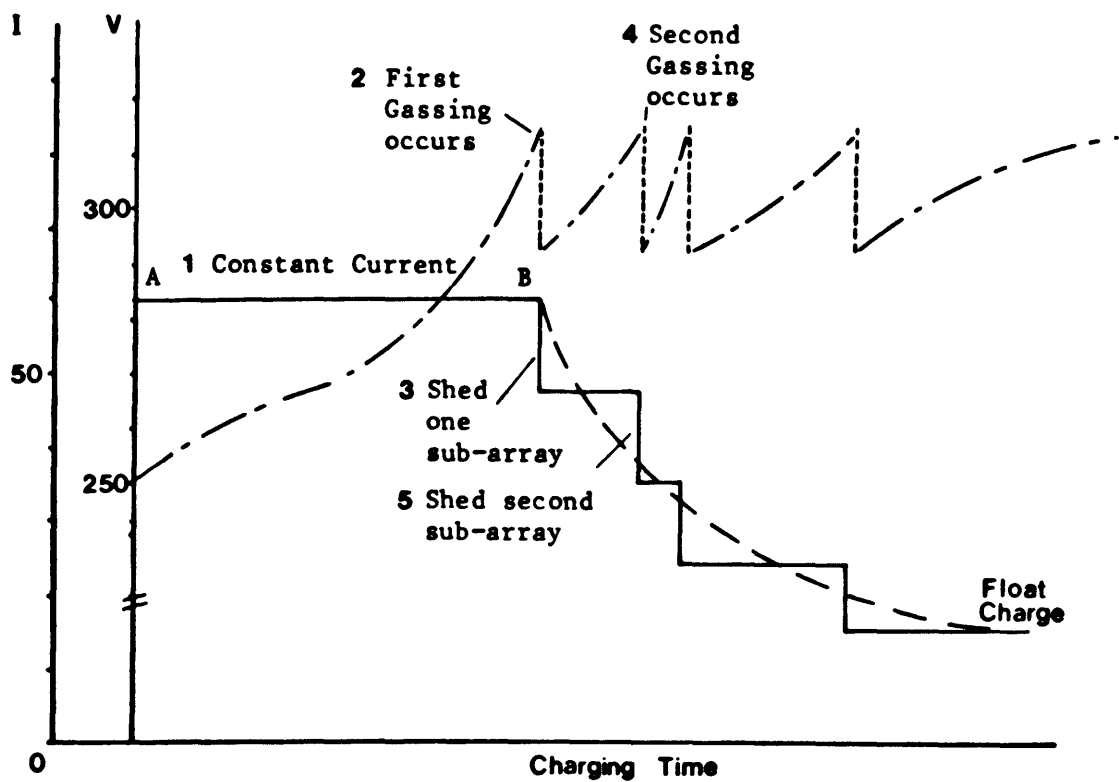


Figure 3.2 Charging Characteristics of Fotovoltaic Project

Figure 3.1 shows the theoretical charging routine. In section A-B the battery voltage is less than the gassing voltage and the current is regulated and maintained at a constant value. When gassing occurs at point B the current is adjusted to maintain the voltage at this level.

In the Fotovoltaic system the battery charging current is regulated by switching subarrays to and from the battery. In figure 3.2 the current step at B represents the disconnection of a subarray. This charging procedure does not follow a theoretical current-voltage curve but it is sufficiently accurate to bring the battery to full charge. The computer model assumes that a proper current-voltage characteristic exists.

Deep-Discharge

During deep-discharge of lead-acid cells a non-conducting material, lead sulphate (PbSO_4), is deposited on the lead plates. This reduces the area of plate and the cell capacity while it increases the internal resistance of the cell. During prolonged deep-discharge the lead sulphate crystallises and cannot be removed during recharging.

In the Fotovoltaic Project deep-discharge is avoided by disconnecting the loads and inverters when the voltage is less than 1.865 V/cell. If the battery discharges below the 1.8 V/cell limit, the line-commutated inverter is operated in the converter mode and the batteries are recharged from the utility grid. Due to this control feature the deep discharge state is not modelled.

However, the power management model (Chapter 4) does simulate the recharging of the batteries using the line-commutated inverter.



Battery Gassing and Overcharge

Water decomposition takes place at 1.23V, which is far below the nominal 2V of a lead-acid cell. Consequently, hydrogen and oxygen are always generated in the lead acid cell [51].

Fortunately, the rates of both hydrogen and oxygen evolution are very slow in the cell. When the battery approaches the state of full charge, an increasing fraction of current is used for electrolysis. An overcharge current is used solely to decompose water i.e. it does not increase the Ah capacity.

The disadvantages of battery overcharging are:

- it reduces the battery efficiency as the energy is used to disassociate water,
- it increases water loss
- the corrosion rate of the positive grid as well as the shedding rate of the active material is increased [63].

The advantages of overcharging are:

- the bubbling during overcharge has a stirring effect and this equalises the acid concentration. This is necessary since some high density active material may fall to the base of the cell and this reduces the battery capacity.
- The stirring effect prevents the formation of layers of lead sulphate. Existing layers may also be removed during gassing.

The software control of the Fotovoltaic System prevents extreme overcharging but allows some battery gassing. This is done by maintaining the battery voltage at the gassing voltage (2.35 V/cell) during the charging process.

Mathematical models have been suggested to simulate battery gassing [56]. The most successful equation to model the Fotavoltaic system's operation was:

$$V_{\text{gas}} = \text{No of cells} \times 0.05 \times \ln(I+1)$$

where I is the charging current.

If the battery State-of-charge is greater than 0.9 or if the battery voltage during charging is greater than 2.23 V/cell V_{gas} is added to the equation developed in section 3.2.4.

Charge Factor

The capability of a battery to store the charge current is called the charge acceptance. It depends on the construction, age, and temperature of the battery. The ratio of the current needed for full charge to the available current for discharge is called the charge factor, the reciprocal value of the charge efficiency. Gassing, is a parasitic use of current, and when it occurs, the charge factor is always greater than 1.0. Below the gassing voltage, the total charging current is available for discharge and the charge factor is 1.0.

From experimental data and from manufacturers' specifications the VARTA bloc batteries have a charge factor of 1.1.

In the battery model the increase in the battery Ah is calculated as follows:

$$\text{Ah}(t) = \text{Ah}(t-1) + I(t)/cf$$

$$cf = 1.0 \quad \text{battery not gassing}$$

$$cf = 1.1 \quad \text{battery is gassing.}$$

$$\text{Ah}(t) = \text{Ah of battery at time } t$$

$$\text{Ah}(t-1) = \text{Ah of battery during previous hour}$$

$$I(t) = \text{mean charging current during hour } t$$

$$cf = \text{charge factor of battery}$$

This function is described by SUBROUTINE NEWAH in the power management model.

3.2.4 Battery Charge/Discharge Characteristics

During charge/discharge the external voltage is

$$V = V_0 + IR_i$$

where R_i is the internal resistance of the battery

V_0 is the no load voltage.

I is the charge/discharge current. Charging is positive, discharging is negative.

The internal resistance includes the free electrolyte, the separators, the porous active materials and the polarization of the chemical materials.

$$R_i = R_{i0} + R_p$$

where R_{i0} = a fixed resistance

R_p = polarization resistance [1].

Shepard [50] establishes that the polarization resistance is inversely proportional to the unused active material. A number of empirical models have been developed [50,56,66,] describing the polarization resistance effects. These models were tested using data recorded at Fota.

The final model is summarised as follows:

1. A linear relationship was established between the battery no load voltage and the battery state of charge.

Figure 3.3 shows this relationship

$$V_1 = (Ah(m) - 60) 0.158 + 250$$

$Ah(m)$ = mean Ah during sampled hour

$$= Ah(t_0) + (1/2)*Cf$$

$Ah(t)$ = Ah at the beginning of the sampled hour

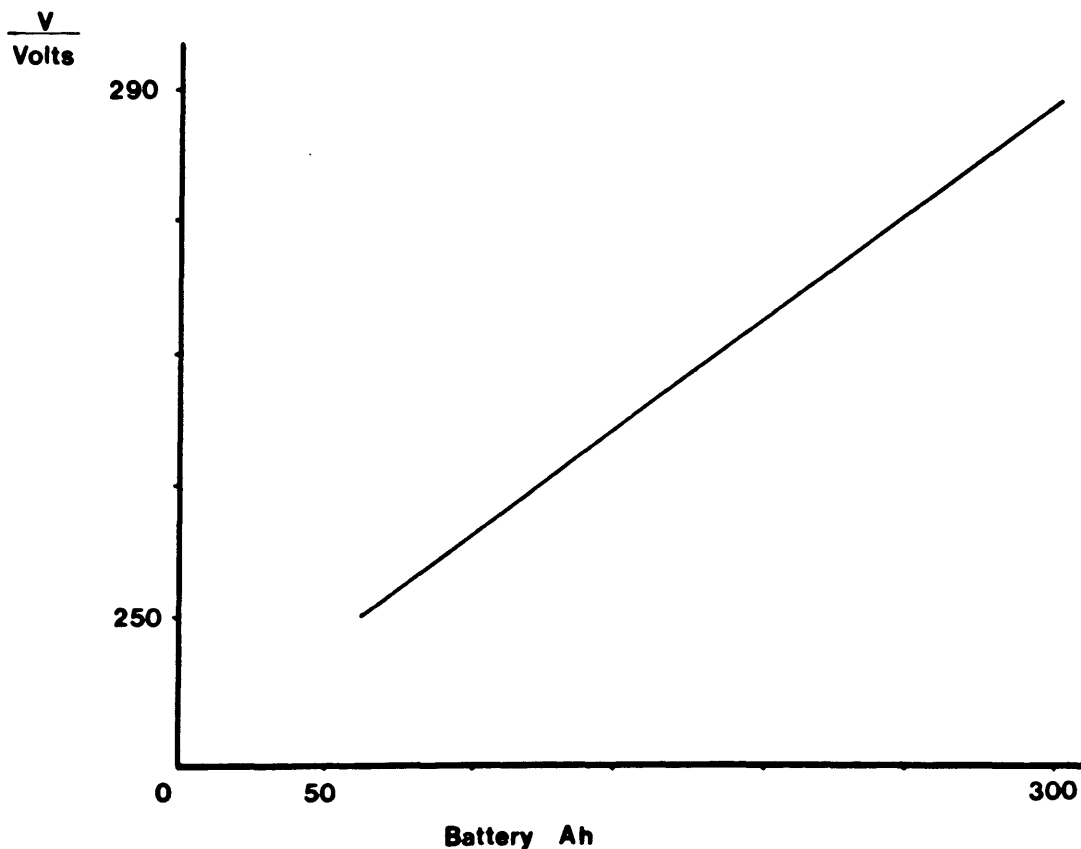


Figure 3.3 Relationship between the battery no-load voltage and the battery Ah.

* This model was developed using night time data i.e. when the charge/discharge current is zero. The battery voltage is a measured parameter and the Ah is calculated by the summation of the charge/discharge current.

$I/2$ = extra Ah at $t + \frac{1}{2}$

cf = charge factor

2. A constant internal resistance exists, and its contribution to the external voltage is:

$$V_2 = R_{i0} \times I$$

R_{i0} = constant resistance = 0.0536 (measured)

I = mean charge/discharge current

3. The voltage increase due to polarization is described as:

$$V_3 = N_c \times 0.05 \times \ln(\text{Abs}(I)+1)$$

N_c = number of cells in series = 134

I = mean charge/discharge current

The final voltage at the battery terminals is:

$$V = V_1 + V_2 + V_3$$

$$= (\text{Ah}(m) - 60)/0.158 + 250$$

$$+ (0.0536 \times I(t))$$

$$+ 134 \times 0.05 \times \ln (\text{Abs}(I) + 1)$$

3.2.5 Effect of Temperature on Battery Model

The capacity of a lead-acid battery is greatly dependent on the temperature of the electrolyte [54]. At high temperatures the capacity increases and at low temperatures the capacity decreases.

In the computer model, correction factors are introduced to allow for extremes in temperature. The correction factors are suggested by the battery manufacturers and also by some authors [56].

In this model the correction factor for the battery state of charge is:

$$Q = Q(20^{\circ}\text{C})(1-0.007(20-T))$$

where Q = battery Ah capacity/nominal capacity (C10)

T = ambient temperature.

3.2.6 Verification of the Battery Model

The final battery model is presented in figure 3.4. This plot describes the battery voltage as a function of the charge/discharge current and the battery Ah. The upper limit of 310V and the lower limit of 250V are the limits used by the microcomputer.

The battery voltage and current are the most important parameters in the control of the Fotavoltaic System. In the modelling of the power management, the battery model is used to:

- calculate the battery voltage for any charge/discharge current
- calculate the current required to produce gassing
- determine if battery overcharging occurs
- determine if the battery is capable of supplying the loads
- determine if the batteries are deep-discharged
- calculate the battery Ah at the beginning of the simulation.

These conditions are the basis of the power management algorithms described in the following Chapter.

The battery model is verified by plotting the simulated net battery energy versus the real net battery energy and by examining its statistical summary.

The scatter plot and the statistical summary are shown in figure 3.5. The slope of the regression line is 0.988 and the y-intercept is 0.05 indicating that the regression line is the 45° diagonal. The R^2 value is

FIGURE 3.4 FINAL BATTERY MODEL

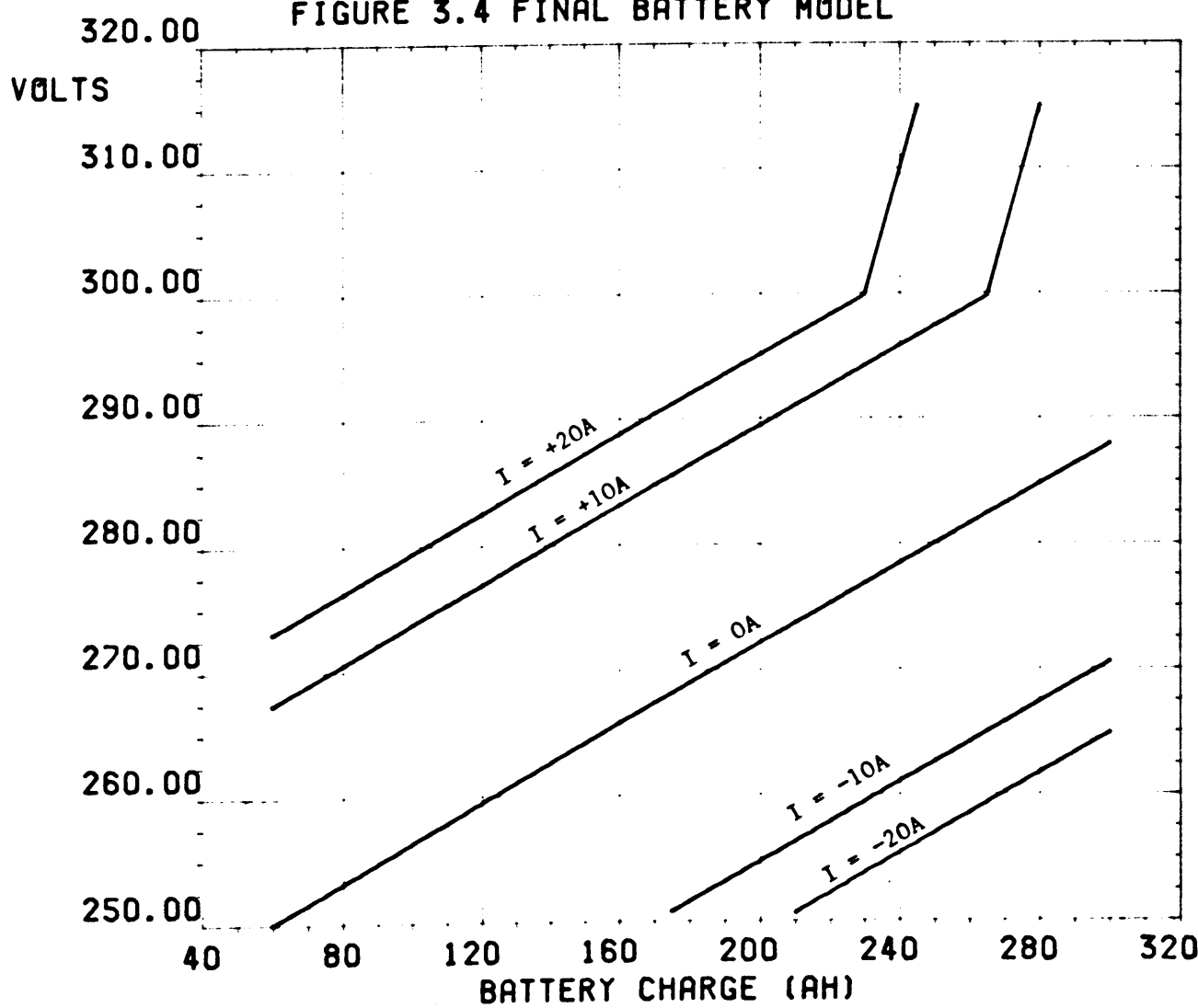
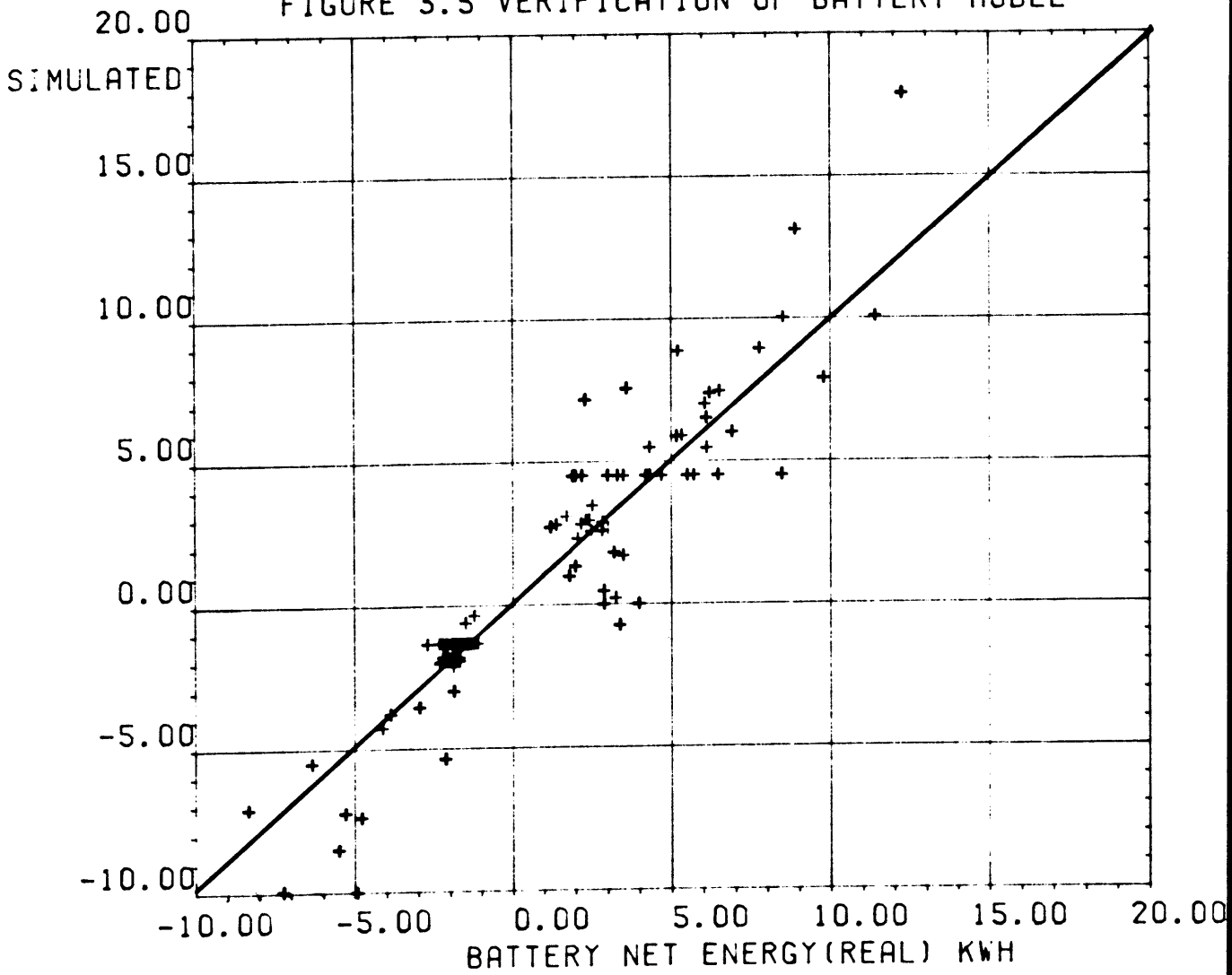


FIGURE 3.5 VERIFICATION OF BATTERY MODEL



Statistical Summary of Figure 3.5

R Squared	=	0.86
Slope of Regression Line	=	0.988
Intercept on Y Axis	=	0.05
Standard Error of Estimate	=	1.33
Number of Points Plotted	=	168

0.86 i.e. the simulation explains 86% of the real variation about the mean value. The main source of error in this model is due to the fact that the model calculates the battery net energy/hour whereas in the real situation battery charging and discharging may occur during the sampled hour. However, the final battery model is sufficiently accurate for use in the power management model.

3.3 Model of Self-Commutated Inverter

The three 10kVA self-commutated inverters, known as 'solarverters', use high powered transistors for commutation. Above 10% of full load the operating efficiency is constant at 95%.

The three solarverters supply three independent loads on the dairy farm. The loads, which are selected to operate in the high efficiency region, are:

Solarverter 1 - Milking machine 1 (2.2kw), washing pump (2.2kw) and air compressor (500w).

Solarverter 2 - Milking machine 2 (2.2kw), milk pump (500w), feeder motors (2.2kw).

Solarverter 3 - Milk cooler (3.5kw), milk agitator (500w).

The model of the solarverter was developed by measuring its real operating efficiency and its no-load demand. The inverter input energy/hour is plotted as a function of its output energy/hour in figure 3.5. The linear plot demonstrates the constant efficiency of the solarverter. The slope of the line is the reciprocal of the operating efficiency and the y-intercept is the no-load demand. These values are contained in the statistical summary presented in table 3.1.

FIGURE 3.6 SOLARVERTER INPUT AND OUTPUT ENERGY

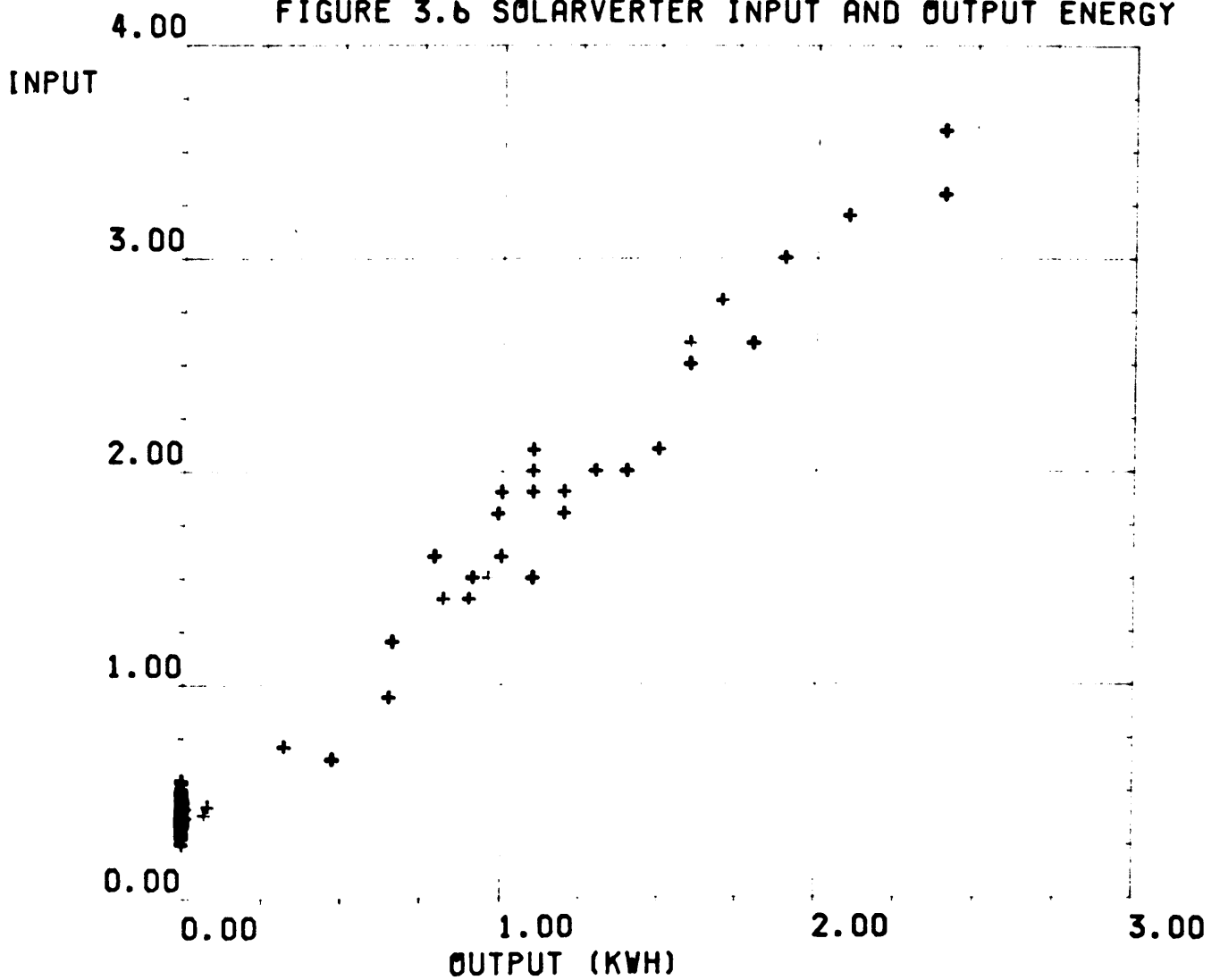


TABLE 3.1 Statistical Summary of Figure 3.6

R Squared	=	0.964
Slope of Regression Line	=	1.06
Intercept on Y Axis	=	0.32
Standard Error or Estimate	=	0.1
Number of Plotted Points	=	181

The R^2 of 0.964 shows that the regressions line explains 96.4% of the real variation. The slope of the line is 1.06 giving an efficiency of 94.3%. The y-intercept, representing the no-load demand is 0.32 kwh/h.

When the solarverters are disconnected from the system their DC energy demand is zero. They are disconnected when an overload is detected or when an emergency switch is operated on the dairy farm. These interruptions are inherent in the hardware and are not controlled by the microcomputer.

During the verification phase the interruptions are simulated using software flags. Their starting and ending times are supplied as input data to the model in SUBROUTINE LOG. This information is obtained from the system log book.

3.4 Model of Line-Commutated Inverter

The 50kVA line-commutated inverter, known as the 'Minisemi', is designed to deliver excess energy from the PV system to the utility grid. During periods of prolonged low insolation it is used in a converter mode to recharge the batteries from the utility grid. In the first year of operation the solarverters were unreliable and the minisemi was also used to supply energy to the loads.

This section describes the minisemi model in which the efficiency is expressed as a function of the output energy.

The minisemi uses thyristors for commutation and consequently its operating efficiency is lower than that of the solarverters. A non-linear relationship exists between the operating efficiency and the AC power. A quadratic equation [5] can be developed to describe this curve.

The hourly energy values used by the model are calculated by averaging sixty power samples. If the minisemi power varies during a sampled hour the resulting energy efficiency is not a quadratic function of the output energy. In fact, it is very random, e.g. if a value of 12kwh is recorded as the minisemi output energy it may be a) 12kwh for 1 hour or b) 36kwh for 20 minutes. The former operates at an efficiency of 66% and the latter at 85%.

A further example, shown in figure 3.7, is a scatter plot of the minisemi energy efficiency versus the minisemi output energy for September 1985. A very random plot is obtained.

From this analysis it is clear that the apparent minisemi energy efficiency is very dependent on its performance during the sampled hour. To overcome this problem a separate model is developed for each mode of operation of the minisemi. The modes are:

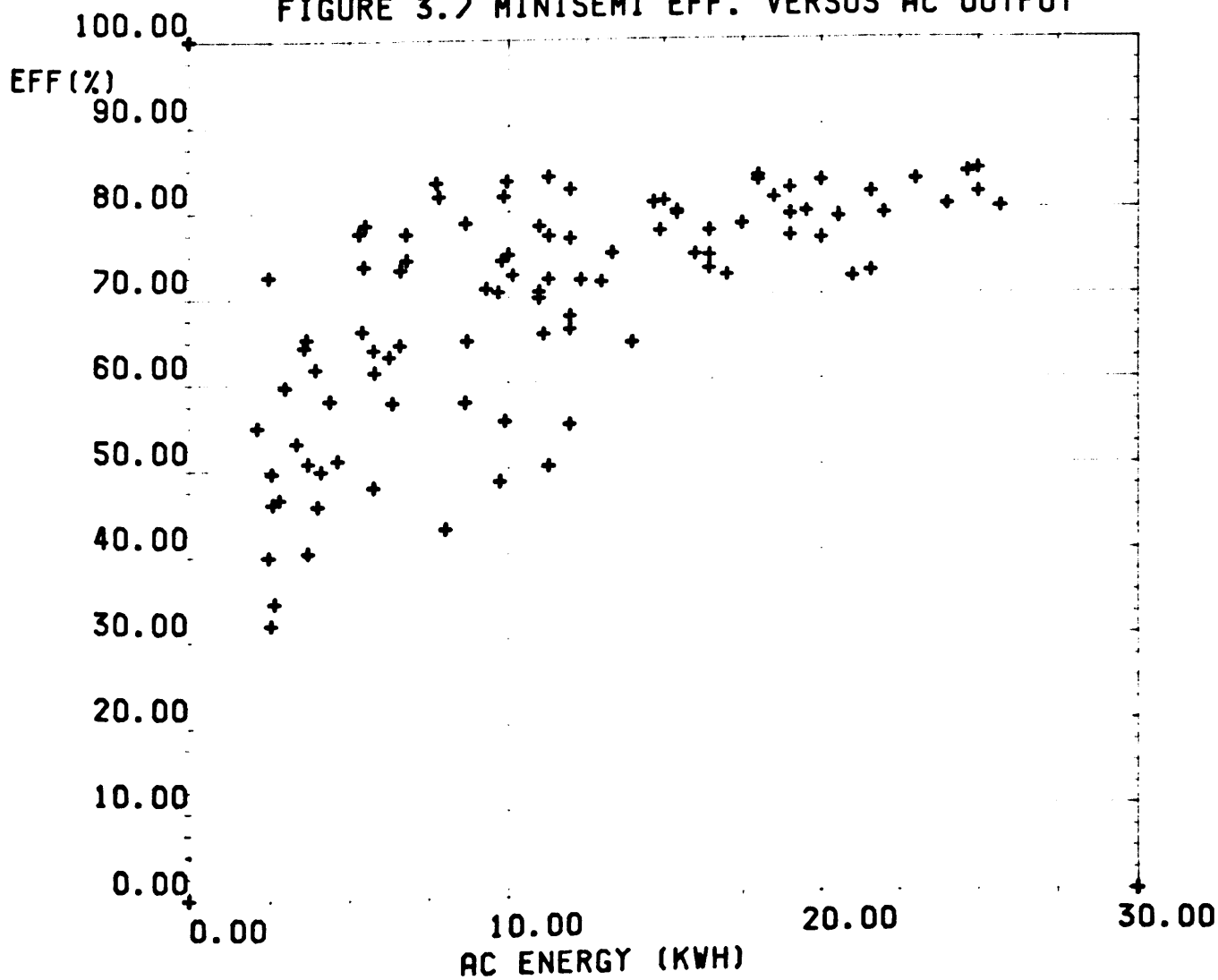
1. Minisemi supplying dairy farm loads
2. Both batteries gassing, minisemi delivers excess to the utility grid
3. High insolation with cloud, minisemi delivers energy to the utility grid
4. Emergency charging of batteries from the utility grid (converter mode).

These modes of operation are described in detail in Chapter 4 but they are introduced here to describe the minisemi model.

3.4.1 Minisemi supplying dairy farm loads

The minisemi delivers energy to the dairy farm through the utility grid. The energy path is shown in figure 3.8. This operation occurs when the solarverters are not available to supply the loads (Section 3.3).

FIGURE 3.7 MINISEMI EFF. VERSUS AC OUTPUT



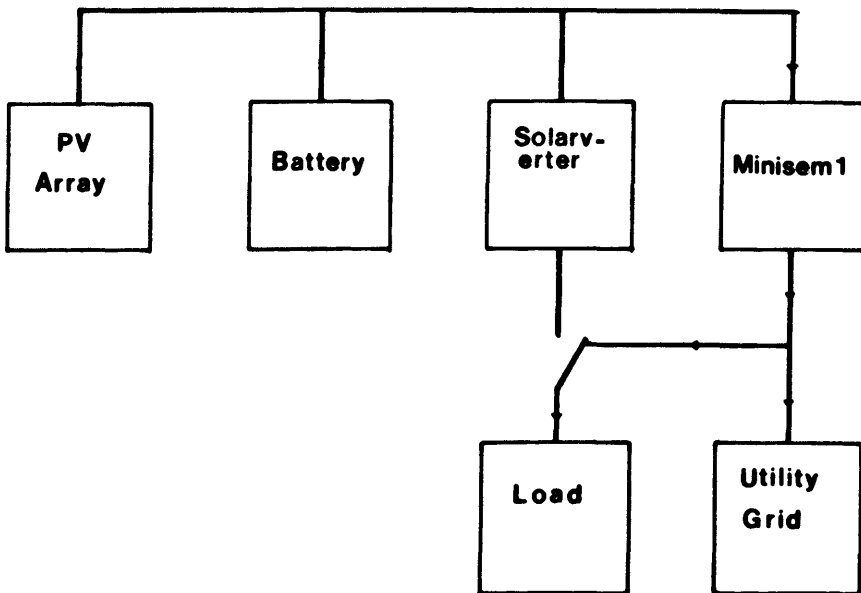


Figure 3.8 Energy Path used to supply loads with the Minisem

The dairy farm load demand varies between 2.5 kwh/h and 12.0 kwh/h and a linear model describes the minisemi efficiency in this region. A scatter plot of the minisemi efficiency versus the load demand is shown in figure 3.9 and a statistical summary is presented in table 3.2. The regression line is summarised as:

$$n = 31.57 + 3.36 E_{out} \quad (2.5 < E_{out} < 12.0)$$

where:

n = Energy efficiency

E_{out} = AC output energy

The regression line has an R^2 of 0.35. The variation about the regression line in figure 3.9 is due to the fact that in this operating region small changes in output power (1kw) will cause large changes in operating efficiency

3.4.2 Both Batteries Gassing, Minisemi Delivers Excess Energy to the Utility Grid.

When both batteries begin gassing the charging current is reduced by delivering energy to the utility grid. The amount of energy delivered is dependent on the excess charging current. This mode of operation normally occurs during periods of constant insolation i.e. when there is very little variation in the cloud cover. Consequently, the energy is delivered to the utility grid at a constant rate. A plot of the efficiency versus output energy, shown in figure 3.10 is very similar to the efficiency versus power curve supplied by the manufacturer.

Two models were developed: one analytically and one statistically.

Analytical methods [5] have been developed to describe the efficiency versus power curves of inverters. In this analysis three points are selected from the curve and the following equation is solved:

$$n(f) = n_1 \frac{(f-f_1)(f-f_2)}{(1-f_1)(1-f_2)} + n_{f1} \frac{(1-f)(f-f_2)}{(1-f_1)(f_1-f_2)} + n_{f2} \frac{(1-f)(f_1-f)}{(1-f_2)(f_1-f_2)}$$

FIGURE 3.9 MINISEMI SUPPLYING LOADS

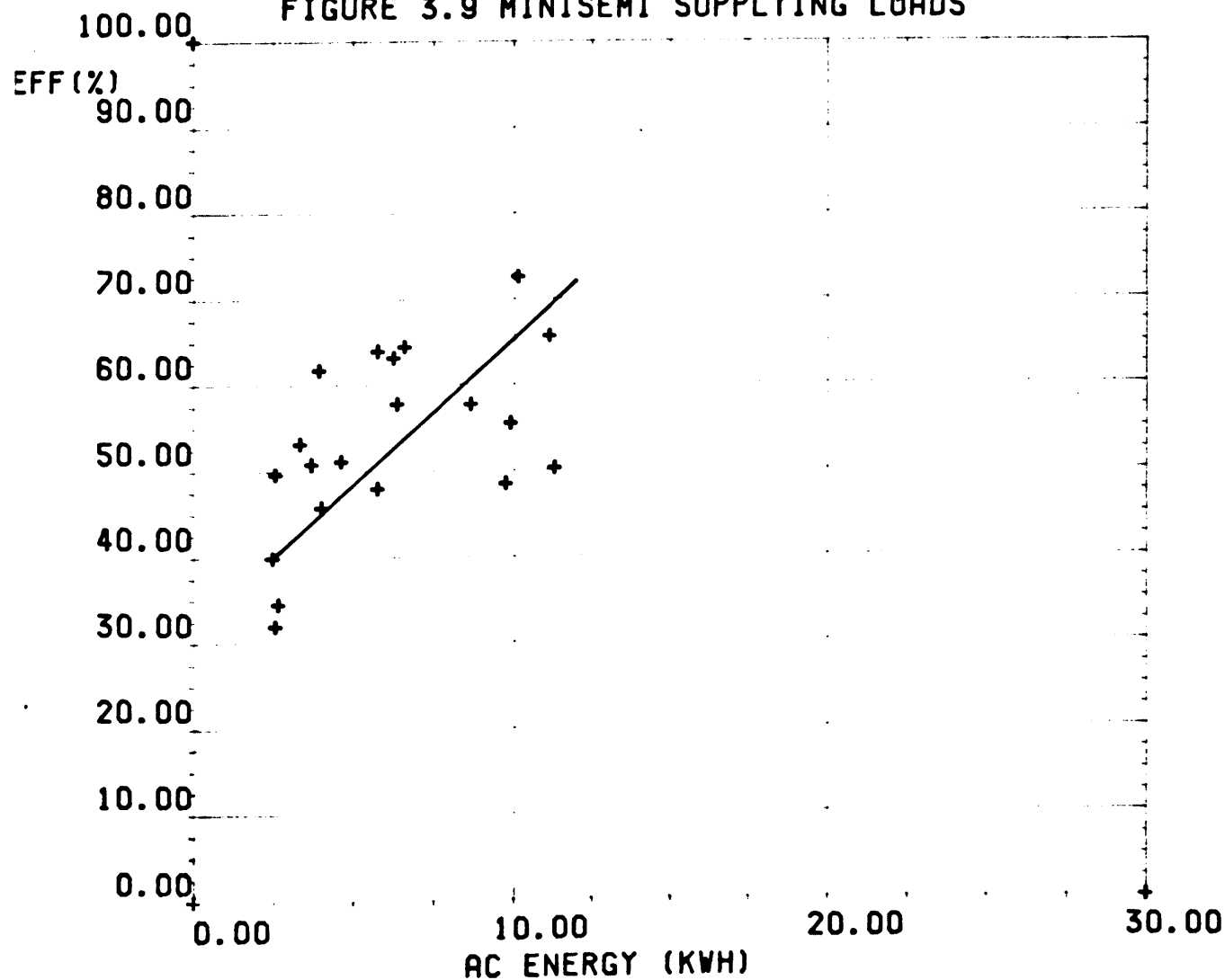


TABLE 3.2 Statistical Summary of Figure 3.9

R Squared	=	0.35
Slope of Regression Line	=	3.36
Intercept on Y Axis	=	31.57
Standard Error or Estimate	=	10.7
Number of Plotted Points	=	26

where:

n_1 = the efficiency at full load ($f=1$)

n_{f1} = the efficiency at the fractional load f_1

n_{f2} = the efficiency at the fractional load f_2

Three points were selected from the curve shown in figure 3.6 and the following equation was solved:

$$n = 38.5 + 2.17 E_{out} - 0.035 E_{out}^2$$

This equation was verified using the methods outlined in section 1.5.6 and it has an R^2 of 0.51.

The statistical model was developed by assuming that a quadratic relationship exists between the efficiency and the output energy i.e.

$$n = AE_{out}^2 + BE_{out} + C$$

where:

n = the efficiency of the minisemi

E_{out} = the AC output energy

A,B,C = constants

A regression analysis of the calculated efficiency (n) versus E_{out}^2 and E_{out} provided an equation:

$$n = 50.6 + 2.56 E_{out} - 0.055 E_{out}^2$$

This equation has an R^2 of 0.65.

A higher R^2 is difficult to attain due to some power variations during the sampled hour.

The statistical model is more accurate than the analytical model but it requires a larger amount of data. The analytical model is easier to develop and it is very suitable for modelling inverters which do not have operating data.

FIGURE 3.10 MODE 3 OPERATION OF MINISEMI

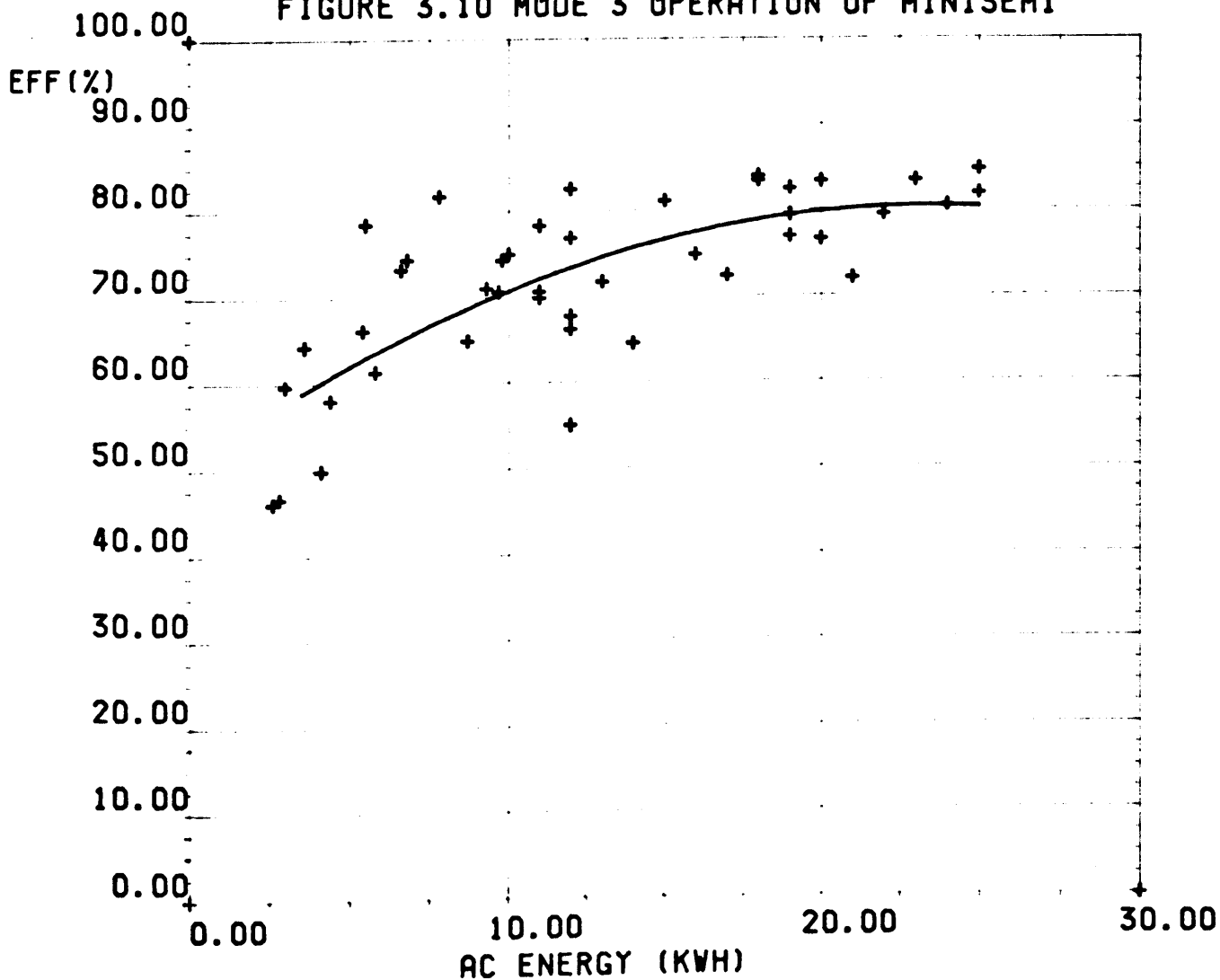


TABLE 3.3 Statistical Summary of Figure 3.10 (Step Wise Regression)

$$N = A + BE_{out} + CE_{out}^2$$

Step 1 E_{out}

R squared = 0.5

Step 2 E_{out}, E_{out}^2

R squared = 0.65

Constant A = 50.6

Constant B = 2.56

Constant C = -0.055

Standard Error = 6.9

Number of Plotted Points = 44

If the DC input energy is known then the AC output energy is calculated using the above equation

$$n = \frac{E_{out}}{E_{in}}$$

$$= 50.6 + 2.56 E_{out} - 0.055 E_{out}^2$$

which gives:

$$0 = 50.6 + (2.56 - \frac{1}{E_{in}}) E_{out} - 0.055 E_{out}^2$$

E_{out} is calculated by solving this quadratic equation.

3.4.3 Minisemi Operation During High Insolation with Varying Cloud Cover

During periods of high insolation with varying cloud cover, the battery is discharged to approximately 80% at full charge. At this charge, the battery will accept large current changes caused by variations in the array output.

In this mode, energy is delivered to the utility grid at full minisemi rating. Consequently, the operating efficiency is very high. A scatter plot of the efficiency versus AC output energy is shown in figure 3.11. A linear regression model describes this plot, i.e.,

$$n = 76.48 + 0.12 \times E_{out}$$

This regression line has an R^2 of 0.68. The variation about the line is mainly due to measuring point errors.

3.4.4 Minisemi Model During Emergency Charging

Emergency charging of the battery occurs during winter time or during prolonged periods of low insolation. During this mode of operation the minisemi delivers a constant 30A DC at an efficiency of 71%. In this mode the DC energy is the output and the AC energy is the input.

FIGURE 3.11 MODE 4 OPERATION OF MINISEMI

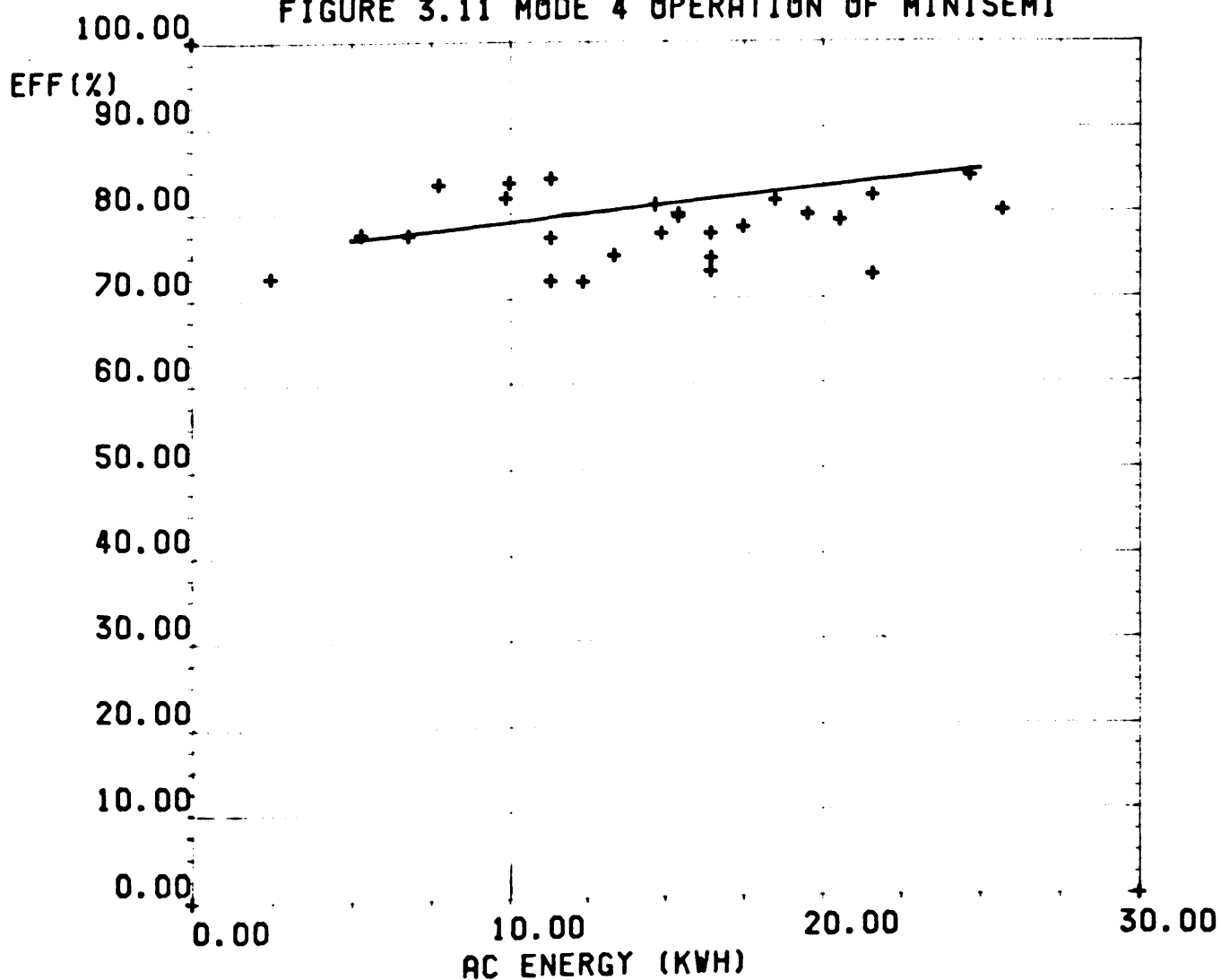
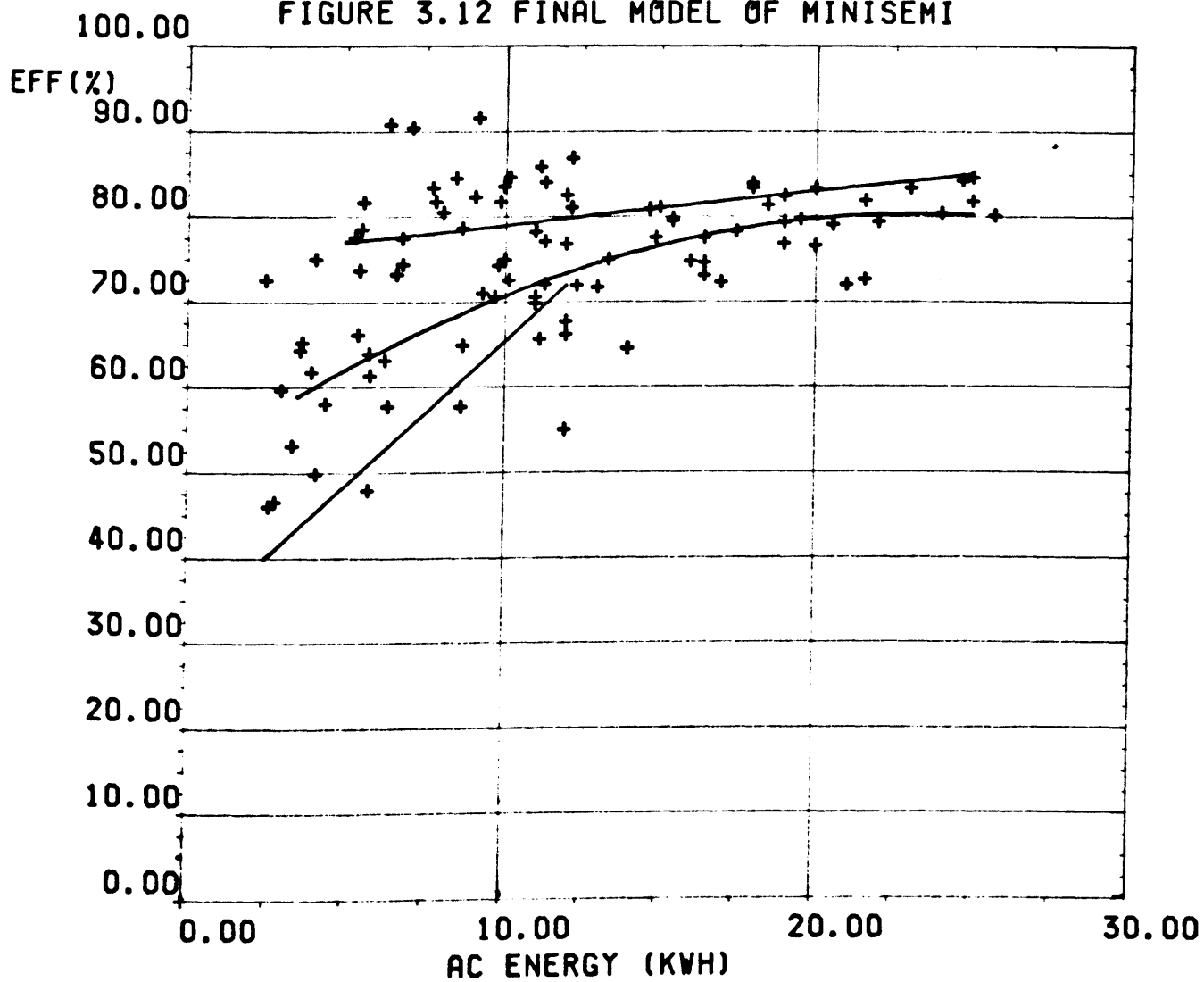


TABLE 3.4 Statistical Summary of Figure 3.11

R Squared	=	0.68
Slope of Regression Line	=	0.12
Intercept on Y Axis	=	76.48
Standard Error or Estimate	=	3.85
Number of Plotted Points	=	26

FIGURE 3.12 FINAL MODEL OF MINISEMI



Summary of the Minisemi Model

The scatter plot of the minisemi efficiency versus the AC output energy, shown in figure 3.17, is explained by combining the three models as in figure 3.12. From this analysis it is clear that the exact mode of operation must be determined during each sampled hour. The conditions which initiate and terminate each mode are described in Chapter 4.

3.5 Conclusion

Batteries and inverters were in use long before photovoltaics were accepted as a terrestrial source of energy. Despite this, information on the modelling of these units is not plentiful. The models which have been developed by the manufacturers deal specifically with the internal design and are not suitable for system modelling. Some battery and inverter models have been developed theoretically and verified using data from small ($< 5\text{kWp}$) PV systems. The modelling techniques described in this chapter are very accurate and are suitable for modelling the batteries and inverters of other PV systems.

CHAPTER 4

Power Management Model

4.1 Introduction

The power management model links the individual hardware models to simulate the overall performance of the system. In addition, it simulates non-optimized switching strategies and this characteristic is not available in existing PV computer models [1-5]. This chapter describes the power management of the Fotavoltaic Project and the techniques used to develop its model.

4.2 Power Management of the Fotavoltaic Project

The power management of the Fotavoltaic Project is implemented using a complex switching strategy. The configuration of the thirty switches, which interconnect the different sub-units, is determined by the PV array output, the battery state-of-charge and the load demand. The microcomputer monitors the system every two seconds and, if necessary, it updates the configuration of the switches.

The switching strategy and the microcomputer control create a very flexible power management system. The advantages of this are:

- some problems [19] may be corrected using clever software rather than including oversized hardware.
- The performance of various hardware configurations may be investigated.

As a result of this flexible power management and the study of the system operation during its first year (1984) seven power management modes were developed for the present automatic system control.

Each of these modes, taken as a separate entity, can be compared to the overall power management of most other projects in the CEC pilot program. Therefore, the techniques used to model the different power management modes of the Fotavoltaic Project may be applied directly to the modelling of other projects. The only difference would be in the sizing of the components.

4.2.1 Layout of the Fotavoltaic Project

The layout of the Fotavoltaic Project is shown in figures 4.1 and 4.2. The PV array is divided into thirteen subarrays. Each subarray is connected to either battery 1 or battery 2 when switch K27 is closed. If K27 is open, the subarrays are connected to battery 2 or they are open-circuited. During array shutdown the subarrays are connected to battery 1 busbar and K27 is opened.

The three 10kVA self-commutated inverters (solarverters) are connected to battery 1 or battery 2 or they can be disconnected to reduce the no-load losses. The three load groups are connected to either the solarverters or to the utility grid. It is also possible to have one load group connected to a solarverter and the other load groups connected to the utility grid.

The 50kVA line-commutated inverter (minisemi) is connected to battery 1 or battery 2. It may also be disconnected from both batteries to minimise the no-load losses. On the AC side the minisemi is connected to the utility grid using a manually operated switch. An internal switch is used to select inverter/converter operation. The power flow through the minisemi is regulated using a 0-10V signal from the microcomputer.

The thirty switches described in this section are all controlled by the microcomputer. 25K of control software, which is stored on EPROMS, is used to implement the complex switching strategy described in the following sections.

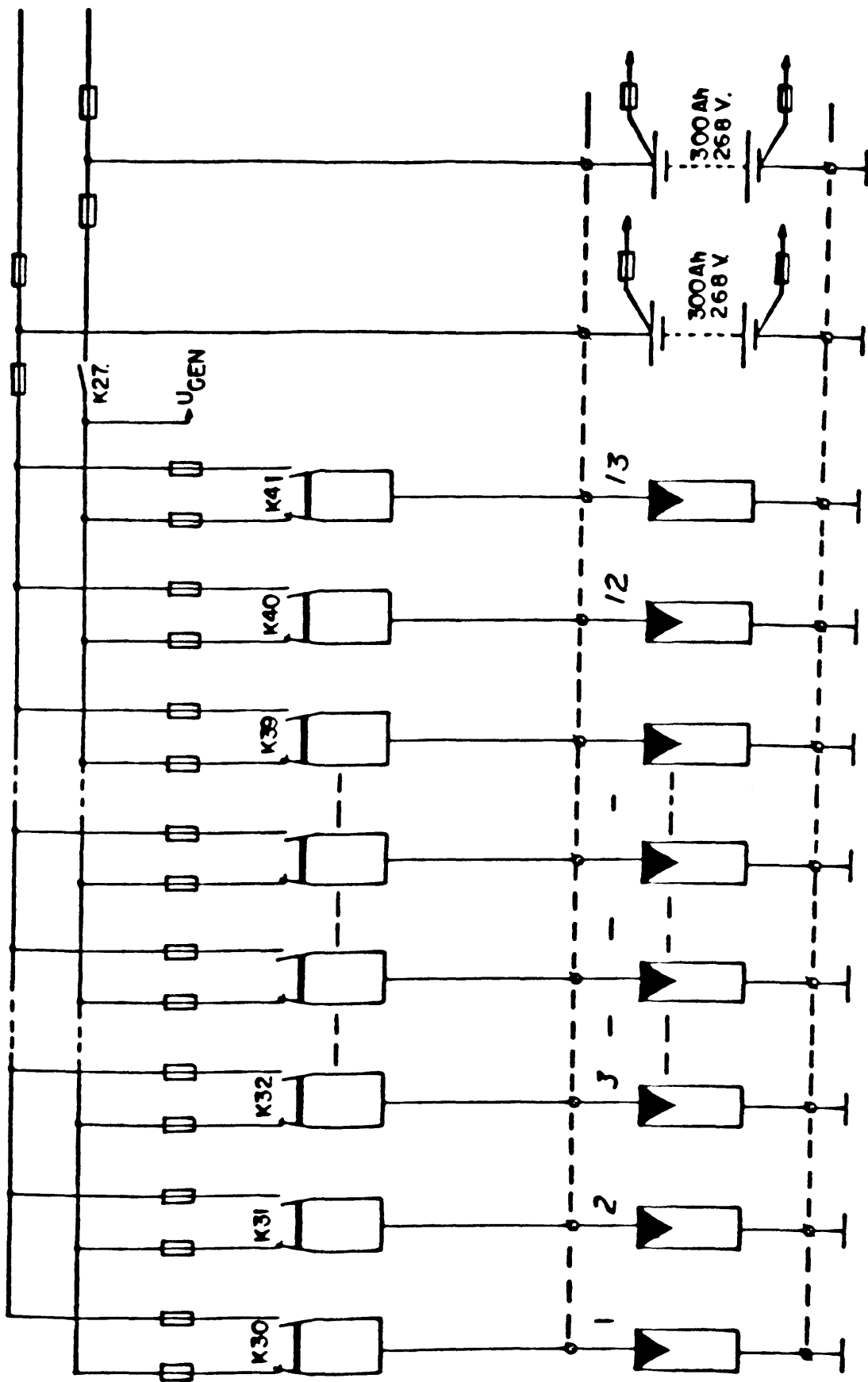


Figure 4.1 DC Power Distribution

SOLARVERTER 1.

SOLARVERTER 2.

SOLARVERTER 3.

MINISEM 1

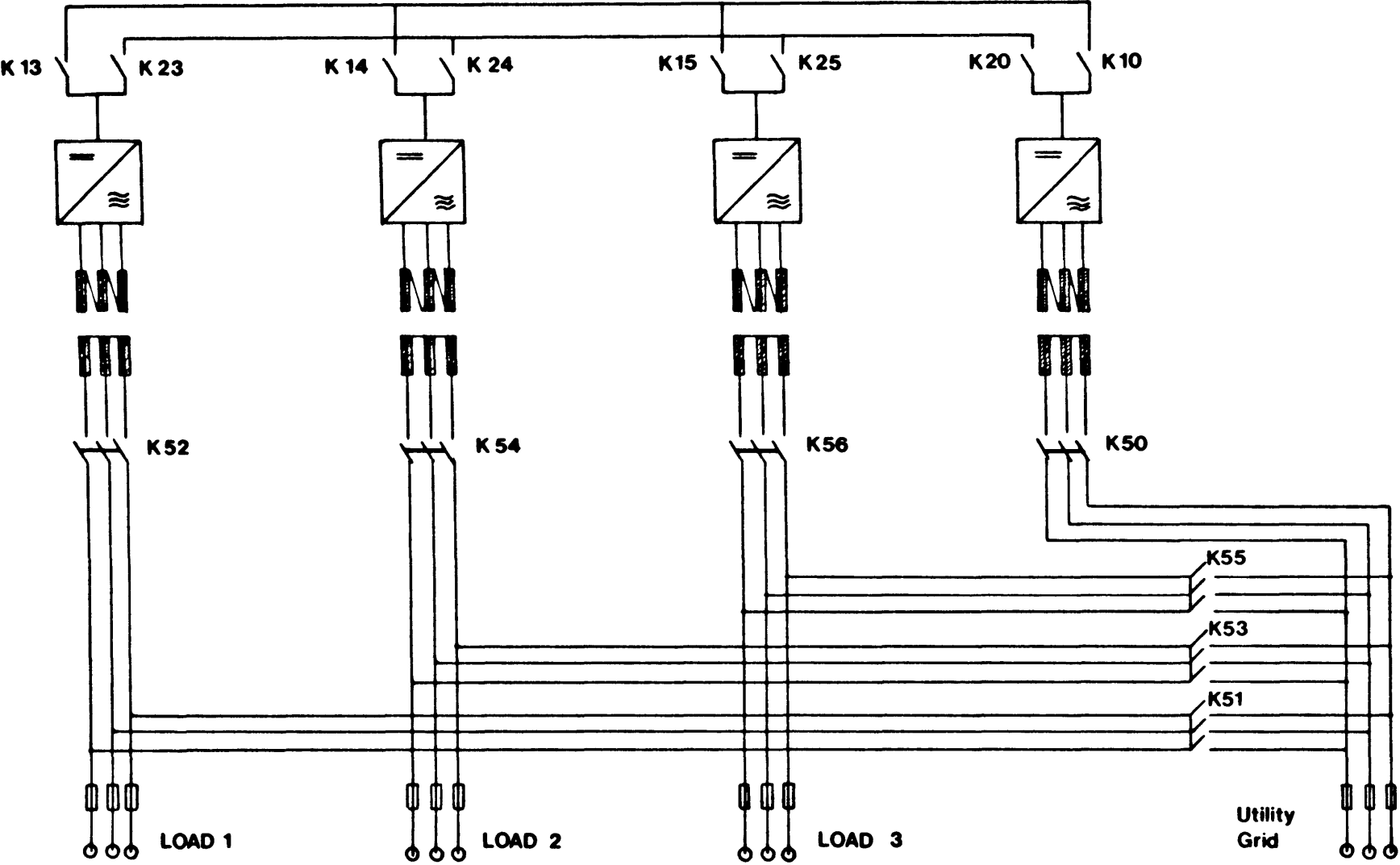


FIGURE 4.2

A.C. POWER DISTRIBUTION

Double Battery Operation

Double battery operation was selected to provide each battery with more charge/discharge cycles. Also each individual battery reaches full charge more often than if one large battery was used.

The microcomputer selects one battery as the working battery and the other as a stand-by battery. The working battery supplies the loads and the stand-by battery is unloaded and is brought to full charge. Battery charging, described in Chapter 3, is implemented by connecting and disconnecting subarrays to maintain the battery's voltage and current within predefined limits. During charging, priority is given to the working battery.

4.2.2 Power Management Modes

This section describes the seven power management modes which are used to control the Fotovoltaic Project. The different modes are:

1. Battery charging and load management when both batteries are connected (K27 closed).
2. Battery charging and load management when only battery 2 is connected (K27 open).
3. Delivery of excess energy to the utility grid when both batteries are gassing.
4. Delivery of excess energy to the utility grid during periods of high insolation and varying cloud cover.
5. Operation of the system if the line-commutated inverter is disconnected.
6. Nighttime/low insolation operation.
7. Emergency charging of the batteries from the utility grid.

The algorithm which selects the mode of operation for any sampled hour is shown in figure 4.3. The following section describes the main features of each mode of operation and Appendix C contains the detailed control algorithm which simulate each mode.

Mode 1 - Battery charging and load demand when both batteries are connected (K27 closed).

This mode of operation normally occurs during the first three hours after array start-up and during the last three hours before array shut-down. It also occurs at midday during low insolation periods. The priority is to supply the load and to provide both batteries with a proper charge characteristic. This mode of operation ends when battery overcharging exists.

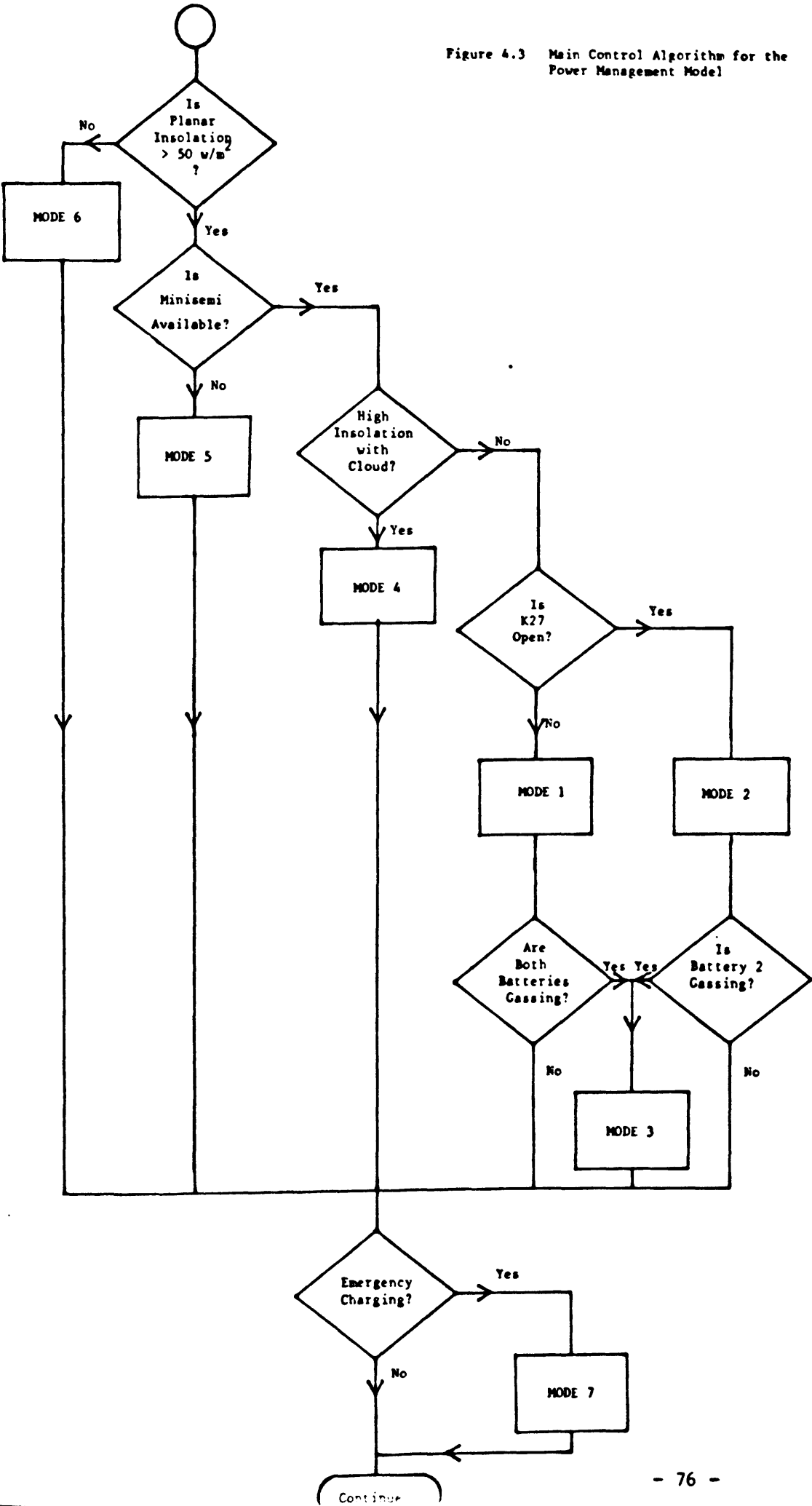
Mode 1 is equivalent to the complete power management of the Pellworm Project.

Mode 2 - Battery charging and load demand when only battery 2 is connected (K27 open).

Mode 2 begins when battery overcharging exists, i.e. when the battery voltage exceeds 320V (2.4V/cell). When a battery is in a highly charged state its voltage increases rapidly (3.1.6) with small increases in current. During periods of high insolation ($> 0.6\text{kwh/m}^2$) the subarray switchings of mode 1 are not fast enough to protect the battery from overcharging. Mode 2 operation was introduced to prevent overcharging and to reduce the energy losses caused by array shutdowns. Overcharging is prevented in this mode by open-circuiting individual subarrays.

Mode 2 operation is equivalent to the power management of the Vulcano Project. This project consists of a 50kwp PV array, a single 1500Ah battery, a 50kVA self-commutated inverter and a 140kVA line-commutated inverter. The system supplies energy to a remote hamlet on Vulcano Island (Sicily).

Figure 4.3 Main Control Algorithm for the Power Management Model



Mode 3 - Delivery of excess energy to the utility grid when both batteries are gassing

If the working battery begins gassing its charging current is reduced by disconnecting subarrays and by connecting them to the stand-by battery. Should the stand-by battery begin gassing the charging current is reduced by delivering the excess energy to the utility grid. The amount of energy delivered to the grid is determined by the excess charging current of the stand-by battery. In Chapter 5 this operation is improved by increasing the operating efficiency of the minisemi.

Mode 4 - Delivery of excess energy to the utility grid during periods of high insolation with varying cloud cover.

The minisemi is capable of accepting a maximum of 34kW of DC power. During midday the PV array is capable of generating up to 45kW and also at midday the dairy farm load demand is typically zero. The battery must therefore accept the 11kW balance. If the battery is in a highly charged state it cannot accept 11kW and subarrays are disconnected to avoid overcharging. When high insolation with varying cloud cover exists, extra subarrays are disconnected to reduce the variation in the battery charging current. In May 1984 this power management mode was analysed and the following improvements were implemented. Periods of high insolation with varying cloud cover are predicted, by the microcomputer, by comparing the mean planar insolation with the maximum planar irradiance.

The recorded data for March, April and May 1984 were analysed and it was found that if the mean planar insolation was greater than 0.45 kWh/m^2 and the maximum planar irradiance was greater than 0.7 kW/m^2 there was a high probability of subarray disconnections in the following hours. When the new software control recognises this condition (0.45 kWh/m^2 , 0.7 kW/m^2) the battery is discharged by delivering energy to the utility grid. Therefore, at midday the battery is not fully charged and is

capable of accepting the 11kW balance. Figure 4.4 and figure 4.5 show scatter plots of the PV array output energy versus the planar insolation for May 1984 (prior to improvement) and July 1984 (after improvement). The low energy values at high insulations during May 1984 were due to subarray disconnections. In July 1984 no subarrays were disconnected.

This mode of operation is not used by other PV projects but it could be used to overcome some existing problems especially at Hoboken and Giglio. The techniques used to model Mode 4 operation could readily be used to optimize the performance of these two projects.

Mode 5 - Operation of the system if the line-commutated inverter is disconnected

The microcomputer disconnects the minisemi from the batteries when it detects an interruption. During the first year of operation the main interruptions were caused by fuse failures. These problems were later solved by improving the software and by including extra hardware protection at the DC input.

During the first year a considerable amount of control software (2K) was written to operate the system in the absence of the minisemi. The data which was recorded during these interruptions was used to develop the model for Mode 5. This mode prevents overcharging by open-circuiting subarrays. The number of subarrays connected to each battery is determined by their charging characteristics.

This power management mode is very popular in PV systems which operate as stand alone systems. Typical examples are Aghia Roumeli, Kaw and Rondulinu.

Figure 4.4 PV Array Output Versus Planar Insolation
for May 1984

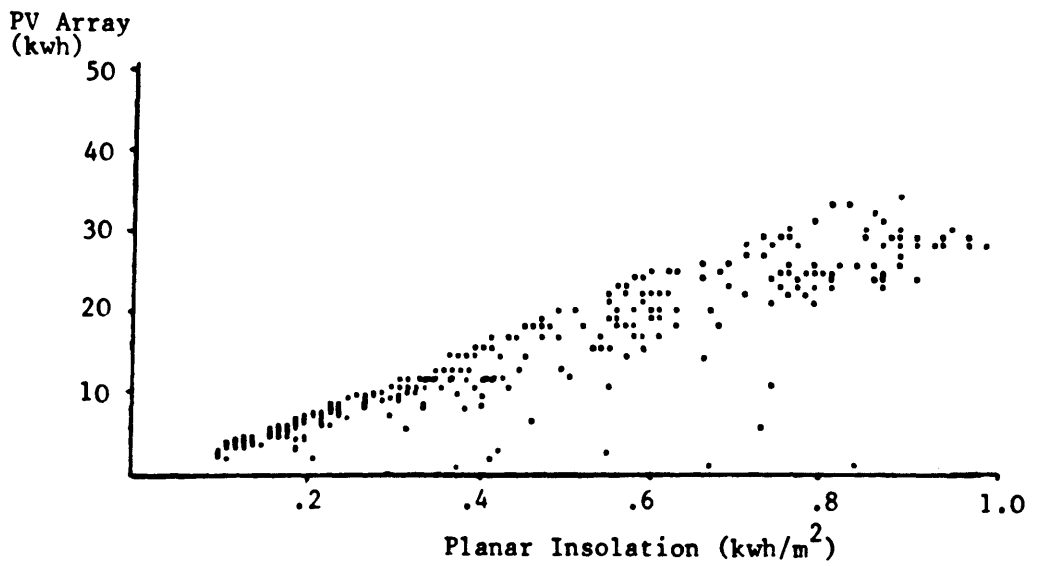
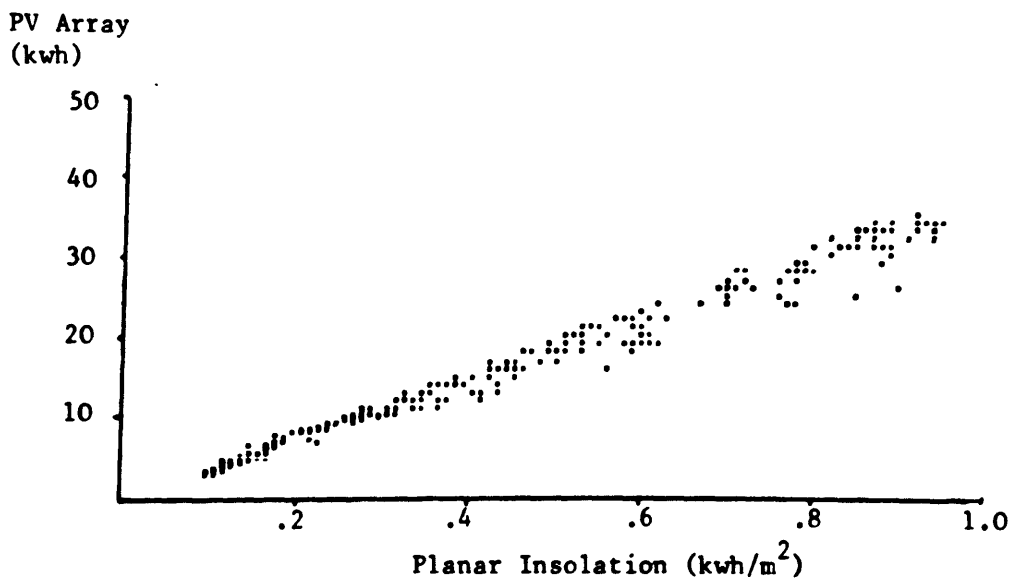


Figure 4.5 PV Array Output Versus Planar Insolation
for July 1984



Mode 6 - Night-time and low insolation operation

During these periods the PV array is not available and the load demand is distributed between both batteries. The model simulates the load management and the battery protection. This mode begins at array shut-down and ends at array start-up.

Mode 7 - Emergency charging from the utility grid

If both batteries are less than 240V (1.8 V/cell) emergency charging begins. During emergency charging the loads are connected to the utility grid, the solarverters are disconnected from the batteries and the minisemi is operated in the converter mode. Battery 1 is recharged from the utility grid and battery 2 is recharged using the complete PV array. When both batteries reach gassing voltage, emergency charging ends and mode 1 operation begins.

This operation occurs only during periods of prolonged low insolation.

Load Management

These seven modes of operation describe the switching strategies of the PV array, battery and minisemi. Associated with each mode is a load management strategy which switches the loads between the solarverters and the utility grid and switches the solarverters between battery 1 and battery 2.

When the PV array is operating the three solarverters are connected to the working battery and the stand-by battery is unloaded. At night the solarverters are distributed between both batteries. This reduces the discharge current of each battery and allows more energy to be extracted.

If a battery voltage is less than 250V a software flag is set indicating that the battery is not available for load supply. When this occurs all three solarverters are connected to the second battery. Should this voltage be less than 250V both batteries are not available and the load groups are disconnected from the solarverters and reconnected to the utility grid. The batteries will again be available for load supply when they begin gassing. When this occurs the loads are not reconnected to the solarverters until the next midday, thus avoiding interruptions to the milking process.

The load can also be supplied using the minisemi. This operation is described in section 3.4.1.

4.3 Model Development for the Power Management

The techniques used to model the power management are similar to those which are used to model the hardware components. First a model concept is established; this concept is transcribed into software and finally the simulation is verified by comparing the results to the real data. This section describes these three phases of the development.

4.3.1 Model Concepts for the Power Management

The seven power management modes, described in the previous section, were modelled using the following concepts:

- Each mode was defined and described in detail
- The effect on each mode of varying array outputs, battery states of charge and load demands were examined.
- The conditions which initiate and terminate each mode were defined.

The initial model concepts were developed by manually examining three months recorded data. The data for each hour was examined, the mode of operation was defined and hypotheses were established to explain the variations of each mode. When these initial concepts were defined special software packages were developed to analyse, by computer, all subsequent data.

The development of the model concepts was time consuming both in man hours and in computer hours, yet it resulted in a better understanding of the system and this led to system improvements.

4.3.2 Model Implementation for the Power Management

In this phase the model concepts were converted to control algorithms and the software logic was written. Figure 4.3 shows the main control algorithm of the power management. The algorithms which simulate the seven power management modes are presented in Appendix C. The hardware models, described in the previous chapters, are used to implement the processes and decisions which are described in these algorithms.

The software logic uses flags to store information on the status of the system. Some flags are also used to transfer information from one sampled hour to the next. Sixty flags are used and Appendix D contains a listing of the significance of each flag. This list is a summary of the logical operations implemented during each hourly simulation.

Appendix D also contains a listing of fifty three variables which are used by the software. This list is a summary of the parameters calculated during each hourly simulation.

4.3.3 Verification of the Power Management Model

The hardware models were verified by assessing their accuracy in simulating the input and output energies of the units. The power management model is verified by assessing its accuracy in simulating the DC and AC energy distributions.

The procedures used during this verification are summarised as follows:

First, the simulation for the complete sampled period is analysed. Figure 4.6 shows both the actual and the simulated energy for the sampled period October 1985. Table 4.1 is the energy summary of this graph. In this example the DC and AC energy distributions are modelled showing a difference of less than 8%.

The daily simulations are next analysed. These results are presented as daily energy summaries and an example is shown in table 4.2. The aim of this daily analysis is to assess the accuracy of the model during different climatic conditions.

Finally, the hourly simulations are analysed. This is the most important verification procedure since the model operates on an hourly basis. The battery net energy, inverter input energy and the inverter energy to the loads are used as parameters to assess the accuracy of modelling the DC and AC energy distributions. These parameters are analysed using the scatter plots and the regression analysis techniques outlined in section 1.5.6.

Figure 4.7 is an example of a scatter plot for the inverter input energy. The statistical parameter R^2 is 0.96 i.e. the simulation explains 96% of the real variation.

FIGURE 4.6 REAL AND SIMULATED ENERGY.

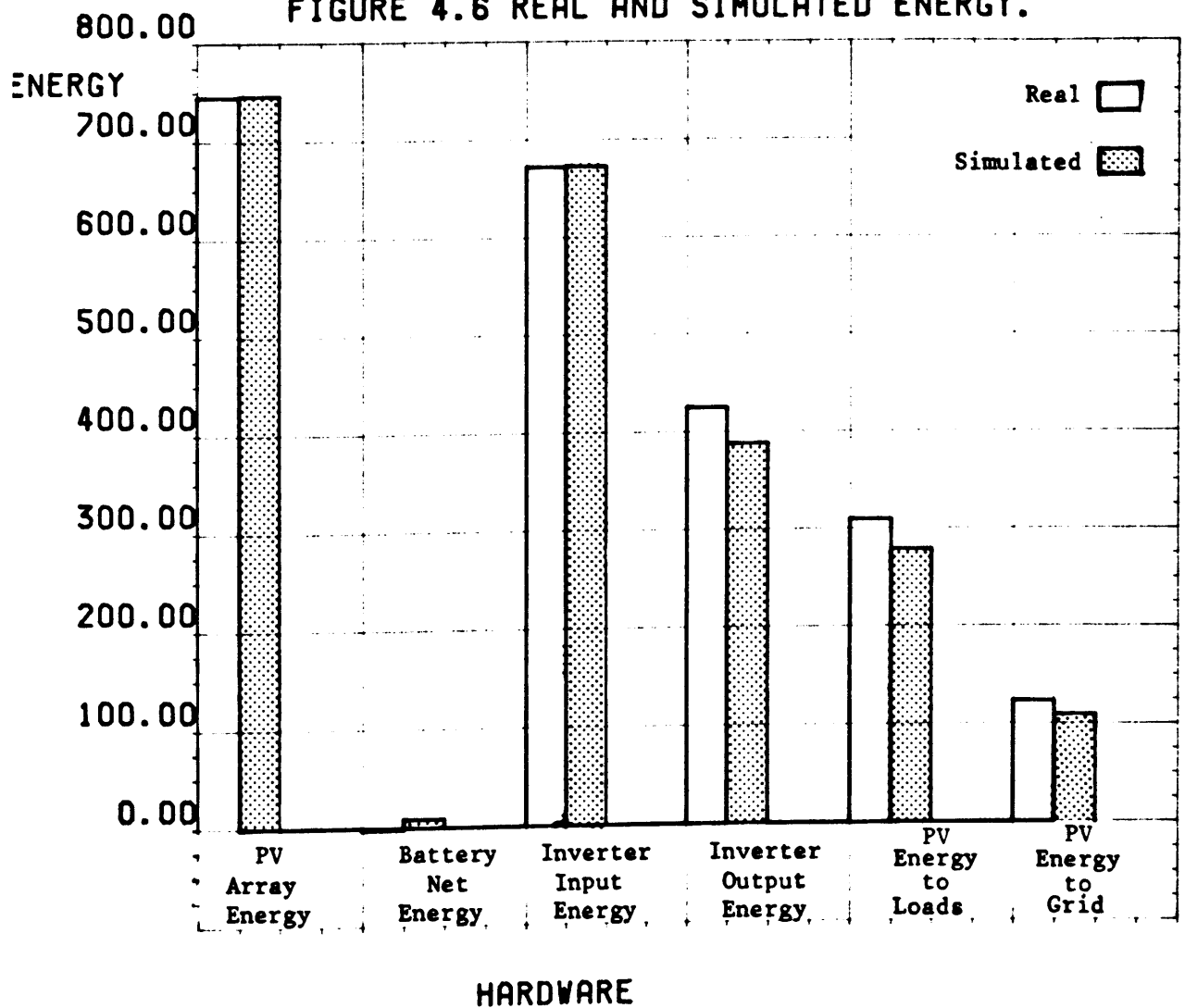


TABLE 4.1 ENERGY SUMMARY OF COMPLETE SAMPLED PERIOD.
OCTOBER 1985

	measured kWh	simulated kWh	error %
array output energy:	744.91	746.61	0.2
battery net. energy:	-1.75	9.03	3.5
inverter input energy:	672.54	673.18	0.1
inverter output energy:	424.92	388.37	-8.0
energy to utility grid:	309.77	278.85	-1.7
PV energy to load:	123.82	109.52	-4.5
ESB energy to load	207.68	221.97	6.0
% of inverter operation	0.63	0.58	-7.9

ESB: ELECTRICITY SUPPLY BOARD

TABLE 4.2 DAILY ENERGY SUMMARIES OF SIMULATION.

OCTOBER 7 1985			
	measured kWh	simulated kWh	error kWh
array output energy:	121.54	123.62	2.08
battery net. energy:	9.88	4.25	-5.63
inverter input energy:	103.39	110.97	7.58
inverter output energy:	67.37	68.82	1.45
energy to utility grid:	55.92	56.26	0.34
PV energy to load	15.00	12.56	-2.44
ESB energy to load	21.55	23.99	2.44
% of inverter operation	0.65	0.62	-0.03
OCTOBER 8 1985			
	measured kWh	simulated kWh	error kWh
array output energy:	43.12	42.95	-0.17
battery net. energy:	-9.11	-4.70	4.41
inverter input energy:	33.60	39.25	5.65
inverter output energy:	10.22	9.93	-0.29
energy to utility grid:	1.86	2.26	0.40
PV energy to load	8.12	7.68	-0.45
ESB energy to load	30.16	30.61	0.45
% of inverter operation	0.30	0.25	-0.05
OCTOBER 9 1985			
	measured kWh	simulated kWh	error kWh
array output energy:	67.37	66.95	-0.42
battery net. energy:	-0.21	-6.45	-6.24
inverter input energy:	58.70	65.00	6.30
inverter output energy:	26.70	31.30	4.60
energy to utility grid:	19.20	15.21	-4.00
PV energy to load	13.23	16.09	2.86
ESB energy to load	29.55	26.69	-2.86
% of inverter operation	0.45	0.48	0.03
OCTOBER 10 1985			
	measured kWh	simulated kWh	error kWh
array output energy:	14.31	15.58	1.27
battery net. energy:	-10.63	-7.29	3.34
inverter input energy:	15.31	17.61	2.30
inverter output energy:	1.40	1.66	0.26
energy to utility grid:	1.66	1.66	0.00
PV energy to load	1.57	0.00	-1.57
ESB energy to load	31.92	33.50	1.57
% of inverter operation	0.09	0.09	0.00

Improvements to Power Management Model

The aims of the verification phase are to assess the accuracy of the simulation and to recommend changes in the model concepts. The hourly simulations are verified and the model concepts are improved using the following procedures.

Scatter plots are obtained and they are examined for outliers. The outliers represent errors in the model. An example of an outlier is shown in figure 4.7. The hourly simulations which produce the outliers are determined by examining the data of the scatter plots. A detailed analysis of an hourly simulation is performed by examining:

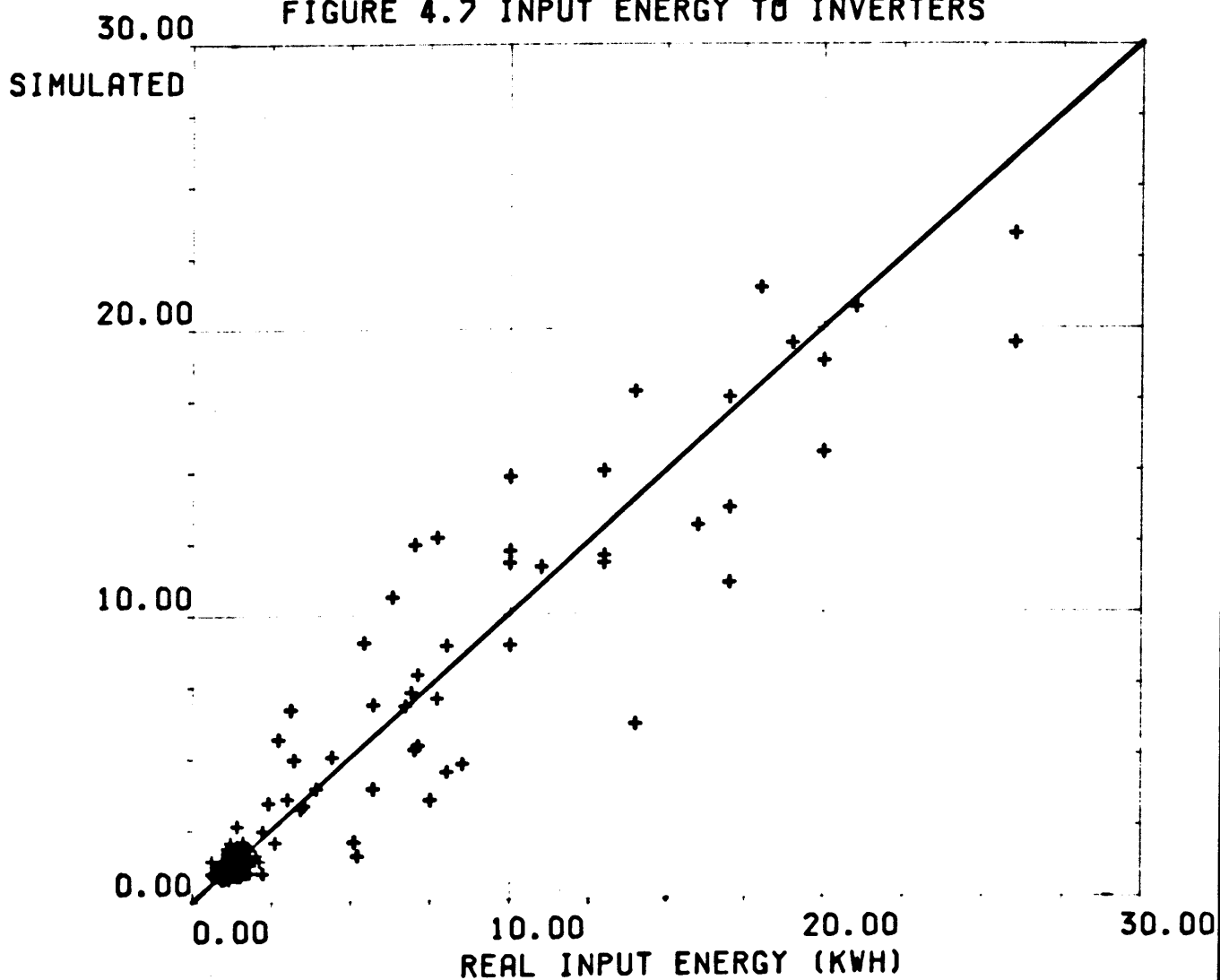
- its mode of operation
- its input data
- its simulated DC and AC energy distribution
- the values of the software variables
- the state of the software flags.

During the verification phase this information is printed for each hourly simulation. An example is presented in table 4.3.

The first line of table 4.3 describes the mode of operation during the hour. The next eleven lines describe the input data. The data lines "2" and "3" occur twice. The first line "2" represents the real data and the second line "2" represents the equivalent simulated data. A similar procedure is adopted for line "3". This information is used to compare the real and simulated energy distributions.

The software variables (VAR (1) to VAR (53)) describe the calculations which were performed during the sampled hour and the logic variables (COND (1) and COND (60)) describe the state of the software flags.

FIGURE 4.7 INPUT ENERGY TO INVERTERS



Statistical Summary of Figure 4.7

R Squared	=	0.9
Slope of Regression Line	=	0.91
Intercept on Y Axis	=	0.29
Standard Error or Estimate	=	1.54
Number of Plotted Points	=	180

TABLE 4.3 DATA USED DURING THE VERIFICATION OF THE HOURLY SIMULATIONS.

MODE 2

%FOIA%03-10-85,12.00

1,	0.43,	0.67,	8.70,	153.00,	1.90,	2.60,	2.00,	0.00,											
2,	15.00,	21.00,	25.00,	0.00,	5.50,	2.50,	19.00,	13.15,	16.00,	0.00									
2,	15.00,	24.19,	24.32,	0.00,	4.50,	0.00,	19.47,	15.81,	15.46,	0.00									
3,	0.00,	0.00,	0.00,	0.35,															
3,	0.09,	0.09,	0.00,	0.18,															
4,	1.90,	1.90,	1.80,	1.80,	1.70,	2.00,	2.20,	1.80,	1.80,	2.00									
5,	2.10,	2.00,	1.30,	22.00,	24.00,	21.00,	13.00,	15.00,	10.00,	4.00									
6,	288.00,	5.20,	29.00,	20.00,	97.00,	275.00,	0.34,	22.00,	25.00,	14.00									
7,	0.40,	1.10,	0.30,	0.70,	0.61,	1.40,	19.00,	19.00,	38.00,	42.00									
8,	1.90,	2.30,	2.00,	952.00,	951.00,	11.00,	1.10,	0.01,	0.00,	0.68									
VAR(1)=	267.22	VAR(2)=	270.69	VAR(3)=	168.96	VAR(4)=	207.56												
VAR(5)=	0.00	VAR(6)=	0.00	VAR(7)=	0.00	VAR(8)=	0.00												
VAR(9)=	267.22	VAR(10)=	292.12																
VAR(11)=	0.00	VAR(12)=	0.00	VAR(13)=	0.00	VAR(14)=	0.00												
VAR(15)=	18.47	VAR(16)=	0.48	VAR(17)=	0.51	VAR(18)=	0.00												
VAR(19)=	0.00	VAR(20)=	0.00																
VAR(21)=	0.00	VAR(22)=	4.50	VAR(23)=	0.00	VAR(24)=	16.62												
VAR(25)=	0.00	VAR(26)=	0.00	VAR(27)=	0.00	VAR(28)=	6.41												
VAR(29)=	0.00	VAR(30)=	26.00																
VAR(31)=	0.00	VAR(32)=	0.00	VAR(33)=	77.48	VAR(34)=	0.00												
VAR(35)=	82.08	VAR(36)=	1.10	VAR(37)=	0.00	VAR(38)=	-4.82												
VAR(39)=	24.32	VAR(40)=	0.67																
VAR(41)=	0.60	VAR(42)=	0.00	VAR(43)=	15.64	VAR(44)=	0.00												
VAR(45)=	0.00	VAR(46)=	0.00	VAR(47)=	0.00	VAR(48)=	0.00												
VAR(49)=	0.58	VAR(50)=	24.19																
COND(1)=	F	COND(2)=	F	COND(3)=	F	COND(4)=	F												
COND(5)=	F	COND(6)=	F	COND(7)=	T	COND(8)=	F												
COND(9)=	F	COND(10)=	F																
COND(11)=	F	COND(12)=	F	COND(13)=	F	COND(14)=	F												
COND(15)=	F	COND(16)=	F	COND(17)=	F	COND(18)=	F												
COND(19)=	T	COND(20)=	F																
COND(21)=	F	COND(22)=	F	COND(23)=	F	COND(24)=	F												
COND(25)=	F	COND(26)=	F	COND(27)=	F	COND(28)=	T												
COND(29)=	F	COND(30)=	F																
COND(31)=	F	COND(32)=	F	COND(33)=	T	COND(34)=	F												
COND(35)=	F	COND(36)=	F	COND(37)=	T	COND(38)=	F												
COND(39)=	F	COND(40)=	T																
COND(41)=	T	COND(42)=	F	COND(43)=	F	COND(44)=	F												
COND(45)=	F	COND(46)=	F	COND(47)=	T	COND(48)=	F												
COND(49)=	F	COND(50)=	F																
COND(51)=	F	COND(52)=	F	COND(53)=	F	COND(54)=	F												
COND(55)=	F	COND(56)=	F	COND(57)=	F	COND(58)=	F												
COND(59)=	F	COND(60)=	F																

This data combined with the control algorithms provide a fast and efficient method for improving the power management model.

4.4 Conclusion

The Fotavoltaic Project has a complex power management. During the development of its model seven power management models were identified and a separate model was developed for each. The modes cater for all possible combinations of PV array, battery, inverters, loads and utility grid. Their models can be used to simulate all existing PV systems except those which have DC/DC converters. A DC/DC converter was not installed in the Fotavoltaic system.

The verification procedures described in this chapter provide a fast and efficient method of debugging the model. Using an accurate model similar procedures would examine the hourly and daily performance of any PV system.

The double battery operation provides ideal battery management but it requires a complex software control. Consequently, the power management model is more complex and more difficult to develop than if one battery was used.

The development of the power management model requires a thorough knowledge of both the control software and the characteristics of the hardware components.

CHAPTER 5

OPTIMIZATION TECHNIQUES

5.1 Introduction

Optimization techniques have been developed by PV system designers [82,83,87] to minimise the overall cost of the generated energy. These techniques identify the optimum component sizes taking into account the component costs, the component characteristics, the load variation and the geographical location. The computer model described in this thesis can perform similar optimizations.

The main advantages of this computer model over existing computer models are:

- (a) Existing computer models assume that the PV array, battery, inverters and loads are single units and that the power management is optimized. This computer model simulates the performance of a PV system in which the main hardware units are divided into subunits (13 subarrays, 2 batteries, 4 inverters, 3 loads) and the power management is not optimized. It can therefore be used to improve the performance of an existing non-optimized system.
- (b) Some optimization techniques [87] use analytical methods based on mean monthly data. These analysis techniques are very fast but they provide very little information on the detailed performance of the system. Since this computer model operates on an hourly basis it can examine detailed performance such as; the occurrence of battery deep-discharge or overcharge, energy loss due to

overcharging, performance during extreme variations of insolation or load demand etc. These details play an essential part in the optimization of the performance efficiency and reliability of a PV system.

Experience with PV systems [101] has shown that poor system performance is due to:

- hardware failures
- non-optimized hardware design
- non-optimized power management
- undersizing of components
- changes in the load demand
- changes in the load profile.

This chapter describes how the computer model can be used to address these problems. The techniques are presented in four main sections which are summarised as follows:

- (1) The PV system performance is improved as a result of analysing the response of the model to simulated changes in both the hardware design and the power management. These are the least expensive changes which can improve the system performance.
- (2) The computer model examines how the performance can be improved by changing the size of individual components. The model calculates the minimum battery and inverter sizes required to achieve maximum performance. These modelling techniques can be used, for example, when a PV system needs to be updated due to an increase in the daily load demand.

- (3) In this section the computer model calculates the optimum PV system design using meteorological data and load profiles as inputs. This involves calculating the optimum PV array tilt and also calculating the optimum PV array/battery combination to reduce the overall cost. These techniques are the basis for the design of any PV system.
- (4) The computer model examines how PV system design and cost vary with the load profile. Four load profiles are selected for analysis i.e.
- night-time load only
 - daytime load only
 - constant demand
 - variable load demand.

A PV system is designed for each. Component sizes and system costs are compared.

Throughout this chapter the analysis is based on the data from the Fotovoltaic system. It is important to remember, however, that this is just an example and that similar techniques can be applied to any other PV system.

5.2 Optimization Parameters

The optimization of a PV system involves the attainment of maximum performance, efficiency and reliability at the minimum cost. This section describes the parameters which measure these characteristics.

a) System Performance

The performance of a PV system is measured by examining the main aims of the system design. In the Fotavoltaic project the main aim of the PV system is to supply the dairy farm load independent of the utility grid. A secondary aim of the design is to deliver all excess energy to the utility grid.

The performance of the system is therefore assessed by measuring the fraction of the total load which is supplied by PV i.e.

$$\% \text{ of load supplied by PV} = \frac{\text{PV energy to load}}{\text{Total load energy}} \times 100$$

The total load energy consists of the PV energy and the energy from the utility grid. The optimum value for this parameter is 100%.

b) System Efficiency

The overall design efficiency is measured by expressing the total AC energy produced as a fraction of the total horizontal insolation.

$$\text{ODE} = \frac{\text{Total AC output energy}}{\text{Total horizontal insolation}} \times 100$$

This is a measure of the combined efficiencies of the PV array, battery and inverters. i.e.

$$\text{ODE} = n_{\text{tilt}} * n_{\text{array}} * n_{\text{battery}} * n_{\text{inverter}}$$

where

$$n_{\text{tilt}} = \text{tilt efficiency of the array} \left(= \frac{\text{planar insolation}}{\text{horizontal insolation}} \right)$$

η_{array} = PV array efficiency efficiency (DC energy/planar
insolation)

$\eta_{battery}$ = battery efficiency = $\Delta E_{stored} / (E_{in} - E_{out})$

where ΔE_{stored} = change in the amount of energy stored

E_{in} = input energy (charging)

E_{out} = output energy (discharging)

$\eta_{inverter}$ = inverter efficiency = AC Energy/DC Energy

The overall design efficiency can therefore measure improvements due to changes in the hardware design or in the power management.

c) System reliability

The reliability of the system is optimized by operating the components within the limits specified by the manufacturers. In the optimization software the simulated data is tested for the following conditions:

- Deep-discharge is not allowed (< 1.865 V/cell)
- Overcharging is not allowed (> 2.4V/cell)
- The instantaneous battery voltage is always greater than 240V and less than 350V. (This is the input voltage range of the inverters).
- Subarray switchings are minimised to improve the reliability of the DC contactors.

If these conditions occur during the optimization a message is printed describing the potential fault e.g.,

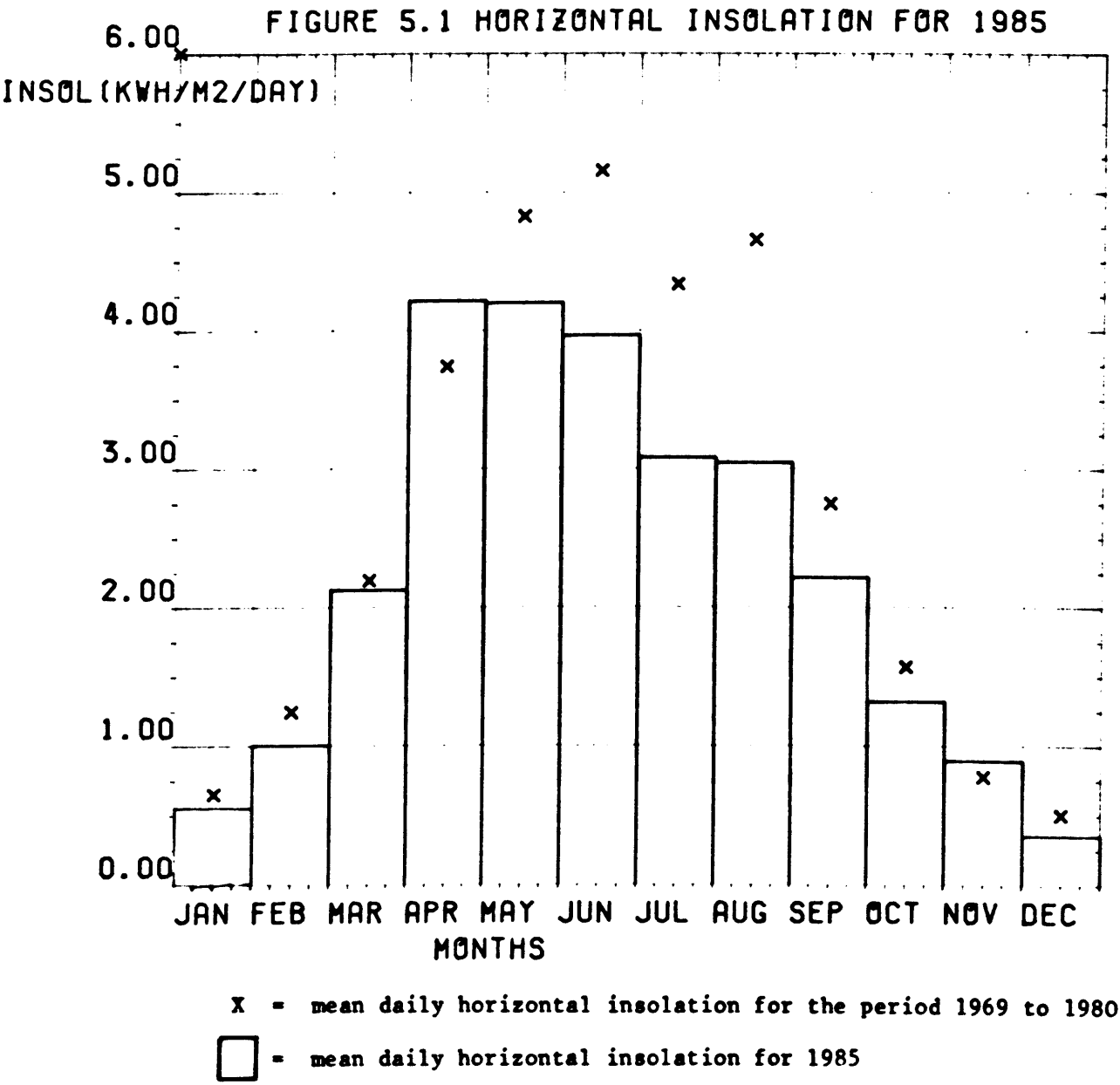
DEEP-DISCHARGE CONDITION AT 13-09-85, 13:00

d) System Costs

The cost of the components is expressed in \$ and the rates were obtained from Maycock [99] and from manufacturers data sheets.

In the following analysis the data for 1985 was selected.

Figure 5.1 shows the mean daily horizontal insolation per month for 1985 (histogram) and for the period 1969 to 1980 (asterisk). This plot shows that the insolation for each month, except April and November, was below normal. In fact the data for the months May, to October represent the worst insolation for the period 1969 to 1986. The total insolation for the year was 15% below normal. Based on these factors the data can be used to optimize the system performance for worse case conditions.



5.3 Modelling of Changes to the Hardware Design and Power Management

The PV system performance is improved as a result of analysing the response of the model to simulated changes in both the hardware design and in the power management. This section describes the techniques which are used to simulate the following hardware and software changes and it discusses the results of each simulation.

Hardware

- (a) One 600 Ah battery is used instead of two 300 Ah batteries.
- (b) The load demand is matched to the available insolation by including an ice-producing facility in the dairy farm.
- (c) (a) and (b) are used in combination.

Software

- (d) The power management of the minisemi is adjusted to operate it only in its high efficiency region.

5.3.1 Simulations of Changes in the Hardware Design

(a) One 600 Ah battery is used instead of two 300 Ah batteries. Double battery operation was selected as it improves the battery performance by providing more charge/discharge cycles than would be the case if only one large battery was used. Also each battery reaches full charge at regular intervals.

The main disadvantage of double battery operation is the extra complexity and consequently the extra software required for the power management. In the Fotavoltaic system 25K of control software is required to control and monitor the system. If a single battery was used this could be reduced to 15K.

Another disadvantage is that the load capacity is reduced by using two smaller batteries rather than one large battery. This is discussed in further detail on the following page.

This section describes the techniques used to simulate the performance of a 600 Ah battery and it compares the results with the existing double battery operation.

The simulation of a single 600 Ah battery operation requires the development of the following models.

- A model of the 600 Ah battery
- A model of its power management
- A model of its load capacity.

The model of the 600 Ah battery is calculated using the concepts described in Chapter 3. The external voltage is:

$$V = V_1 + V_2 + V_3$$

where V_1 = no-load voltage as a function of Ah capacity

V_2 = voltage due to the constant internal resistance

V_3 = the polarization resistance.

The no-load voltage is calculated using the concepts outlined in section 3.2.4, i.e. a linear relationship exists between the no-load voltage and the battery state of charge.

At 20% SOC (120 Ah) $V = 250V$

At 100% SOC (600 Ah) $V = 289V$

Using this linear relationship the no-load voltage is defined as:

$$V_1 = 250 + 0.08 (Ah-120)$$

A 600 Ah battery is equivalent to two 300 Ah batteries in parallel.

Therefore, the external voltage of a 600 Ah battery at a current I is equal to the external voltage of a 300 Ah battery at a current $I/2$. The 300 Ah model is adjusted to give:

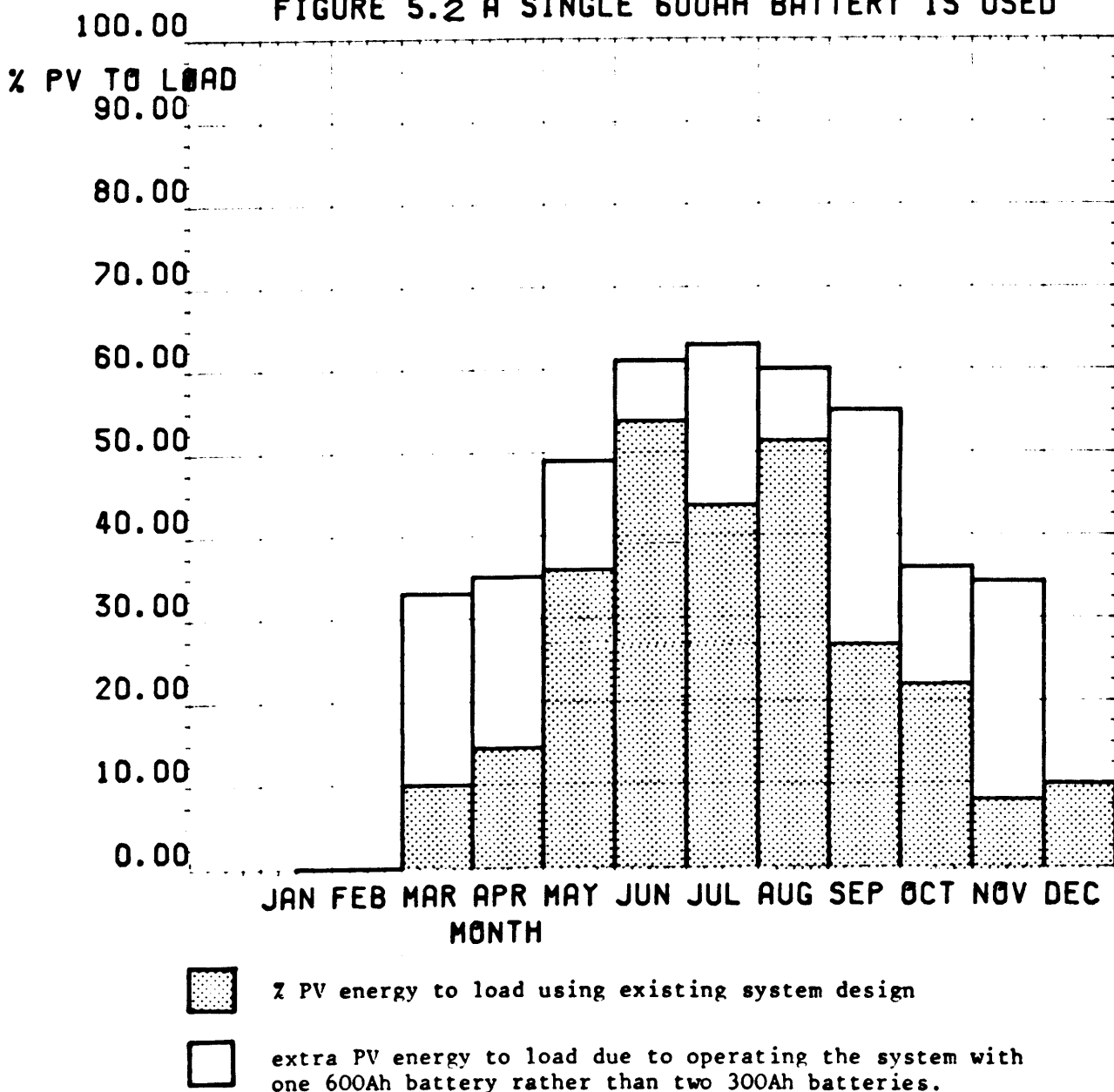
$$V_2 = 0.0536 * I/2$$

$$V_3 = 6.7 \ln (I/2 + 1)$$

The power management of a single battery operation is already described by Mode 2 operation.



FIGURE 5.2 A SINGLE 600AH BATTERY IS USED



Battery Load Capacity

The load capacity of a battery refers to the amount of energy which can be removed at a given load demand. This section compares the load capacity of a single 600 Ah battery with that of two independent 300 Ah batteries.

In the Fotavoltaic System the minimum battery voltage allowed by the microcomputer is 250V. During the milking period, at low insolation, the discharge current is 31A.

Using the 300 Ah battery model (described in Section 3.2.4) this 31A will cause a voltage drop of 24.84V and both batteries must have a minimum capacity of 217Ah to prevent the battery voltage reaching 250V. Therefore the maximum amount of Ah which can be removed during these conditions is $2 * (300 - 217) = 166\text{Ah}$.

Using the 600Ah battery (described above) a 31A discharge will cause a voltage drop of 19.43V and the battery must have minimum capacity of 314 Ah to prevent the battery reaching 250V. Therefore, the maximum amount of Ah which can be removed using a 600 Ah battery is $600 - 314 = 286\text{ Ah}$.

This calculation shows that by using a single 600 Ah battery instead of two independent 300 Ah batteries an extra 119 Ah can be removed. This is equivalent to 32 kWh which is then available to the loads.

The results of the simulation are presented in figure 5.2. The figure shows that the system performance could be improved during each month of the year if a single battery was used. During the Spring and Vernal equinoxes the system is very much dependent on the performance of the battery because the sun, at these times of the year, is low in the sky during morning and afternoon milking. The extra load capacity of the

600 Ah battery is, therefore, most beneficial during these periods and as can be seen in figure 5.2 the system performance actually increases considerably.

In summary, by using a 600 Ah battery the PV system is capable of supplying 47.2% of the annual load demand during worse case conditions. This compares with 29% using the existing double battery operation.

b) The Dairy Farm Load is Matched to the PV Array Output using an Ice Producing Unit

Milking occurs during the early morning (7:30-10:00) and the late afternoon (16:30-18:00). The milk is collected every morning and is transported to the local creamery. At midday there is no load demand on the dairy farm and the PV energy is used to charge the batteries or, if excess energy exists, it is sent to the utility grid.

During the milking periods and the nighttime the milk is cooled using a 3.5 kW compressor. The disadvantages of this operation are:

- it increases the load demand during the milking periods.
- it discharges the batteries at nighttime.

The load demand on the dairy farm could be better matched to the available PV energy by the installation of an ice-producing unit. The ice, produced during mid-day, could then be used to cool the milk during the milking periods and the nighttime. The existing cooler can be used to produce the ice and therefore no changes are required to the inverter design or the power management. A detailed description of the ice producing unit and the amount of ice required is presented in Appendix E. Based on these calculations the operation may be summarised as follows:

1. The ice producing unit should not be used during the milking periods or during the night-time.
2. The unit should operate continuously between 10:00 and 16.30 to produce sufficient ice for the dairy farm.
3. The existing compressor could be used to produce the ice.

The results of this simulation are presented in figure 5.3.

Figure 5.3 shows that the performance increases during each month of the year. The increase is due to the better daily matching of the load to the PV array output and also to the reduction in load demand during the morning and afternoon milking periods.

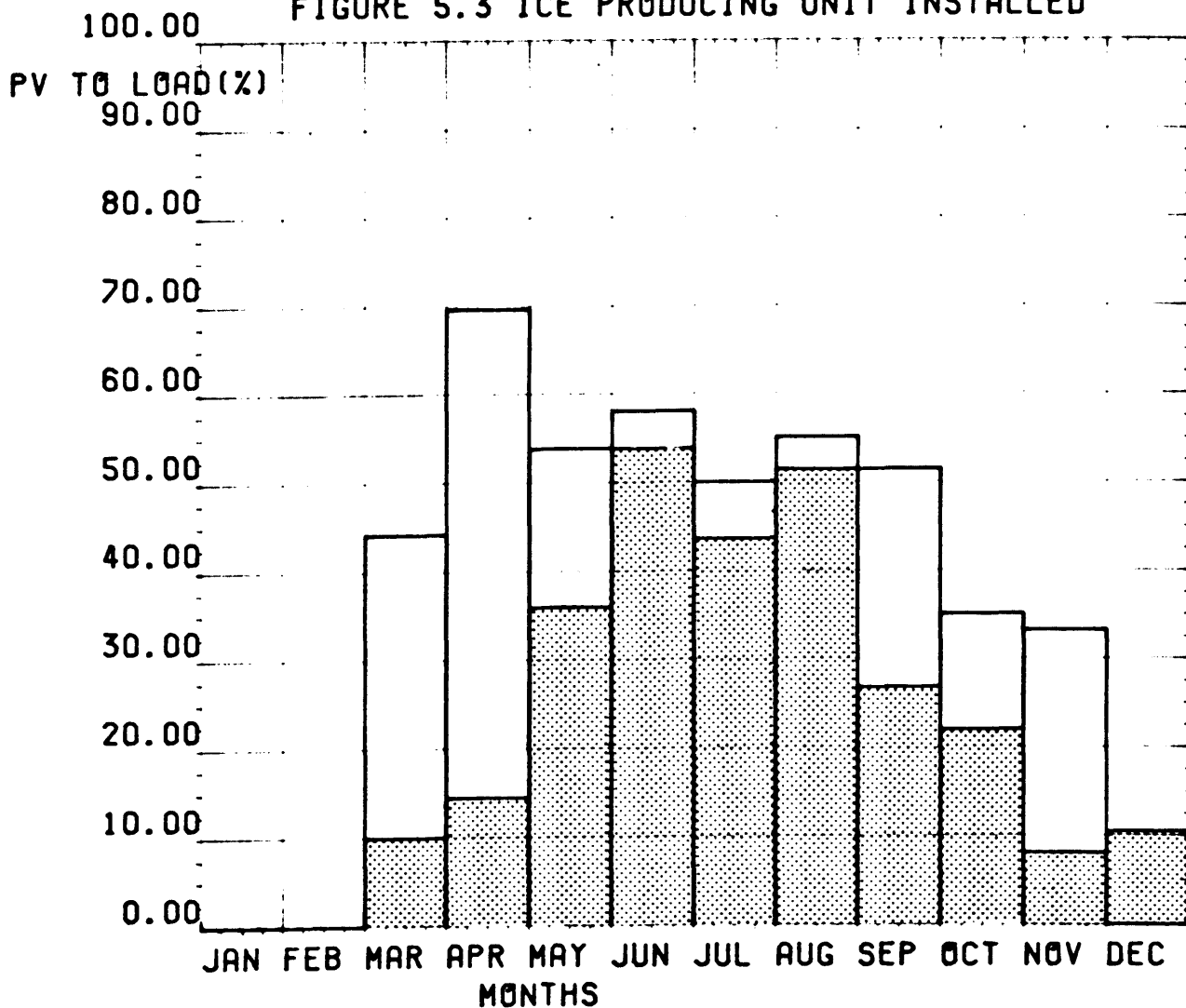
In summary, by using an ice-producing unit on the dairy farm the PV system is capable of supplying 50% of the annual load demand during worst case conditions, compared with the existing performance of 29%.

(c) A Single 600 Ah Battery is used in Combination with an
Ice-Producing Unit

The computer model simulates the operation of a 600 Ah battery in combination with an ice-producing unit by combining the two previous simulations. The results are presented in figure 5.4.

These results show that by using this design the PV system is capable of supplying 65% of the total load demand during worst case conditions.

FIGURE 5.3 ICE PRODUCING UNIT INSTALLED



% Load supplied by PV using existing system design

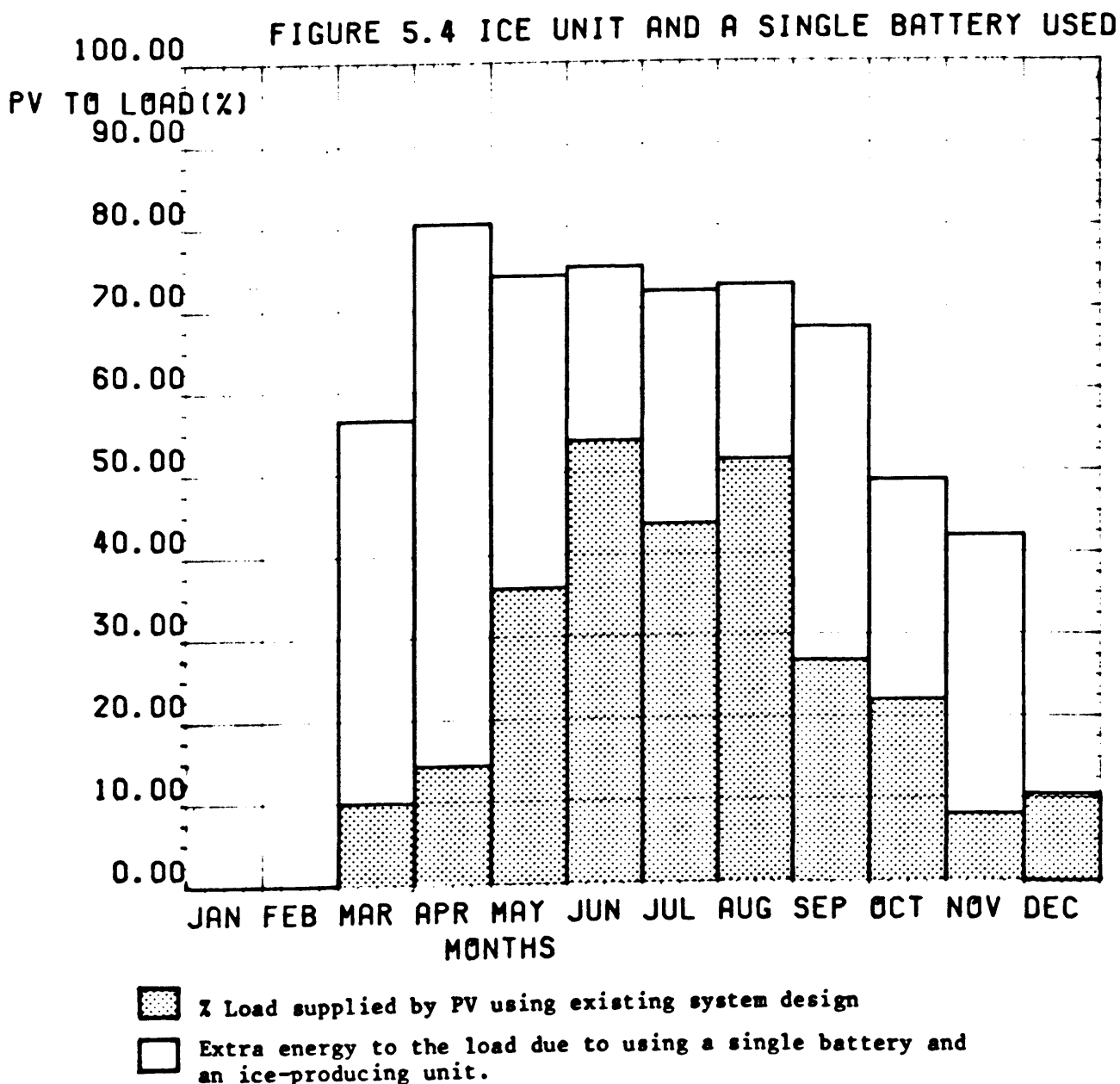


Extra energy to the load due to the installation of an ice producing unit.

These three simulations show that the performance of the system can be considerably improved. The main problem associated with these hardware changes are:

- the cost of the ice-producing unit and the rewiring of the batteries
- new control software is required.

In the following section (section 5.4) the model examines how the performance can be further improved by changing the size of the battery.



5.3.2 Simulation of Changes in the Power Management

In this section the model is used to determine the improvements which can be implemented by changing the power management of the system.

(d) Operate the minimsemi only at its highest efficiency.

When both batteries begin gassing the excess energy is delivered to the utility grid. The amount of energy delivered depends on the excess charging current of the stand-by battery. Presently, if the PV system generates 10kWh excess energy it is delivered to the utility grid as 10kw for one hour at an efficiency of 71%. It is more efficient, however, to deliver 30kw for 20 minutes at 85% efficiency.

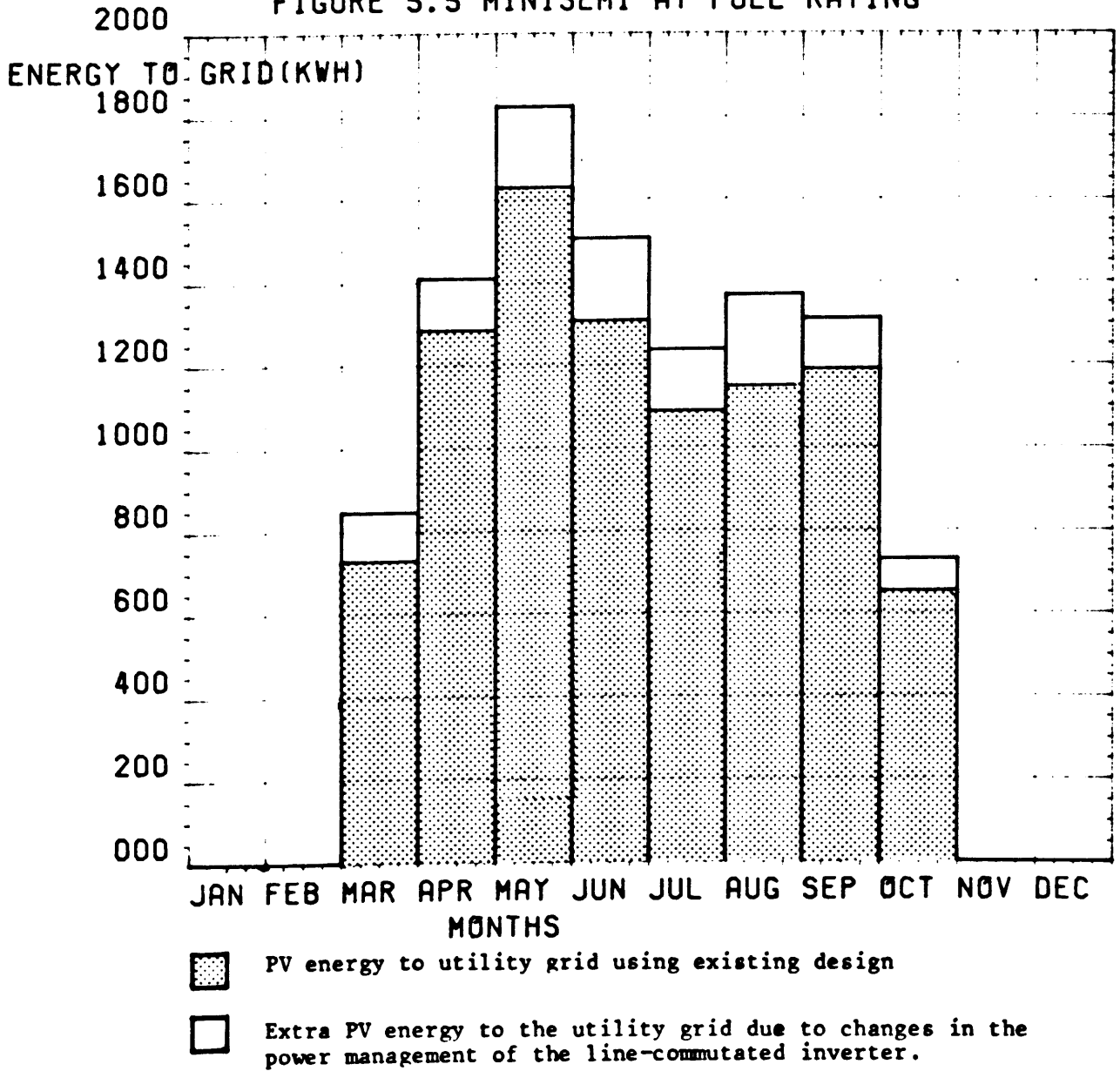
The main disadvantage of this control is that, because more energy flows through the battery, the energy losses increase. The purpose of this study is to examine if the battery losses are compensated for by the increase in efficiency of the minisemi.

In this simulation the minisemi is assumed to operate only at its highest efficiency of 85%. This is simulated by changing the minisemi efficiency model of mode 3 from a quadratic equation to a fixed value of 0.85. Improvements are measured by examining the AC energy delivered to the utility grid.

Simulations were performed on the data for the months March to October 1985 and the results are presented in figure 5.5. These results show that during each month there is an increase of over 10% in the energy delivered to the utility grid. The net increase for the year is 12.9%.

This is an example of how a PV system performance can be improved by implementing a simple (and inexpensive) software change. However, without the use of a computer model the merits of this operation would be difficult to predict.

FIGURE 5.5 MINISEMI AT FULL RATING



5.4 Optimization of Component Sizes

These techniques are the basis for updating an existing system in which the components are undersized or the load demand has increased. This section examines how the existing performance can be improved by changing the size of individual components. The model calculates the minimum battery and inverter size required to achieve maximum performance.

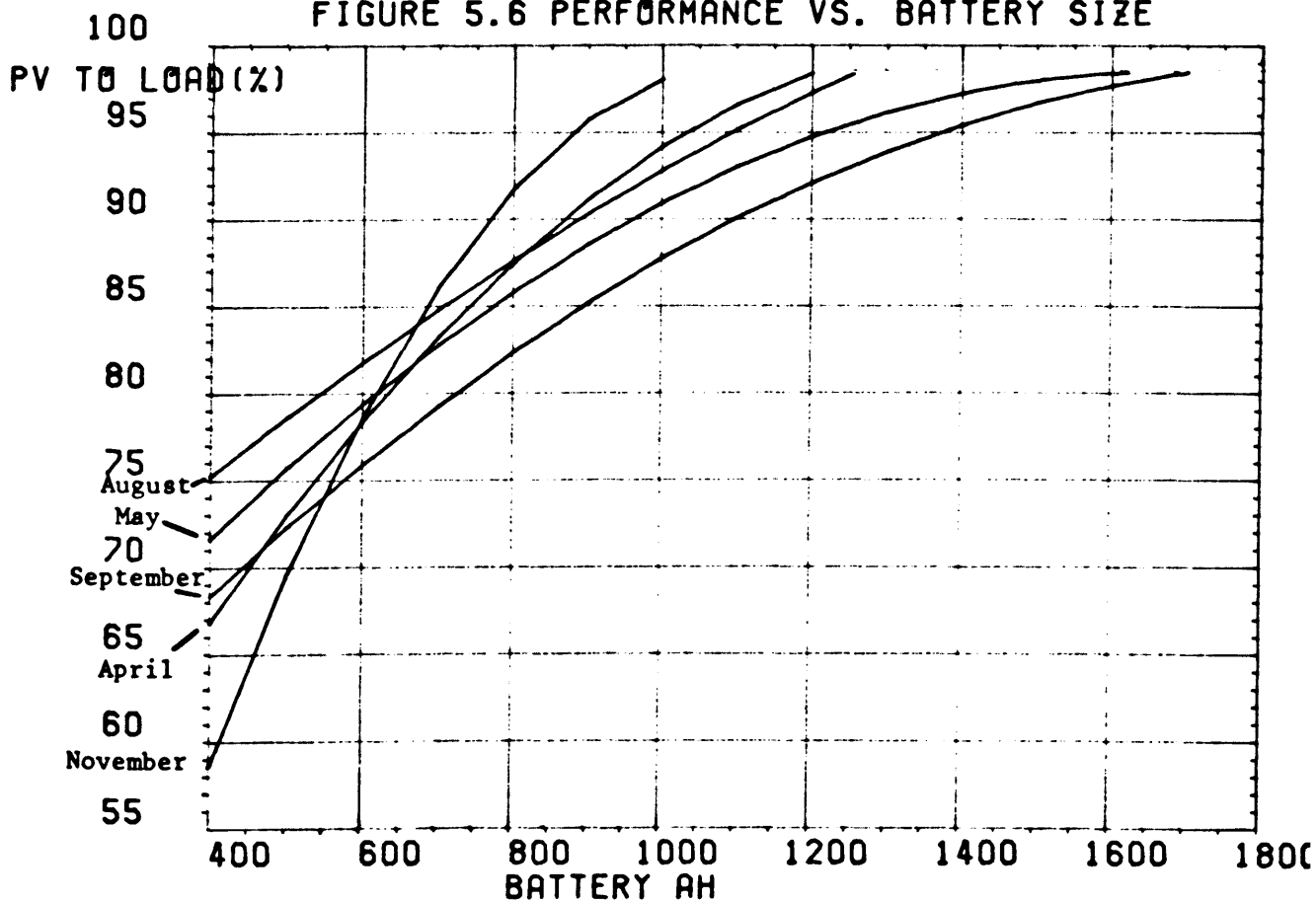
5.4.1 Minimum Size of the Battery

Even though 1985 data represents worst case conditions the PV system produced sufficient AC energy to supply the total AC load. In the previous section the model showed that by improving the hardware design the system could supply a maximum of 65% of this energy to the load. The remaining 35% had to be sent to the utility grid as the 600 Ah battery was not capable of storing the total energy produced by the PV array. In this section the model is used to calculate the minimum battery size required to maximise the amount of PV energy supplied to the load.

The minimum battery size is determined by plotting the % LOAD SUPPLIED BY THE PV as a function of the BATTERY Ah for different months. The results of these simulations are shown in figure 5.6. These results show that if the PV system is required to supply 100% of the load during worst case conditions a 1700 Ah battery is required. However, if a 90% supply is acceptable during worst case conditions then a 1093 Ah battery is sufficient (N.B. 600 Ah @ 268 V cost \$41,000) (13% of the total PV array/battery cost).

Figure 5.6 also shows that September represents the worst case conditions. This is due to the fact that the PV array output is low during the milking periods and the load demand is high at 60 kWh/day (63% of summer load).

FIGURE 5.6 PERFORMANCE VS. BATTERY SIZE



5.4.2 Optimum Size of the Line-Commutated Inverter

The optimum size of the line-commutated inverter is determined by simulating the system performance with different sized inverters and by analysing the changes in the OVERALL DESIGN EFFICIENCY. The existing inverter accepts a maximum of 34kW DC. In this analysis the system is simulated with inverter sizes ranging from 15 kW to 34kW. The 15kW size is the minimum size required to recharge the batteries from the utility grid.

When an inverter cannot deliver all the excess energy to the utility grid subarrays are open-circuited and this causes a reduction in the PV array output and in the OVERALL DESIGN EFFICIENCY. However, advantages of using a smaller inverter are that they are cheaper and also they operate closer to full rate (and maximum efficiency) more often than larger inverters. The optimum inverter size occurs when the efficiency losses due to subarray disconnections are compensated for by the increased operating efficiency of the inverter.

The simulations are implemented using data from May 30 to June 3rd 1985. This period had very high insolation (6.5kWh/m/day) and the maximum excess energy was delivered to the utility grid each day.

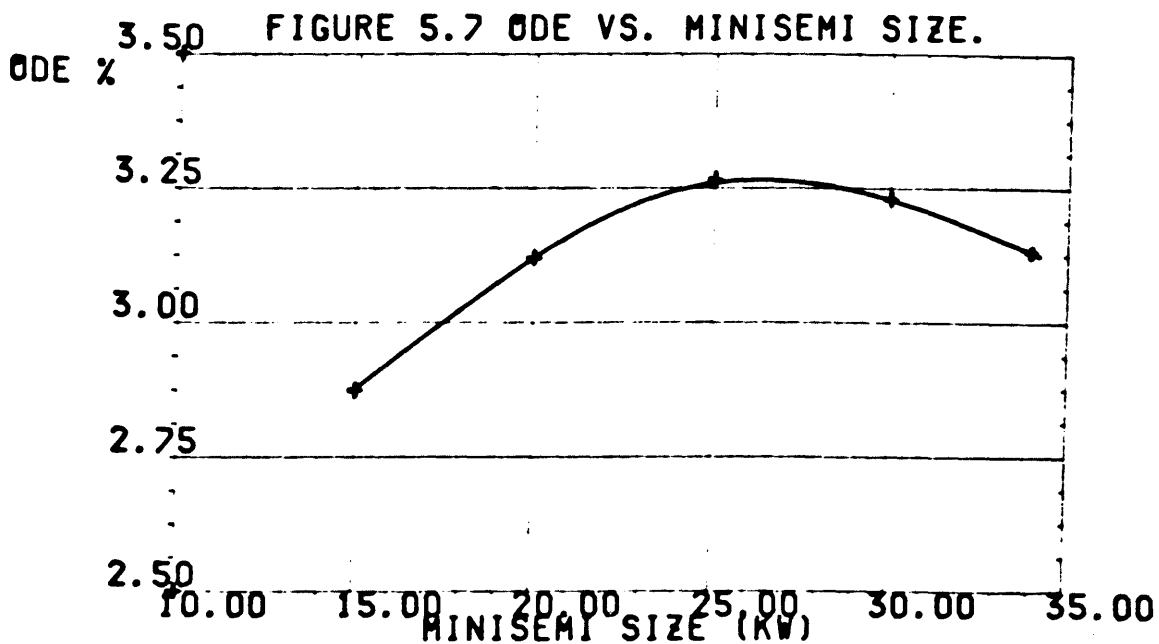
The results of the simulations are shown in figure 5.7. Figure 5.7 is a plot of the OVERALL DESIGN EFFICIENCY (ODE) versus the minisemi rating and it shows a weak maximum about the 25kW range.

Below the 25kW range the ODE is low because energy is lost due to subarray disconnections since this size of inverter cannot deliver all of the excess energy to the utility grid.

At the 25kW range some energy is lost due to subarray disconnections but this is compensated for by the extra AC energy generated due to the high efficiency operation of the inverter.

Above the 25kW range all excess energy is delivered to the utility grid but at a lower efficiency.

These results show that the optimum inverter size is 25kW (36kVA) rather than the existing 34kW (50kVA). In the initial design a cheaper inverter and a cheaper interface to the utility grid could have been installed.



5.5 Optimum System Design

This section describe how the computer model is used to calculate the optimum design from the meteorological data and the load profile. The optimum design is the design which produces maximum performance at minimum cost.

The first task [94,95] in designing a PV system is to specify the requirements of the user. This involves specifying the critical loads and the acceptable performance during worst case conditions. In this study the computer model also examines how the system design and cost vary with the requirements of the user.

The second task is to identify the worst case condition. In most PV applications worst case conditions occur in December. However, in this application the seasonal load demand is matched to the PV array output and figure 5.6 shows that worst case conditions occur in September.

This section describes how the computer model is used to calculate the optimum PV array tilt and the optimum PV array/battery combination to reduce the overall costs. Identical procedures can be used in the optimization of any other PV system design.

5.5.1 Optimum Tilt of the PV Array

The insolation on the plane of the array is dependent on the latitude, tilt, day of the year, time of the day and the direct and diffuse components of the insolation. When a PV system is designed the array tilt is selected to match the array output with the seasonal demands of the user. Neville [98] has developed an analytical equation to calculate the optimum tilt at any latitude. However, the equation

does not consider local weather conditions as it assumes clear sky conditions at all times. It is therefore not suitable for Irish applications where the diffuse fraction is 60% of the total insolation.

In this study the optimum tilt is calculated for the long term (1969-1978) average global insolation. The data which has been recorded at Fota since January 1984 is not a good representation of the average insolation. It was therefore necessary to select sections of each month in which the mean daily insolation was equal to the long term average. Evans [4] states that 'three is a sufficient number of days to accommodate weather variations for any month'. In this analysis the statistical significance of the results was improved by selecting five days from each month.

A computer program was written to examine the data from each month and the periods selected are listed in table 5.1

The computer model is used to calculate the mean daily planar insolation for each tilt angle and for each month and the results are presented in figure 5.8.

The optimum PV array tilt is the tilt which produces the maximum PV array output during worst case conditions. Worst case conditions for the Fotovoltaic system occur during March and September. Figure 5.8 shows that due to the high diffuse component of the insolation during the months September to March the effect of the PV array tilt is minimal.

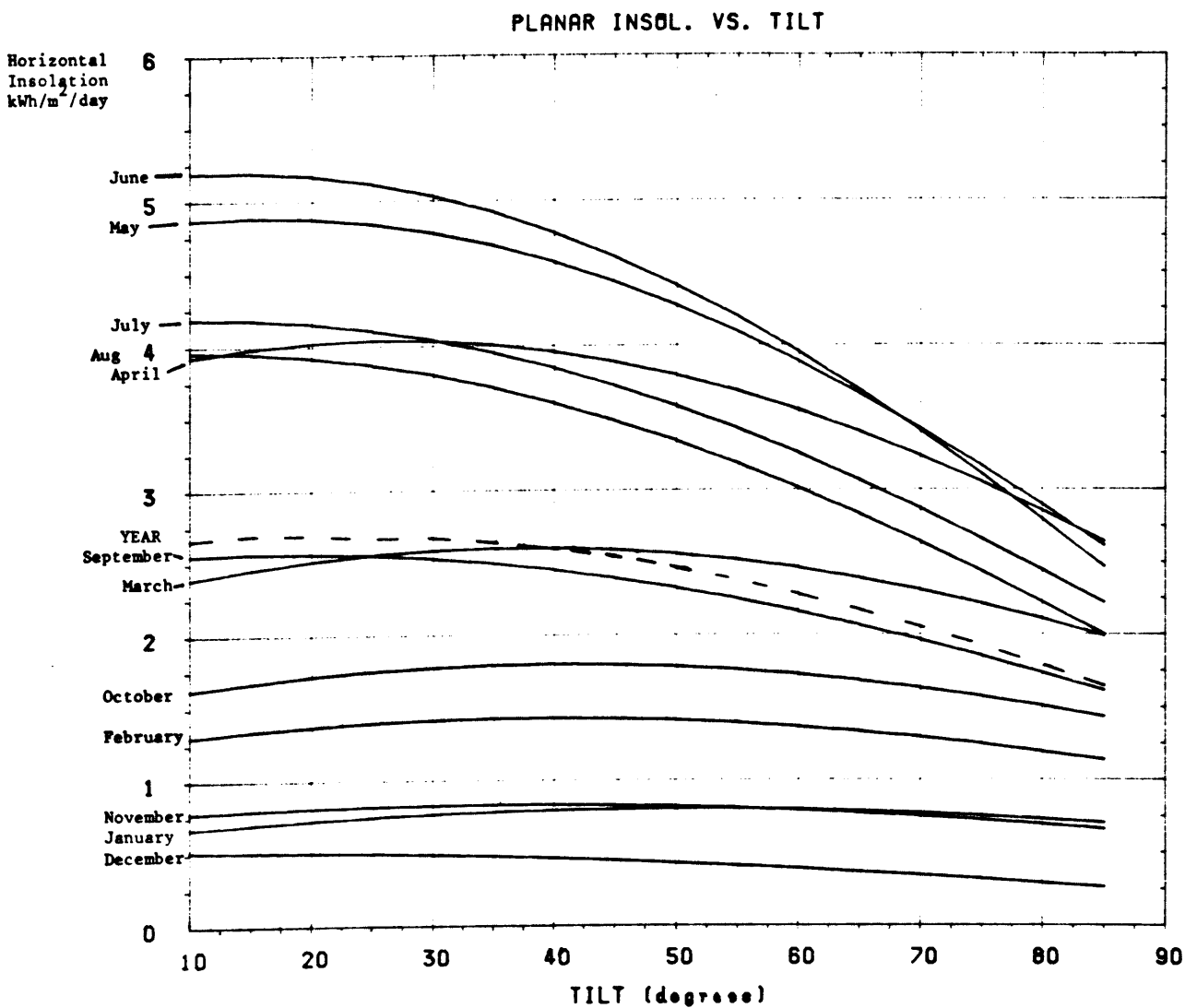
During September, the maximum PV array output occurs for any angle between 10° and 33° . During March the maximum PV array output occurs for any angle between 25° and 60° . Consequently the optimum angle for March and September lies between 25° and 33° . A plot of the mean daily planar insolation for the year shows that within this region (25° - 33°) the

Table 5.1 Periods Selected to Calculate the Optimum PV Array Tilt

The mean daily horizontal insolation of the following periods is the same as the mean daily horizontal insolation for the period 1969 to 1980.

Month	Period (date)	Mean for Period kWh/m ² /day	Mean 1969-1980 kWh/m ² /day
January	27-31	0.65	0.649
February	23-27	1.205	1.24
March	14-18	2.211	2.19
April	6-10	3.739	3.73
May	9-13	4.75	4.82
June	1- 5	5.08	5.15
July	14-19	4.31	4.33
August	2- 6	4.03	4.06
September	10-14	2.78	2.74
October	7-11	1.492	1.56
November	16-20	0.746	0.773
December	7-11	0.471	0.502

Figure 5.8 Mean Daily Planar Insolation for Each tilt and For Each Month



maximum yearly output occurs for an angle of 25°. By specifying the worse case conditions the computer model can calculate the optimum tilt using the procedures outlined above.

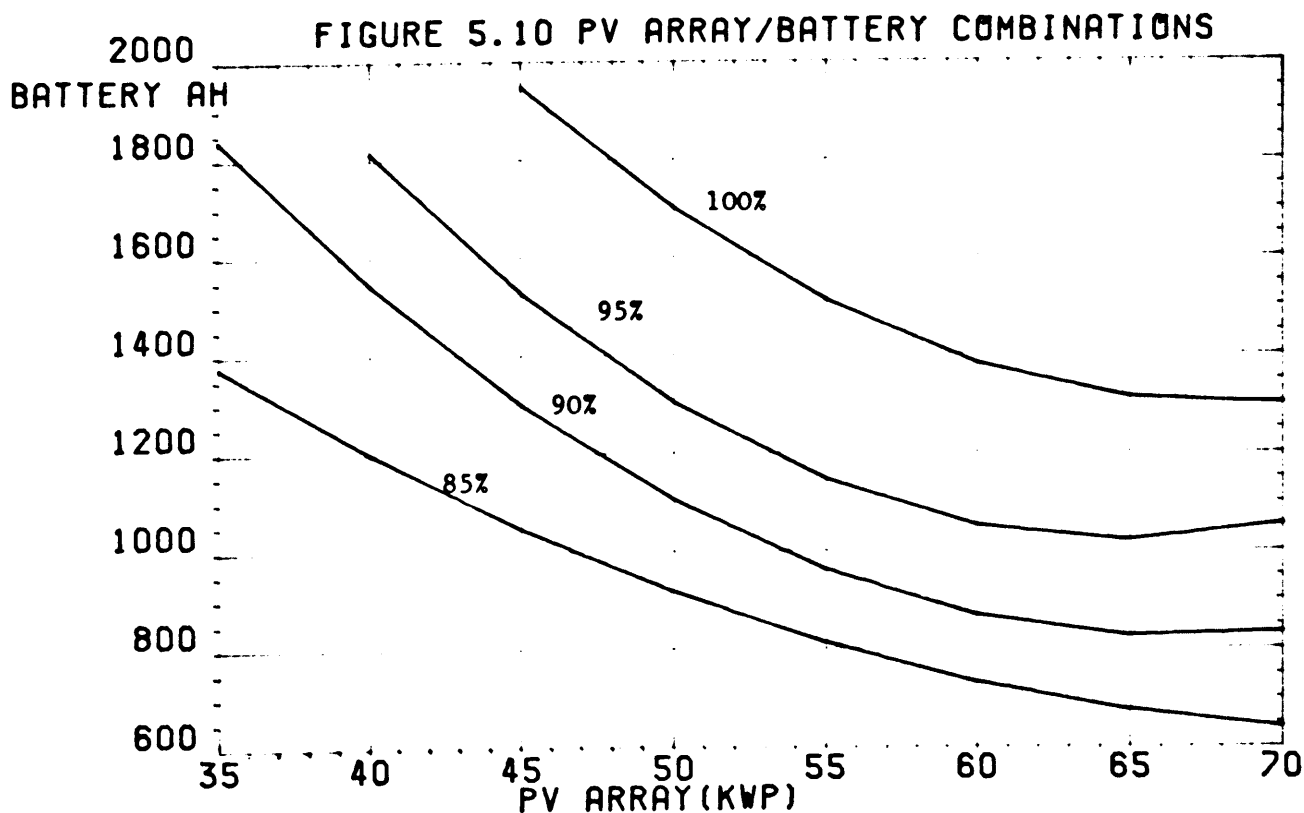
The main disadvantage of this analysis is that it requires a large amount of data and consequently the analysis is slow. However, the results are very accurate and they can be used to calculate the optimum tilt for a PV application in the region. The procedures are far more accurate than existing analytical methods [98] as they take into account the local climatic condition.

5.5.2 Optimum PV Array/Battery Combinations

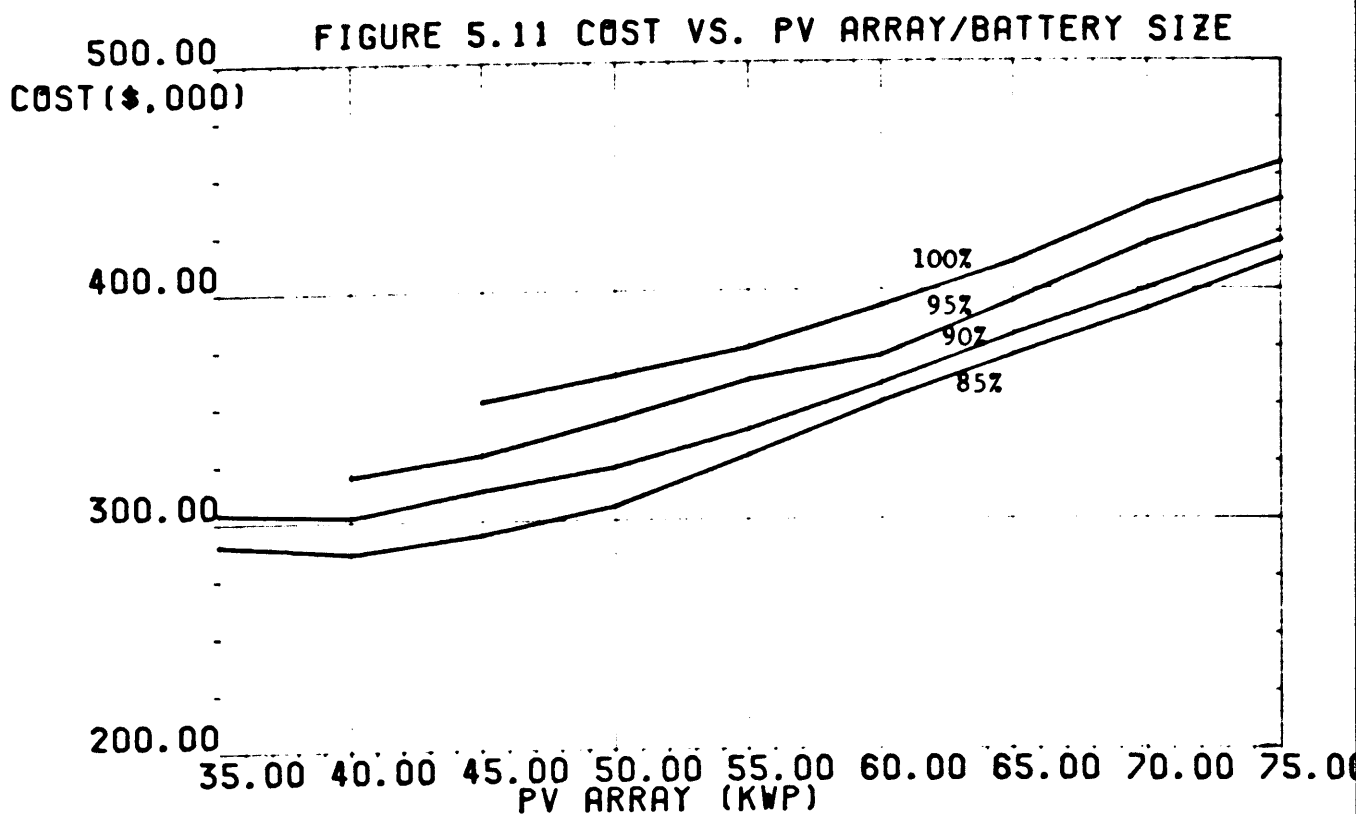
The optimum PV array battery combination provides maximum performance at minimum cost. This is the basis for the design of any PV system. This section describes how the minimum cost is calculated and how it varies with the requirements of the user.

The first task of the computer model is to examine how the system performance varies with different combinations of PV array and battery. The results of these simulations are presented in figure 5.10. Figure 5.10 shows the combinations which supply 100%, 95%, 90% and 85% of the load during worst case conditions.

These results identify the minimum PV array size (and its corresponding storage) and the minimum storage (and its corresponding PV array size). The optimum combination lies between these limits. For example, figure 5.10 shows that if 100% performance is required the minimum PV array size is 40 kWp (+ 1950 Ah) and the minimum battery size is 1300 (Ah + 75 kWp). The minimum battery size actually represents the minimum size which is required to support the daily loads during low insolation periods. The minimum PV array size is the size which supplies the basic needs of system.



This plot shows the combinations of PV array/battery which will supply 100%, 90% and 85% of the load during worse case conditions.



This plot shows the cost of the PV array/battery combination presented in figure 5.10.

The optimum combination is determined by minimising the cost i.e.,

$$\text{COST} = A * \text{PV Array} + B * \text{Battery Size}$$

where A, B are the unit costs of the PV array and battery.

$$(A = \$5/\text{Wp Maycock [99]}, B = \$0.25/\text{Wh (Varta)})$$

The total cost is calculated for each combination shown in figure 5.10 and the results are presented in figure 5.11.

Figure 5.11 shows that if 100% performance is required the minimum cost of the PV array and battery is \$352,000. Furthermore, if 90% is acceptable during worst case condition the cost can be reduced by 14% (\$50,000). In practice this system should be designed to supply 90% of the load during worst case conditions and a backup generator should be included to supply the loads during periods of prolonged low insolation.

The above calculations are based on minimising the initial investment cost. It is also important to minimise the system cost over the lifetime of the plant. The Fotovoltaic System has a lifetime of twenty years but the battery lifetime [100] is limited to ten years. Therefore, when calculating the system cost over its lifetime it is necessary to consider the cost of replacing the battery.

i.e.

$$\text{lifetime cost} = A * \text{PV size} + 2 * B * \text{Battery size}$$

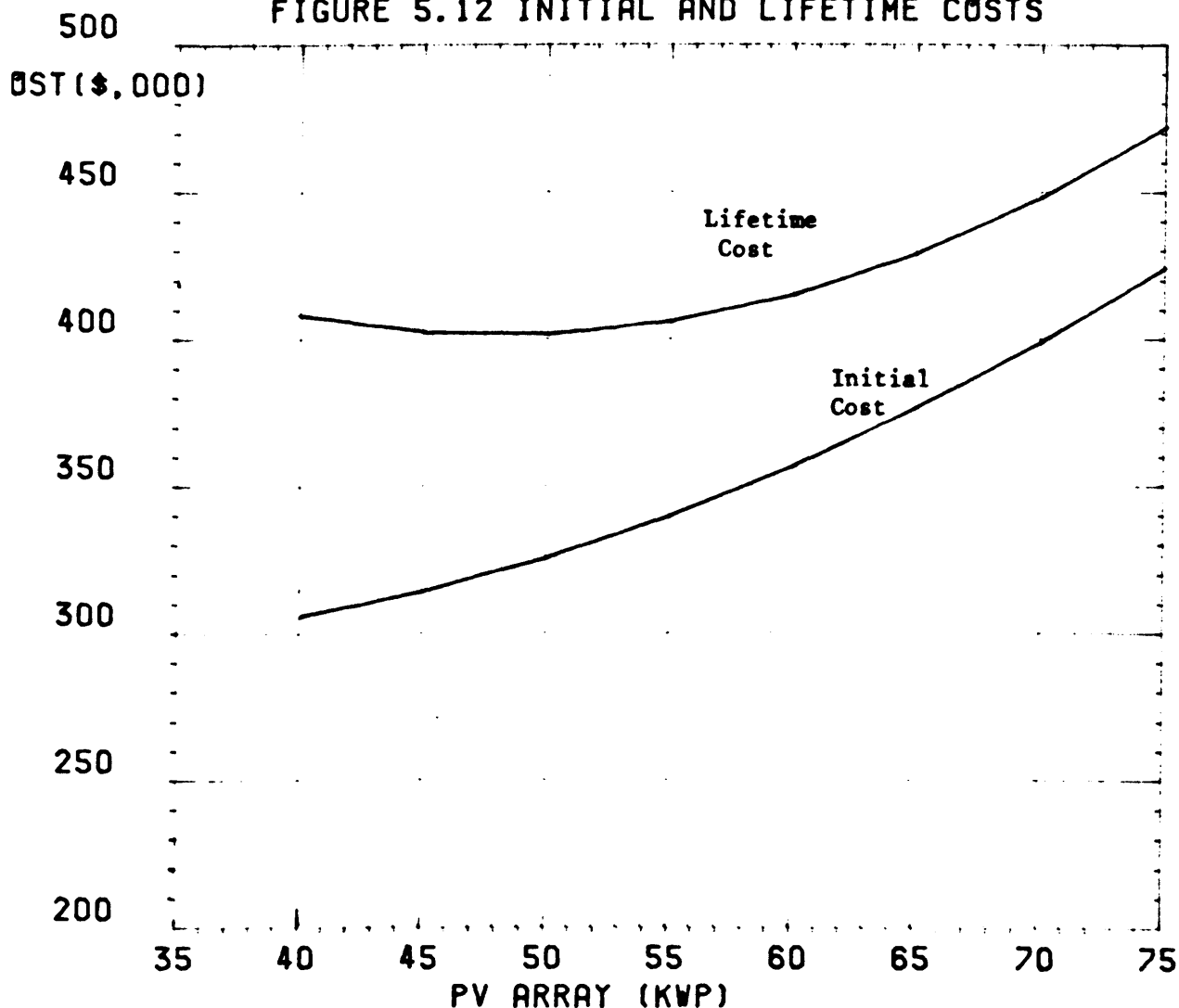
where A,B are the unit costs of the PV array and battery.

Figure 5.12 shows a plot of the initial cost and the lifetime cost for the 90% performance data (figure 5.11). This plot shows that the minimum lifetime cost occurs for a combination of a 50 kWp PV array and a 1093 Ah battery. The minimum initial cost occurs for a combination of 40 kWp PV array and a 1533 Ah battery. The initial cost and lifetime cost for each combination are summarised as follows:

	Initial Cost	Lifetime Cost
50kWp, 1093 Ah	\$323,000	\$396,000
40kWp, 1533 Ah	\$302,000	\$405,000
difference	\$ 21,000	\$ 9,000

Clearly, the optimum cost is the minimum lifetime cost. However, present day calculations for PV systems are based on minimising the initial costs. As PV systems become established as reliable sources of energy with proven lifetimes of up to twenty years the optimum cost will be based on the minimum lifetime cost.

FIGURE 5.12 INITIAL AND LIFETIME COSTS



5.6 PV SYSTEM DESIGN AS A FUNCTION OF THE LOAD PROFILE

The design of a PV system is very dependent on the load profile. If the load profile is matched to the available insolation the battery cost can be reduced considerably. However, if the PV system is treated as a conventional generator where 100% supply on demand is expected (e.g. Greek Island electricity supply policy) the PV system costs increase considerably.

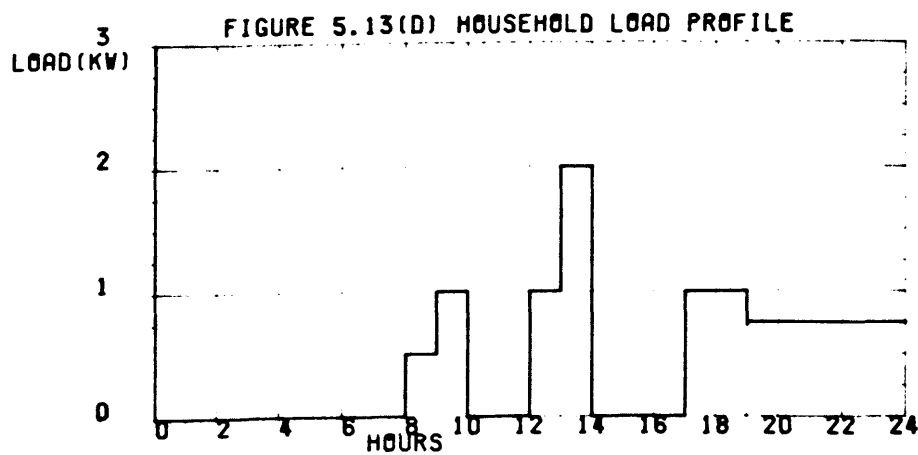
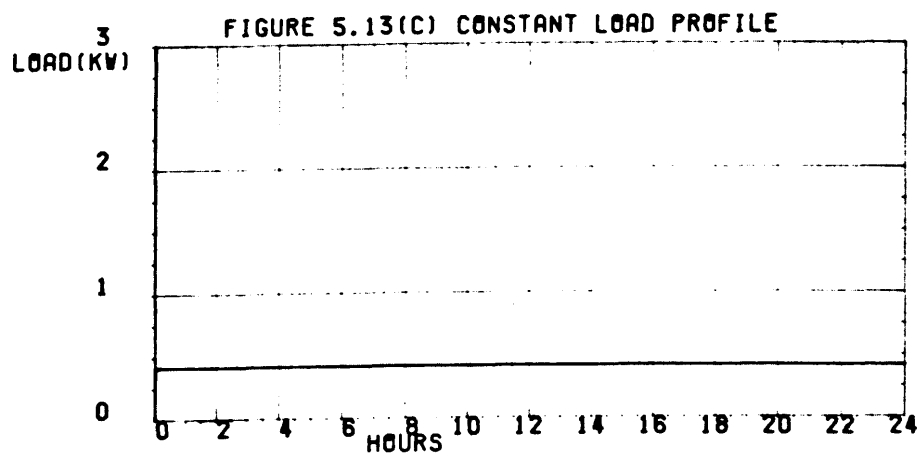
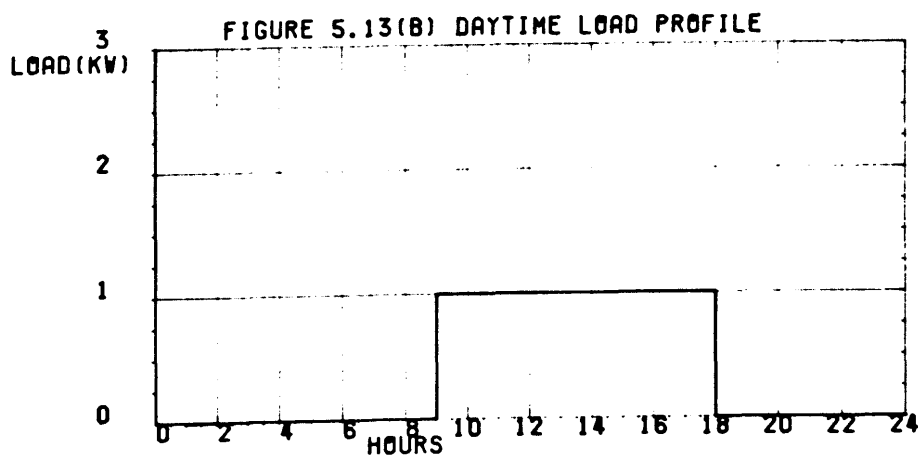
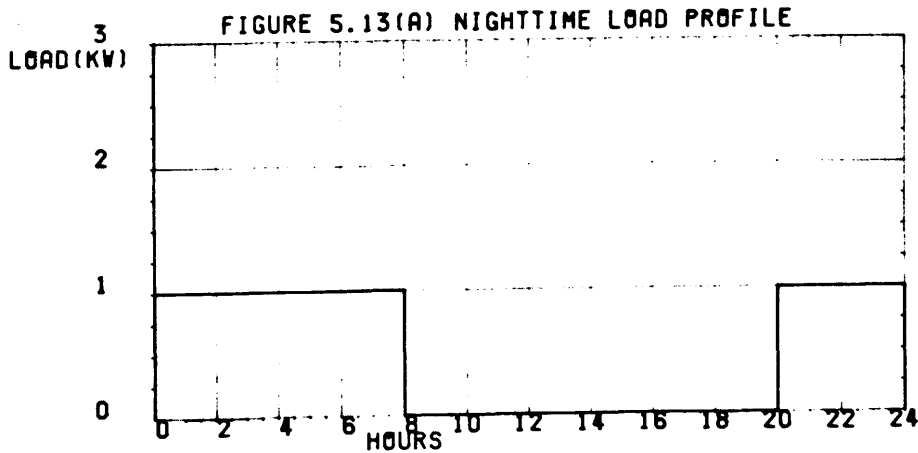
In this study the computer model examines how the PV system design and cost varies with the load profile. Four load profiles are selected for analysis and in each case the total daily load demand is assumed to be 10 kWh.

PV applications in Ireland are limited to situations where the load demand has the same seasonal variation as the available insolation. The most important example are: the dairy industry, tourist industry and recreational facilities. In the following analysis the PV system is designed to supply loads which only occur between March and September. Experience with the Fotovoltaic System (and would apply to all PV systems at Northern European Latitudes) showed that during the winter months (especially December and January) the priority should be to protect the battery rather than supply any load.

The four load profiles selected for analysis are:

1. Night-time load only e.g. public lighting at remote caravan parks
2. Daytime load only e.g. water pumping at remote locations.
3. Constant load demand e.g. refrigeration
4. Variable load demand e.g. holiday homes.

The four load profiles are shown in figure 5.1.3. In this analysis the PV systems are designed to operate in a stand-alone mode. Their configuration is shown in figure 5.14 i.e. a PV array (divided into subarrays for battery management), a single battery and a high efficiency (>90%) self-commutated inverter.



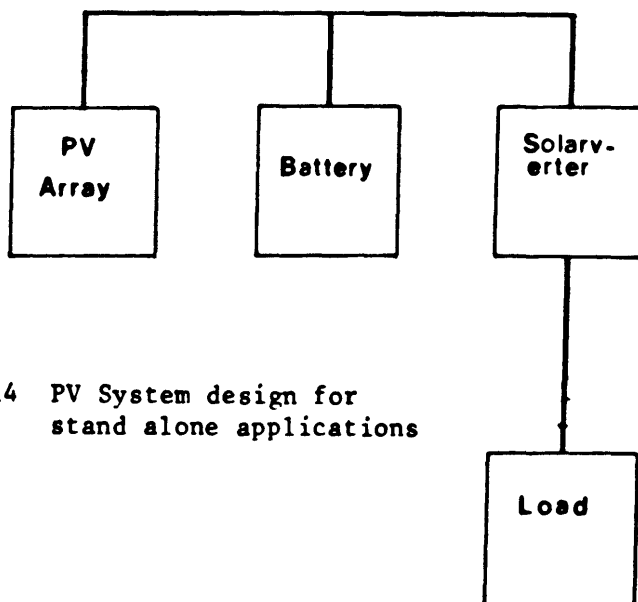


Figure 5.14 PV System design for stand alone applications

The first task in the design of any PV system is to identify the critical loads [94,95]. These are the loads which require 100% supply during specific periods. In the above four examples the loads require 100% supply between the months March and September.

The second task is to identify the worst case conditions. In the above example worst case conditions occur during March and September. The data from 1985 is especially interesting as the insolation for these months was 10% below normal.

The optimum PV array tilt is obtained using the theories outlined in section 5.5. In these applications the optimum tilt is 25° (as in the case of the Fotovoltaic System).



The PV array/battery combinations which supply the complete load demands are selected using the procedures outlined in section 5.5.2 and are presented in figure 5.15. This plot shows that for each load profile there is a minimum battery size. This minimum battery size is actually the battery size which is required to support the load during very low insolation periods.

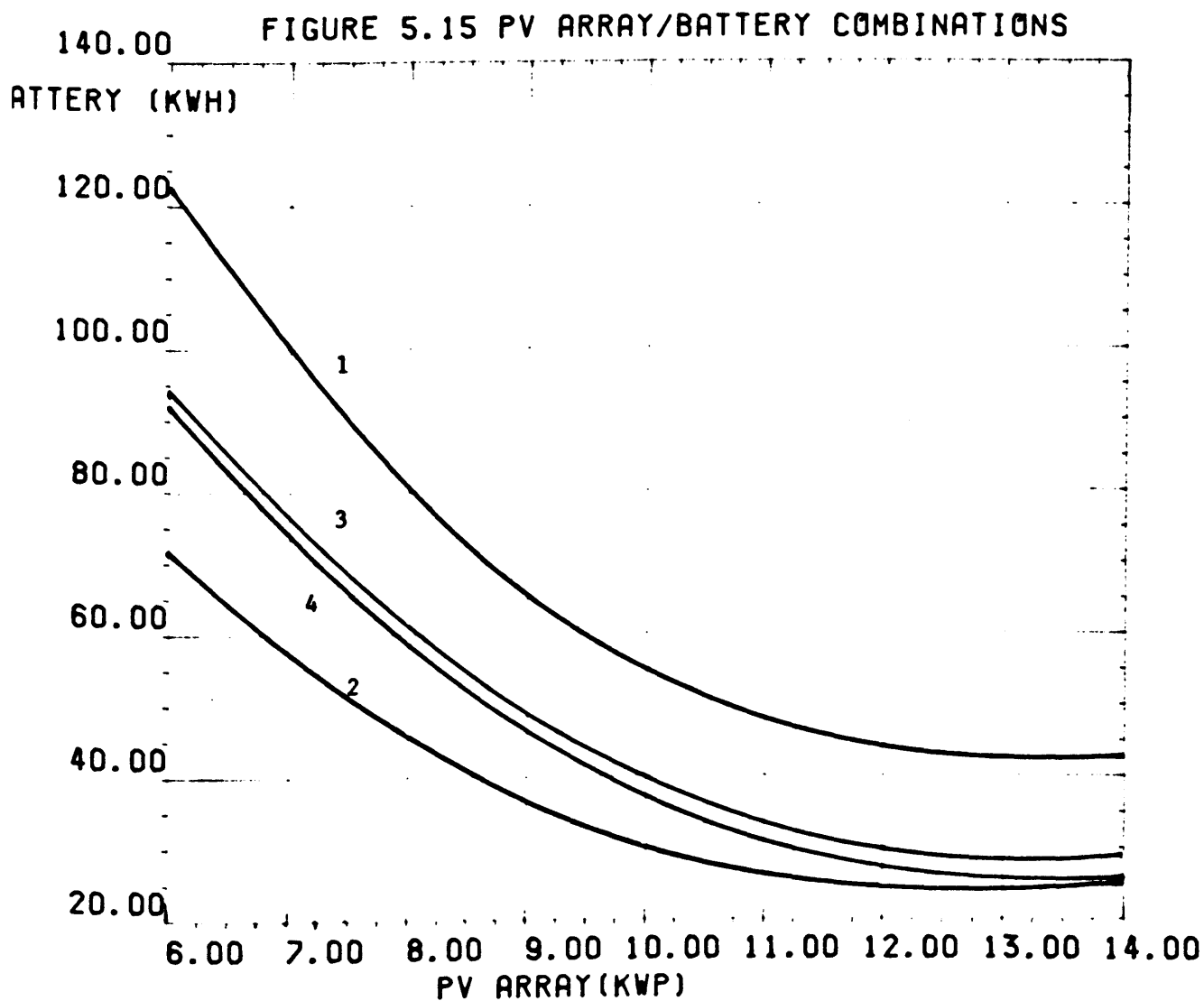
The minimum PV array and battery costs are calculated using the procedures outlined in section 5.5.2. Figure 5.16 is a plot of the initial cost and the lifetime cost as a function of the PV array/battery combination for each load profile.

These results show that even though the total daily load demands are the same the lifetime costs vary from \$62,100 to \$76,800 and the initial costs vary from \$48,000 to \$60,000. The most expensive system, as expected, is the system with the night-time load and the least expensive is the system with the daytime load. In all cases, except for the minimum lifetime cost of the system with the night-time load, the optimum PV array size is 8kWp. The corresponding battery sizes (figure 5.13) vary from 40 kWh to 80 kWh. This shows that the optimum battery size is very dependent on the load profile whereas the optimum PV array size depends on the total daily load.

Existing design rules which use the total daily load rather than the load profile, can accurately predict the optimum PV array size but they cannot predict the optimum battery size. The design of the Fotovoltaic System is a clear example of this, i.e. the 50 kWp PV array is the optimum size to minimise the lifetime costs (section 5.5) whereas the 600 Ah battery is undersized by 45% (optimum = 1000 Ah).

Figure 5.15 PV Array/battery combinations for the following load profiles

1. Nighttime load profile
2. Daytime load profile
3. Constant load profile
4. Household load profile



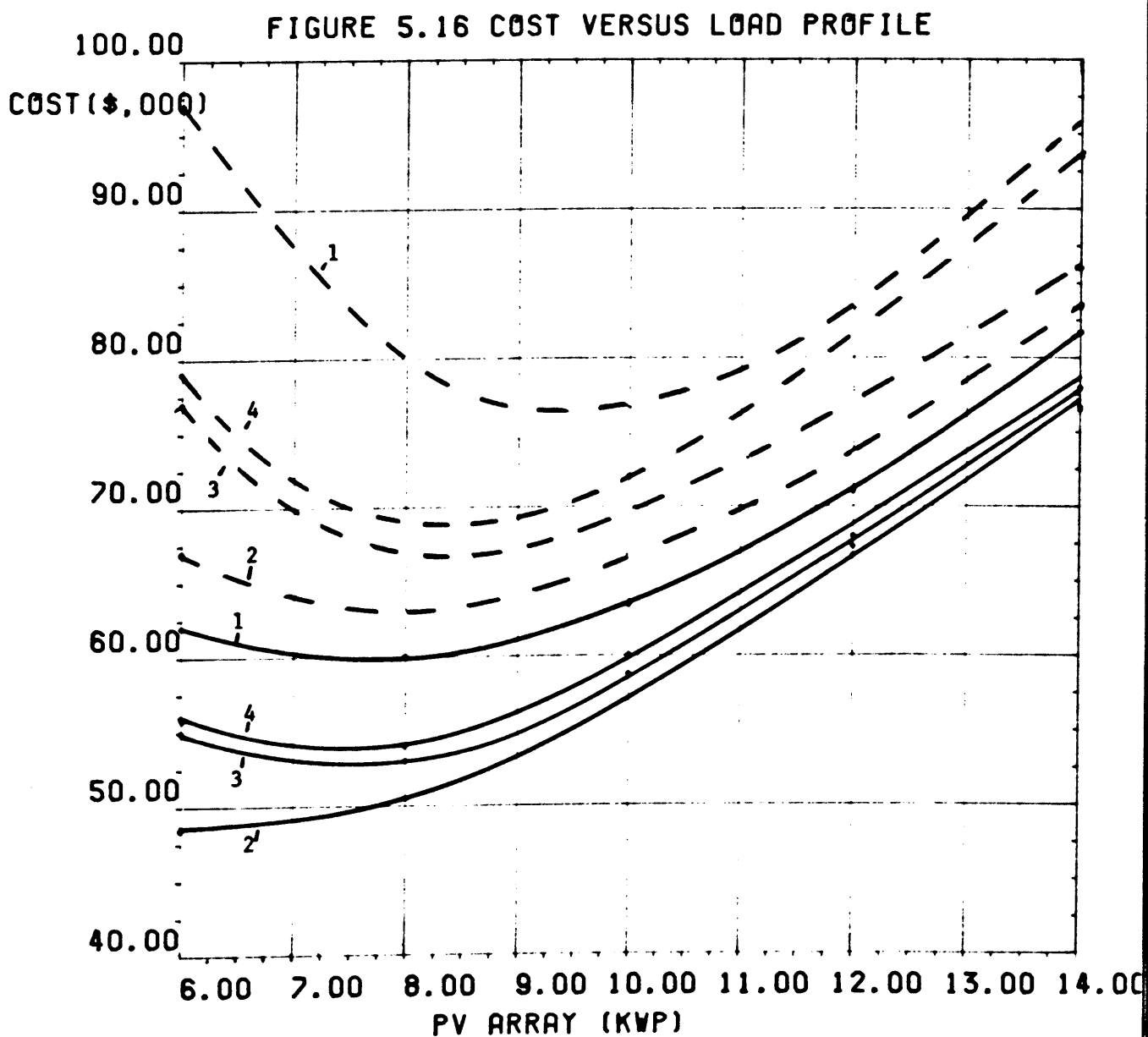
The above analysis described how a PV system is designed for a given load profile. For existing PV systems these techniques can be used to establish guidelines for load management. Load management is necessary when the load profile or the load demand changes. The above examples show how the model can examine criteria such as: matching the daily load to the available insolation; minimising the night-time load and minimising the instantaneous loads. These are the basic criteria for load management in PV systems.

Figure 5.16: Initial Cost and Lifetime Cost Versus
PV array/battery Combinations

1. Nighttime load profile
2. Daytime load profile
3. Constant load profile
4. Household load profile

--- lifetime cost

— initial cost



5.7 Summary

Even though the insolation for 1985 was 15% below normal the PV system generated sufficient energy to supply the total load demand. Despite this, only 29% of the load was supplied by PV while 71% was supplied by the utility grid. During the year 68% of the PV energy (AC) was sent to the utility grid as excess energy. This chapter examines new system designs which would improve the performance of the PV system. It also lists the criteria which should be considered when designing a PV system. The following is a summary of the results.

(a) Hardware Changes

Section 5.3 shows that by using one 600 Ah battery instead of two independent batteries the performance would increase from 29% to 48%. This hardware change would involve rewiring the battery and developing new control software. The system could be further improved by installing an ice-storage unit on the dairy farm. Section 5.3 showed that the performance could increase to over 65%. The only hardware change would be the installation of the actual ice storage unit. The design of the PV system would not change as the existing cooler could produce the ice.

(b) Power Management Changes

Section 5.4 shows that by changing the power management of the line-commutated inverter the amount of AC energy produced would increase by over 10%. This is the least expensive improvement as it only involves changing a few lines of software.

(c) Optimum System Design

The optimum PV array tilt for the Fotovoltaic system is 25°. This angle provides maximum output for the local climatic conditions. The optimum PV array/battery combination was calculated for the minimum

lifetime and initial costs. The minimum lifetime cost occurs for a combination of a 50kWp PV array and a 1093 Ah battery. The lifetime cost is \$396,000 with an initial cost of \$323,000.

The minimum initial cost occurs for a combination of a 40 kWp PV array and a 1533 Ah battery. The initial cost is \$302,000 with a lifetime cost of \$405,000. Present day calculations are based on minimising the initial costs but when PV systems become established as reliable sources of energy the lifetime costs will be used for the optimization. In all cases, however, both combinations should be quoted so that the user can select the design which best suits his financial situation.

(d) The effect of the load profile on the system design.

Section 5.6 shows that the optimum battery size is dependent on the load profile whereas the optimum PV array size depends on the total daily load demand. With the selected four load profiles the computer model shows that if only the total daily load demand was considered the cost could be too high by as much as 14% or the battery would be undersized by up to 45%.

5.8 Conclusion

The Fotovoltaic System was originally designed using calculations which were developed for smaller PV systems. (< 10 kWp) The present performance is an indication of how inadequate these calculations were. A recent report for the CEC [101] showed that the problems encountered in the Fotovoltaic System are common to the other projects in the CEC Pilot Program.

This chapter shows that in addition to optimizing the design of PV systems the computer model could be used to analyse and improve existing systems. The analysis procedures described in this chapter can be easily applied to other systems.

The cost of future PV systems depend on both the reduction in solar cell costs and on the availability of accurate and flexible optimization techniques. This chapter has presented a basis for these techniques.



CHAPTER 6

SUMMARY AND CONCLUSION

6.1 Summary

The summary is discussed under the following headings:

1. The development of the Computer Model,
2. The results of the optimization,
3. Further applications of the Computer Model.

6.1.1 The Development of the Computer Model

The development of a computer model which operates on an hourly basis is very time consuming both in man-hours and in computer-hours. The complete development of this model required two and a half years work. The final model, however, is very accurate and the difference between the real and the simulated data over a period of one month is less than 7%.

The availability of twenty months of hourly recorded data was an excellent basis for the development and verification of the model. In this thesis the component models are presented so that similar models can be developed when less operating data is available. This is important for systems which are already operating but have not accumulated operating data.

The computer model was developed on a VAX 11/780 using FORTRAN 77 language. The complete program has 3240 lines of code and it uses 1 Mbyte of computer memory. Each hourly simulation performs fifty-three calculations and sixty logical operations. A simulation of a weeks performance (168 hours) uses 10.89 seconds of CPU time. In addition to this main software package, three other software packages exist.

The first software package was used to test the model concepts of the individual components. This software was also written in FORTRAN 77 and it has 1063 lines of code. The results of this analysis are well documented and are filed for future reference.

A second software package was developed to optimize the PV system. This software uses the computer model to simulate changes in the hardware design and in the power management.

A third software package was developed to perform a statistical analysis of the results. This software was written in SPSS language [18] and it has 212 lines of code. This program provides seventeen scatter plots and seventeen statistical summaries per simulation and it uses 8.9 secs of CPU time.

The model of the PV array is very accurate and the difference between the real and the simulated data over a period of one month is less than 4%. Though the planar insolation, module temperature and PV array output are measured at the Fotavoltaic system their models were developed so that the complete model can be used at any geographical location and for any climate.

The most difficult models to develop were those of the battery and the line-commutated inverter. This was due to the shortage of relevant data from the manufacturers. The performance curves supplied by the manufacturers were based on instantaneous performance and were only suitable for power analysis. In addition, the existing battery and inverter models are used for internal design and are not suitable for PV system modelling.

In the Fotavoltaic Project the battery state-of-charge is not measured. In the model, however, the state-of-charge is estimated from the summation of battery input/output current measurements. Without a direct

way to measure the state-of-charge the long term predictions of the model are limited. For periods longer than one month the results of simulations are unreliable.

The model of a thyristor commutated inverter is more difficult to develop than that of a transistor commutated inverter. The transistor commutated inverters are very efficient (95% above 10% of full load) and a simple linear relationship exists between the input and output energies. In the thyristor commutated inverters a quadratic relationship exists between the operating efficiency and the AC output power. The relationship between the hourly calculated operating efficiency and the AC output energy is difficult to determine as it is dependent on the performance of the inverter during the sampled hour. In this thesis four different models were required to simulate the performance of the line-commutated inverter.

The power management of the Fotavoltaic Project is very complex and it has seven modes of operation. Each of these modes taken as a separate entity, can be compared to the overall power management of most other projects in the CEC Pilot Program. Therefore, the techniques used to model the different power management modes can be applied directly to the modelling of other projects. The only difference would be in the size of the components.

The development of the computer model provided a better understanding of the system performance and this led to improvements in the power management, data monitoring and system maintenance.

6.1.2 System Optimization

The performance of a photovoltaic system is a complex function of the geographical location, the climatic conditions, the hardware design, the power management, the characteristics of the components, the load profile and the requirements of the user. Chapter 5 describes how the computer model could be used to optimize the performance by analysing the systems response to changes in the above criteria. The optimum design is determined by selecting the components which provide maximum performance at minimum cost.

In this study the Fotovoltaic System was selected for analysis. It is important to remember, however, that similar optimization techniques can be applied to any other PV system.

The major problems associated with the 15 PV systems in the CEC Pilot Program are summarised as follows [101]:

- non-optimum system design
- non-optimum size of components
- inadequate battery management
- changes in load demand
- changes in load profile.

The data which is presently recorded by the PV systems in the CEC Pilot Program is used to calculate the energy produced and the efficiency of operation. These results are adequate for comparing the performance of the 15 PV systems but they do not contain sufficient detail for system improvement.

The techniques presented in chapter 5 and the summary presented in section 5.7 are the type of information which is required to improve system performance. This information provides a system designer with the

advantages and disadvantages of different design strategies and it provides the user with guidelines for load management and system operation.

The availability of optimization techniques such as those presented in chapter 5 are the type of results which the PV Pilot Program might consider.

6.1.3 Further Applications of the Computer Model

The computer model is very versatile and it can be used as follows:

- (a) to model and optimize other PV systems
- (b) as a diagnostics tool to analyse the performance of a PV system
- (c) to examine the degradation of the battery and the PV array

(a) Modelling of Other PV Systems

The main aim in developing the computer model was to optimize the performance of the Fotavoltaic system. The secondary aim was to develop models which could be used to model and optimize other PV systems. This is especially significant to the CEC Pilot Program where the systems' design are very similar to that of the Fotavoltaic Project.

The data used by the model is the same data format which is used at each of the fifteen projects. This format is the standard selected for the CEC program.

Unlike existing computer models [1-5], this model is unique in that it simulates non-optimized PV systems. Because of its complexity it can be used to examine the advantages and disadvantages of different design strategies. These procedures were used to determine the optimum design of the Fotavoltaic system.

The model can be used to transfer experiences from one project to another. For example, the problems incurred at Hoboken and Giglio [6] when conditions of high insolation with varying cloud cover exist have already been overcome at the Fotovoltaic system through the use of prediction analysis. Before the implementation of such control software at Hoboken and Giglio, the model can be used to determine the control parameters and to examine the effect of the software changes.

This is also an example of how the computer model improves a system performance through software improvements rather than the inclusion of oversized hardware.

(b) The Computer Model as a Diagnostic Tool

The computer model can be used to analyse the performance of a PV system. The verification plots, which assess the accuracy of the models, also detect failures in the PV system. The main failures detected are: calibration errors, measuring point failures and hardware failures. These analysis techniques [19] are in regular use in the Fotovoltaic system and are easily applied to other systems.

The most difficult features to detect are intermittent failures. During the analysis of the data for June 1985 a number of outliers appeared on the verification plots of the line-commutated inverter model. These outliers were analysed, and it was found that when inverter 2 was operating the DC current measuring point of the line-commutated inverter was inaccurate. This inaccuracy was caused by high frequency noise from inverter 2. This type of error could not have been detected without the computer model.

The analysis procedures used in the Fotavoltaic system should be further developed into a standard set of analysis procedures. These procedures could be used by system managers to identify faults and to assess the performance of their PV systems.

(c) Examine Degradation of the PV Array and the Battery

The computer model can be used to examine degradation in the PV array and battery.

The rate of degradation of the PV array and the battery is determined by examining the accuracy of their models on an annual basis. The cause of the degradation is then determined by reviewing the model concepts. This analysis is easily implemented using the software packages which were developed to test the model concepts.

The long term aim should be to develop a model for degradation and to incorporate it into the existing models.

6.2 Conclusion

This concluding section examines the present trends in the modelling of PV systems. It examines how this computer model can overcome the disadvantages of existing computer models and it suggests further improvements which can be made to the model.

The earliest work in solar system simulation is that of Speyer [102] in 1959 and Beckberg and Roulet [103] in 1968. These models were designed to calculate the optimum size of the solar collector and storage for a house heating system. In 1969 Schwartzburg [106] developed a computer model to analyse the performance of the PV power system of a satellite. In 1971 Weiner [107] developed a computer model of the Viking Orbiter

Power System. This model was designed to calculate the optimum PV component sizes to support the orbiter during the critical phases of its mission.

Early computer models were custom built and these later became the basis for general purpose models. Since 1974 a number of general purpose models have been developed and the most popular is TRNSYS [105]. TRNSYS was developed at the University of Wisconsin by Duffie and Beckman [104] and it is available on a commercial software package. It is regularly updated to include new developments in the solar technology. Originally TRNSYS was designed to model solar thermal systems but in recent years (1978) it has been updated to simulate PV system performance [5].

The other popular PV computer model is SOLCEL [1]. This was developed at the Sandia National Laboratories and it is designed specifically for PV system analysis and design optimization. This model was the basis for later models such as SOLSTOR [3] which evaluates the economic feasibility of stand-alone PV systems, and SOLREL [108] which analyses the reliability and availability of PV systems.

Both TRNSYS and SOLCEL are written in FORTRAN and the simulations are performed on an hourly basis. They are structured so that PV systems may be modelled by defining the components and their interconnections. TRNSYS and SOLCEL are mainly used to predict the longterm performance of PV systems, to evaluate the life-cycle costs and to assess the reliability and availability of PV systems over their lifetime.

These models are attractive in that they are easy to use and they can simulate various systems design. Their main disadvantages, however, is that in order to make them easy to use they do not give a good insight into the detailed performance of a system. This is the main reason why research groups continue to develop their own models.

Their second disadvantage is that they assume that the components are single units and that the power management is optimized. TRNSYS and SOLCEL could not accurately predict the performance of PV systems in which the components are divided into subunits and the power management is not optimized. For example, they could predict the theoretical maximum performance of the Fotavoltaic system but they could not accurately predict its real performance. This is a serious disadvantage as they cannot be used to examine the feasibility of different power management strategies.

The model presented in this thesis is similar to TRNSYS and SOLCEL in that it is written in FORTRAN, it operates on an hourly basis, and it can be used to predict and optimize the performance of PV systems. The model is unique in that it can simulate the performance of a PV system in which the components are divided into subunits and the power management is not optimized. Chapter 4 showed that even though the power management of the Fotavoltaic system is very complex it could be modelled by defining seven individual power management models. These techniques could then be used to model the different design and power management strategies of the 15 PV pilot projects. The model could optimize these systems performance taking into account the complexity of the system, the layout of the components and the characteristics of the central controller. Such optimization techniques are necessary to determine the feasibility of different design and power management strategies.

The disadvantages of developing a computer model are:

- it is both time consuming and expensive
- a large amount of operating data is required
- techniques must be developed to verify the models
- expertise is required in both PV system design and computer modelling.

In this thesis the component models are presented so that similar models can easily be developed using simplified techniques and with a minimum amount of operating data. The models can be verified using the techniques outlined in section 1.5. Even though these modelling techniques are simplified, the overall development will give the designer a good insight into the detailed performance of the components. With some further development the modelling techniques could be used as a training aid for PV system design engineers.

In summary, TRNSYS and SOLCEL are more useful to a system analyst as they are designed to perform longterm economic and reliability analyses of PV systems. The computer model in this thesis is more relevant to the work of PV system design engineer as it is mainly concerned with the performance of the components within a PV system and their contribution to the overall system performance.

6.2.1 Recommendations for Improvements to the Computer Model

The component models presented in this thesis can be used as general purpose computer models. As such they should be:

- easy to use
- flexible
- accurate.

The overall computer model is examined under these headings and recommendations are made for further improvements.

(a) Is the computer model easy to use?

From a software viewpoint the model is easy to use. The model accepts a minimum amount of input data (five parameters per hourly simulation) and it presents the results in either graphical, statistical

or tabular form. The component models are structured as subroutines and their parameters are defined as subroutine variables.

From a hardware viewpoint the model is not easy to use. A large computer (VAX 11/780) is required, 1 Mbyte of memory is used and a simulation of one weeks operation uses 10.89 seconds of CPU time. This is a big disadvantage if the model is to be used as a general design tool. To overcome this problem the model should be updated to operate on a small computer system or more preferably on a microcomputer. The microcomputer should have a minimum disk storage of 500k bytes and a minimum of 1M byte RAM. This work would involve minimising the number of calculations and logical operations in each hourly simulation.

(b) Is the Computer Model Flexible?

The computer model is flexible. It was developed so that it could model any PV system design at any geographical location and for any climate.

The component models are presented as mathematical equations and the power management models are presented as algorithms. Therefore, the system model can be developed on any suitable computer system and with any computer language.

Component models have only been developed for the components which exist in the Fotavoltaic system. This limits the flexibility of the model. To overcome this problem component models should be developed for all other PV system components e.g.,

- Maximum Power Point Trackers
- Electronic Battery Charge Controllers
- NiCd Batteries.

Manufacturers of PV system components should be encouraged to include a computer model of the components on their data sheets.

(c) Is the Model Accurate?

This thesis has shown that the model can accurately predict the performance of the Fotavoltaic System. The present accuracy is based solely on the data from the Fotavoltaic system and the model has not been verified using data from other PV systems. The component models should be verified using data from the other projects in the pilot program. The power management model should be verified with different battery management strategies and with different inverter layouts.

If computer models are to be used as design tools then the optimization techniques should be versatile and easy to use. To achieve this, general purpose optimization techniques should be developed. These techniques should automatically calculate the optimum design if the user specifies the critical loads and the worst case conditions.

The optimization techniques presented in Chapter 5 are not easy to use. They require expertise in both PV system design and computer programming and they use a large amount of CPU time (e.g. the optimization techniques which calculate the minimum battery size for the Fotavoltaic System uses 1.8 hours of CPU time).

With some improvements the optimization techniques presented in Chapter 5 could be developed into general purpose optimization techniques. This development would require approximately three man months.

The CPU time could be reduced by:

- determining the minimum number of hourly simulations required to calculate the optimum design.

- minimising the number of iterations required to calculate the optimum design.

It is essential to reduce the CPU time especially if the optimization techniques are to be used on smaller and slower microcomputer systems. Future PV systems will require simplified design rules if they are to be implemented on a large scale. The computer model and the optimization techniques described in this thesis can serve as a useful tool in the development of such guidelines.

REFERENCES

CHAPTER 1

1. Linn J.K. PHOTOVOLTAIC SYSTEM ANALYSIS - SOLCEL. System Analysis Division 5743, Sandia Laboratories, Albuquerque, NM 87115, 1977.
2. Edenburn M.W., Grandjean N.R. ENERGY SYSTEM SIMULATION COMPUTER PROGRAM: SOLSYS. Sandia National Laboratories Albuquerque NM 87115 June 1975.
3. Aranson E.A., Caskey D.L. and Caskey B.C. SOLSTOR: DESCRIPTION AND USERS GUIDE. Sandia National Laboratory, Albuquerque NM March 1981.
4. Evans D.L., Facinelli W.A. SIMULATION AND SIMPLIFIED DESIGN STUDIES OF PHOTOVOLTAIC SYSTEMS. Arizona State University, Tempe (USA) 1980.
5. Goldstein L.H., Case R. PVSS - A PHOTOVOLTAIC SYSTEM SIMULATION PROGRAM. Solar Energy Vol. 21. (37:43) 1978.
6. PHOTOVOLTAIC POWER GENERATION Series C Vol. 4 Proceedings of the E.C. Contractors Meeting held at Pellworm July 1983. (Ed. Palz W.) Published by Reidel, Dordrecht, Holland 1983.
7. Wrixon G.T. THE FOTAVOLTAIC PROJECT: A 50kWp PHOTOVOLTAIC SYSTEM TO POWER A DAIRY FARM ON FOTA ISLAND, CORK, IRELAND. Photovoltaic Power Generation. Series C Vol. 4 Published by Reidel, Dordrecht Holland (153:159) 1982.

8. McCarthy S. and Wrixon G.T. THE DEVELOPMENT OF A MICROCOMPUTER FOR THE CONTROL OF A 50kWp PHOTOVOLTAIC POWER STATION. Photovoltaic Power Generation. Series C. Vol. 3 (230:235) 1983.
9. Treble F.S. MONITORING OF THE CEC PHOTOVOLTAIC PILOT PROJECTS. Proceedings of the 5th EC Photovoltaic Solar Energy Conference, Athens, Greece (584:591) 1983.
10. Martin F.F. COMPUTER MODELLING AND SIMULATION. Published by John Wiley and Sons. New York. Boole Ref. 001.4 MART.
11. Graybeal W.T. and Pooch V.W. SIMULATION: PRINCIPLES AND METHODS. Published by Little, Brown and Company (Canada) Ltd. Boole Library Ref. 001.4 Gray.
12. Gordon G. SYSTEM SIMULATION. Published by Prentice Hall. Boole Library Ref. 001.4 GORD.
13. McGovern J.A. MODELLING AND ITS APPLICATIONS TO ENERGY DYNAMICS IN BUILDINGS. Dept. of Mechanical and Manufacturing Engineering, Trinity College, Dublin 1985.
14. Haslett J. and Monaghan P. MATHEMATICAL MODELLING OF THE USE OF SOLAR ENERGY IN BUILDINGS. Report No. 7705, Statistics and Operations Research Laboratory, Trinity College, Dublin, Nov. 1977.
15. Menicucci D. and Fernandez J. PROGRESS IN PERFORMANCE MODEL VERIFICATION. Proceedings of the fifth photovoltaics systems development and evaluation projects integration meeting. Albuquerque NM (156:167) 1984.
16. Draper N.R. and Smith H. APPLIED REGRESSION ANALYSIS. Published by Wiley and Sons, New York. 1981.

17. Naylor T.H., Balintfy J.L., Burdick D.S. and Chu K. COMPUTER SIMULATION TECHNIQUES
18. SPSS: STATISTICAL PACKAGES FOR THE SOCIAL SCIENCES. Published by McGraw-Hill Inc. 1975.
19. McCarthy S., Kovach A. and Wrixon G.T. DATA MONITORING OF THE FOTAVOLTAIC PROJECT. Presented at the first session of the European Workshop Group for Photovoltaic Monitoring, held at JRC ISPRA Nov. 1985.

CHAPTER 2

PLANAR INSOLATION MODEL

20. Liu B.H.Y. and Jordan R.C. DAILY INSOLATION ON SURFACES TILTED TOWARDS THE EQUATOR. Ashrae Journal Vol. 3 (53-59) 1961.
21. Liu B.H.Y. and Jordan R.C. THE INTERRELATIONSHIP AND CHARACTERISTIC DISTRIBUTION OF DIRECT, DIFFUSE AND TOTAL SOLAR RADIATION. Solar Energy Vol. 4, No. 1 (1960).
22. Liu B.H.Y. and Jordan R.C. A RATIONAL PROCEDURE FOR PREDICTING THE LONG-TERM PERFORMANCE OF FLAT-PLATE SOLAR ENERGY COLLECTORS. Solar Energy Vol. 7 No. 2 (53-74) 1963.
23. Iqbal, N. HOURLY VS. DAILY METHOD OF COMPUTING INSOLATION ON INCLINED SURFACES, Solar Energy Vol. 21 No. 6 (485-489) 1978.
24. Collares Pereira M. and Ari Rabl THE AVERAGE DISTRIBUTION OF SOLAR RADIATION - CORRELATIONS BETWEEN DIFFUSE AND HEMISPHERICAL AND BETWEEN DAILY AND HOURLY INSOLATION VALUES. Solar Energy Vol. 22 No. 2 (155-164) 1979.

25. DESIGN HANDBOOK FOR PHOTOVOLTAIC STAND-ALONE SYSTEMS MONEGOM LTD.
4 Professional Drive, Suite 130, Gaithersburg, Maryland 20760 USA
(p. 11-2).
26. Rogers, G.C., Page J.K., Souster C.G. "MATHEMATICAL MODELS FOR
ESTIMATING THE IRRADIANCE FALLING ON INCLINED SURFACES FOR CLEAR
OVERCAST AND AVERAGE CONDITIONS. Meteorology for Solar Energy
Applications (Conference (C18) at the Royal Institution 1979,
United Kingdom International Solar Energy Society) 48-62 (1980).
27. Orgill J.F. and Hollands K.G.T. CORRELATION EQUATION FOR HOURLY
DIFFUSE RADIATION ON A HORIZONTAL SURFACE. Solar Energy Vol. 19,
No. 4 (357-359) 1977.
28. Bugler J.W. THE DETERMINATION OF HOURLY INSOLATION ON AN INCLINED
PLANE USING A DIFFUSE IRRADIANCE MODEL BASED ON HOURLY MEASURED
GLOBAL HORIZONTAL INSOLATION. Solar Energy Vol. 19 No. 5 (477-491)
1977.
29. Erbs, D.G., Klein S.A. and Duffie J.A., ESTIMATION OF THE DIFFUSE
RADIATION FRACTION FOR HOURLY, DAILY AND MONTHLY AVERAGE GLOBAL
RADIATION. Solar Energy Vol. 28, No. 4 (293-302) 1982.
30. Brund, R., A CORRECTION PROCEDURE FOR SEPARATING DIRECT AND DIFFUSE
INSOLATION ON A HORIZONTAL SURFACE. Solar Energy Vol. 20 No. 1
(97-100) 1978.
31. Klein S.A. CALCULATION OF MONTHLY AVERAGE INSOLATION ON TILTED
SURFACES. Solar Energy 19, 325-329 (1977).

MODEL OF MODULE TEMPERATURE

32. Schott T. OPERATION TEMPERATURE OF PV MODULES. A THEORETICAL AND EXPERIMENTAL APPROACH. Sixth E.C. Photovoltaic Solar Energy Conference (held at London 15-19th April 1985). D. Reidel, Dordrecht, Holland.
33. Anis W.R., Mertens R.P. and Van Overstraten R.J., CALCULATION OF SOLAR CELL OPERATING TEMPERATURE IN A FLAT PLATE PV ARRAY. Fifth E.C. Photovoltaic Solar Energy Conference (Proceedings of the International Conference held at Athens Greece 17-21 October 1983). D. Reidel, Dordrecht, Holland (520-524) 1984.
34. Risser V.V. and Fuentes M.K. LINEAR REGRESSION ANALYSIS OF FLAT-PLATE PHOTOVOLTAIC SYSTEM PERFORMANCE DATA. Fifth E.C. Photovoltaic Solar Energy Conference (Proceedings of the International Conference held at Athens, Greece 17-21 October 1983) D. Reidel, Dordrecht, Holland (623-627).
35. Griffith J.S., Rathod M.S. and Paslaski Joel. SOME TESTS OF FLAT PLATE PHOTOVOLTAIC MODULE CELL TEMPERATURES IN SIMULATED FIELD CONDITIONS. Fifteenth IEEE Photovoltaic Specialists Conference, Kissimmee, FL. USA, 12-15 May 1981. Published by IEEE New York (614-620).
36. Hart G.W. and Raghuramon P. RESIDENTIAL PHOTOVOLTAIC SYSTEM SIMULATION: THERMAL ASPECTS. ASME Solar Energy Division, Fourth Annual Technical Conference, Albuquerque, NM 26-30 1982.

PV ARRAY MODELS

37. Hart G.W. RESIDENTIAL PHOTOVOLTAIC SYSTEM SIMULATIONS - ELECTRICAL ASPECTS. Proceedings of the Sixteenth IEEE Photovoltaics Specialists Conference, San Diego, California, USA September 1981.
38. Rasmussen N.E. and Branz H.M. THE DEPENDENCE OF DELIVERED ENERGY ON POWER CONDITIONER ELECTRICAL CHARACTERISTICS FOR UTILITY INTERACTIVE PV SYSTEMS. Proceedings of the Fifteenth IEEE Photovoltaic Specialist Conference, Kissimmee, Fl, USA, 1981.
39. Singer S., Rozenstein B. and Surazi S., CHARACTERISATION OF PV ARRAY OUTPUT USING A SMALL NUMBER OF MEASURED PARAMETERS. Solar Energy Vol. 32, No. 5 (603:607) 1984.
40. Rauschenbach H.S. SOLAR CELL ARRAY DESIGN HANDBOOK. Published by Van Nostrand Reinhold Company.
41. Schmidt W. and Rasch K.D. THE BEHAVIOUR OF SILICON SOLAR CELLS UNDER VARYING INSOLATION CONDITIONS. Proceedings of the fifth EC Photovoltaic Solar Energy Conference, Athens (1147:1154) 1983.
42. Evans D.L. SIMPLIFIED METHOD FOR PREDICTING PHOTOVOLTAIC ARRAY OUTPUT. Solar Energy Vol. 27 No. 6 (555:560) 1981.
43. Roger J.A. and Magum G. PHOTOVOLTAIC SOLAR PANELS SIMULATION INCLUDING DYNAMICAL THERMAL EFFECTS. Solar Energy Vol. 29 No. 3 (245:256) 1982.
44. Knobloch J. EFFICIENCY MEASUREMENTS OF DIFFERENT TYPES OF SOLAR CELLS IN DEPENDENCE ON THE IRRADIATION CONDITIONS. Proceedings of the fifth EC Photovoltaic Solar Energy Conference, Athens (652:656) 1982.

45. Watkins J.L. and Burgess E.L. THE EFFECT OF SOLAR CELL PARAMETER VARIATION ON ARRAY POWER OUTPUT. Sandia Laboratories, Albuquerque, NM 87185.
46. Ngugen P.H. and Ravelet S. COMPUTER AIDED ANALYSIS OF THE EFFECTS OF SERIES AND SHUNT RESISTANCE ON THE PERFORMANCE OF SOLAR CELLS. Proceedings of the 4th EC Photovoltaic Solar Energy Conference, Stresa, Italy, 1982.
47. Loftus M. A REMOTE MONITORING SYSTEM AND A REMOTE IV CHARACTERISATION SYSTEM FOR THE FOTAVOLTAIC SYSTEM. MEngSc Thesis from the National Microelectronics Research Centre, Cork 1985.

CHAPTER 3

BATTERY MODEL

48. Hafen D.P., Wallace R.B. BATTERY MODEL AND COMPUTER SIMULATION OF A MULTIBATTERY/SOLAR ARRAY SPACE CRAFT ELECTRICAL POWER SYSTEM. Proceedings of the Fifteenth Intersociety Energy Conversion Engineering Conference. 1980. pp. 100-105.
49. Applebaum J., Braunstein A. and Bani J., PERFORMANCE ANALYSIS OF A SOLAR-ELECTRICAL SYSTEM WITH A LOAD AND STORAGE BATTERY. Energy Conversion. Vol. 16 1977 pp 105-110.
50. Shepherd C.M. DESIGN OF PRIMARY AND SECONDARY CELLS - AN EQUATION DESCRIBING BATTERY DISCHARGE. Journal of Electrochemical Society Vol. 112 1965 pp. 657-664.

51. Berndt, D., Kiehne H.A. and Tepel R., RELIABILITY AND MAINTENANCE OF STATIONARY BATTERIES. Proceedings of 5th International Telecommunications Energy Conference held in Tokyo, Japan 1983 pp. 27-32.
52. Kiehne H.A. FIELD EXPERIENCE WITH STATIONARY LEAD ACID BATTERIES IN PHOTOVOLTAIC POWER PLANTS. Proceedings of the INTELEC Conference held in Washington DC 1982 pp 249-252.
53. Bode H. LEAD ACID BATTERIES Published by Wiley and Sons, New York.
54. Thione L. and Buccionti. ELECTRICAL BATTERIES FOR ENERGY STORAGE IN PHOTOVOLTAIC GENERATION PLANTS. Photovoltaic Power Generation, Series C, Vol. 1 Reidel, Dordrecht 1982, pp. 100;118.
55. Willmes H. BATTERY SYSTEMS FOR ENERGY SUPPLY IN PHOTOVOLTAIC POWER PLANTS. Photovoltaic Power Generation. Series C. Vol. 1, Reidel Dordrecht 1982. pp. 88-99.
56. Facinelli W.A. MODELLING AND SIMULATION OF LEAD-ACID BATTERIES FOR PHOTOVOLTAIC SYSTEMS. Proceedings of the 18th Intersociety Energy Conversion Engineering Conference held in Orlando, FL. USA August 1983, pp. 1582-1588.
57. Imamura M.S., Conn A.A., Peszko A.J. and Scott R.C. COMPUTER SIMULATION CONCEPT FOR A LARGE SOLAR ARRAY/BATTERY POWER SYSTEM. Proceedings of the 7th ISECEC Conference held in Hilton Inn, San Diego, CA. Sept. 25-29 1972 pp. 607-619.
58. Brench B.L. OPERATIONAL EXPERIENCES IN LEAD-ACID BATTERIES FOR PHOTOVOLTAIC SYSTEM. Proceedings of the 15th IEEE PV Specialists Conference held in Kissimmee, FL, 1981 pp. 642-647.

59. Kornfeil F. SOME OBSERVATIONS ON THE PREDICTION OF THE STATE OF DISCHARGE OF BATTERIES. Journal of the Electrochemical Society Vol. 123 No. 9 September 1976.
60. Sahm D., Karnopp D. SIMULATION OF ELECTRIC BATTERY DYNAMIES USING BOND GRAPH TECHNIQUES.
61. Kappus W. and Bohmann J., THE INFLUENCE OF ACID DIFFUSION ON THE PERFORMANCE OF LEAD-ACID CELLS. Journal of Power Sources Volume (10) 1983 pp. 355-376.
62. Lind H. COMPUTER CONTROLLED BATTERY CHARGING. Telephone Engineering and Management. Vol. 84 No. 10 1980. pp. 80-83.
63. Voss E. RECENT ADVANCES IN LEAD-ACID CELL RESEARCH AND DEVELOPMENT. Journal of Power Sources. Vol. 7 1982, pp. 343-363.
64. Kappus W. and Winsel A. SULPHATE PASSIVATION IN THE LEAD-ACID SYSTEM AS A CAPACITY LIMITING PROCESS. Journal of Power Sources. Vol. 8 1982, pp. 159-173.
65. Vaaler L.E., Brooman E.W. and Fuggiti H.A., COMPUTERISED DESIGN AND EVALUATION OF IMPROVED ELECTRODES FOR LEAD-ACID BATTERIES. Journal of Applied Electrochemistry Vol. 12, 1982, pp. 721-734.
66. Ofry F. and Singer S. MEASUREMENT OF THE STATE OF BATTERY CHARGE USING AN IMPROVED LOADED VOLTMETER TEST METHOD. IEEE Transactions on Instrumentation and Measurement. Vol. 31, No. 3, 1982. pp 154-158.
67. Jones G.J. ENERGY STORAGE IN GRID CONNECTED APPLICATIONS.

68. Horn L. MINIMISING THE GRID WEIGHT OF LEAD-ACID CELLS. In. Progress in Batteries and Solar Cells, Vol. 1, 1978, Published by JEC Press Inc. Boole Library 621.312 KOZA.

INVERTER MODELS

69. Solarverter, System Description AEG-Telefunken, Industriestr. 29, D-2000 Wedel (Holst.), West Germany.
70. Minisemi, System Description. AEG-Telefunken. Industriestr. 29, D-2000 Wedel (Holst.), West Germany.
71. Lakatos L. A NEW METHOD FOR SIMULATING POWER SEMICONDUCTOR CIRCUITS. IEEE Transactions on Industrial Electronics and Control Instrumentations. Vol. IECI-26, No. 1 (2-5) 1979.
72. Hofer K. CLOSED MATHEMATICAL DESCRIPTION OF LINE-COMMUTATED CONVERTER-DRIVES. Proceedings of the Third IFAS Symposium on Control in Power Electronics. Lausanne, Switzerland 1983.
73. Landsman E.E. ANALYSIS AND TEST OF LINE-COMMUTATED INVERTERS FOR USE IN RESIDENTIAL PHOTOVOLTAIC POWER SYSTEMS. Proceedings of the Fifteenth IEEE photovoltaic specialists conference held at Kissimmee, Fl, USA (627-635) 1981.
74. Jewell W.T. and Rizy D.T. INTERCONNECTION PROBLEMS ASSOCIATED WITH SMALL DISPERSED ELECTRIC GENERATORS AND INVERTER DEVICES. Proceedings of the 14th Annual Conference of Modelling and Simulation. Inspec 85B027055.

75. Jewell W.T. SIMULATION OF SOLAR SUB-DIVISION ADDRESSES UTILITY QUESTIONS ABOUT INTEGRATION OF SOLAR PHOTOVOLTAICS. Energy Division, Oak Ridge National Laboratory, Oak Ridge, Tennessee 37830 U.S.A. 1983.

CHAPTER 4

POWER MANAGEMENT MODEL

76. Groumpos P.P., Culler J.E., De Lombard R., Cull R. and Ratajczak A.F. CONTROL ALGORITHMS AND COMPUTER SIMULATION OF A STAND-ALONE PHOTOVOLTAIC VILLAGE POWER SYSTEM. Photovoltaic Power Generation, Series C, Vol. 4, Athens (353-357) 1982.
77. Cull A.C. and Eltimsahy A.H. THE EFFECTS OF CONTROLS AND CONTROLLABLE AND STORAGE LOADS ON THE PERFORMANCE OF STAND-ALONE PHOTOVOLTAIC SYSTEMS. Proceedings of the 15th IEEE photovoltaic specialists conference held at Kissimmee, Fl, USA, (621-626) 1981.
78. Carlvero M., Ciccarella G., Del Maestro G. and D. Domenico D. SIMULATION OF A DESALINATION PLANT SUPPLIED BY A PHOTOVOLTAIC ARRAY WITH MANAGEMENT STRATEGIES SIMULATION (USA) Vol. 42 No. 4 (155-162) 1984.
79. Edenburn M.W., Case G.R. and Goldstein L.H. COMPUTER SIMULATION OF PHOTOVOLTAIC SYSTEMS. Proceedings of the 12th IEEE Photovoltaic Specialists Conference held at Baton Rouge, CA, USA (667-672) 1976.
80. McGarity A.E., Reville C.S. and Cohon J.L. ANALYTICAL SIMULATION MODELS FOR SOLAR HEATING SYSTEM DESIGN. Solar Energy Vol. 32, No. 1 (85-97) 1984.

81. Ofrey E. and Singer S. MANAGEMENT OF EXCESS ENERGY IN AUTONOMOUS PHOTOVOLTAIC SYSTEMS. Solar Energy Vol. 31. No. 5 (445-448) 1983.

CHAPTER 5
SYSTEM OPTIMIZATION

82. Linn J.K. OPTIMIZATION OF TERRESTRIAL PHOTOVOLTAIC POWER SYSTEMS. Proceedings of the 13th IEEE Photovoltaic Specialists Conference held at
83. Huss W.R. EVALUATING THE RELIABILITY AND AVAILABILITY OF PHOTOVOLTAIC SYSTEMS. Simulation Vol.
84. Users Guide to SOREL - A SIMULATION OF RELIABILITY AND AVAILABILITY OF PHOTOVOLTAIC SYSTEMS. Contractors Report, SAND82-7152, Sandia Laboratory, Albuquerque, NM 87185.
85. Ambrose G, Catalanotti S., Cascia U., Troise G. and Concurillo G. COMPARISON BETWEEN POWER AND ENERGY METHODS OF ANALYSES OF PHOTOVOLTAIC PLANTS. Solar Energy Vol. 34, No. 1 (1-8) 1985.
86. Kern E.C. and Pope M.D. DEVELOPMENT AND EVALUATION OF SOLAR PHOTOVOLTAIC SYSTEMS: FINAL REPORT. Final Report Prepared for the US Department of Energy by MIT Lincoln Laboratory. DDE/ET/20279-240 1983.
87. Barra L. AN ANALYTICAL METHOD TO DETERMINE THE OPTIMAL SIZE OF A PHOTOVOLTAIC PLANT. Solar Energy Vol. 33, No. 6 (509-514) 1984.

88. Clarke D.R., Klein, S.A. and Beckman W.A. A METHOD FOR ESTIMATING THE PERFORMANCE OF PHOTOVOLTAIC SYSTEMS. Solar Energy Vol. 33. No. 6 (551-555) 1984.
89. Bucciarelli L. ESTIMATING THE LOSS-OF-POWER PROBABILITIES OF STAND-ALONE PHOTOVOLTAIC SOLAR ENERGY SYSTEMS. Solar Energy Vol. 32 No. 2 (205-209) 1984.
90. Siegel M.D., Klein, S.A. and Beckman W.A. A SIMPLIFIED METHOD FOR ESTIMATING THE MONTHLY-AVERAGE PERFORMANCE OF PHOTOVOLTAIC SYSTEMS. Solar Energy Vol. 26 (413-418) 1981.
91. Documentation of the Computer System Developed for the Purpose of Analysing Photovoltaic Data. EEC Contract No. 2021-82-12 Ed. ISP.IRL.
92. GLOSSARY OF TERMS USED IN SOLAR ENERGY. Solar Energy Vol. 33 No. 1 (97-114) 1984.
93. Beckman W.A. UNITS AND SYMBOLS IN SOLAR ENERGY. Solar Energy Vol. 21, No. 1 (65-68) 1978.

PV SYSTEMS DESIGN

94. Kipperman A.H.M. PHOTOVOLTAIC SYSTEMS. Presented at the Workshop on Photovoltaic Solar Energy, UNARC, Alexandria, Egypt. October 1983.
95. Kipperman A.H.M. THE PHOTOVOLTAIC SOLAR SYSTEM, ANALYSIS AND BASIC DESIGN RULES. Proceedings of the Fourth EC Photovoltaic Solar Energy Conference. Stresa Italy. Reidel, Dordrecht. Holland (280:285) 1982.

96. Ofry E. and Braunstein A., THE LOSS OF POWER PROBABILITY AS A TECHNIQUE FOR DESIGNING STAND-ALONE SOLAR ELECTRICAL (PHOTOVOLTAIC) SYSTEMS. IEEE Transactions on Power Apparatus and Systems Vol. PAS-102, No. 5 (1171-1175) May 1983.
97. Borden C.S. COMPUTER SIMULATION OF THE OPERATION OF UTILITY GRID CONNECTED PHOTOVOLTAIC POWER PLANTS. Proceedings of the National Computer Conference (AFIPS Conference) (341-346) 1980.
98. Neville R.C., SOLAR ENERGY COLLECTOR ORIENTATION AND TRACKING MODE. Solar Energy Vol. 20 No. 1 (7:11) 1978.
99. Maycock P. THE CURRENT PHOTOVOLTAIC SCENE WORLD WIDE. Proceedings of the Sixth E.C. Photovoltaic Solar Energy Conference held at London 15-19 April 1985 (21:27).
100. Thione L. and Bucciatti R. ELECTRICAL BATTERIES FOR ENERGY STORAGE IN PHOTOVOLTAIC GENERATION PLANTS. Photovoltaic Power Generation. Series C. Vol. 1. Published by Reidel Dordrecht Holland 1982 (88:99).
101. Trader K, Wrixon G.T. and McCarthy S., MANUAL OF PHOTOVOLTAIC PILOT PLANTS (STATUS OF OPERATION). A Manual prepared for Commission of the European Communities, Directorate General for Science, Research and Development, March 1986.
102. Speyer E. OPTIMUM STORAGE OF HEAT WITH A SOLAR HOUSE. Journal of Solar Energy. Vol. 3 p. 24 1959.
103. Buckberg M. and Roulet J.R., SIMULATION AND OPTIMIZATION OF SOLAR COLLECTION AND STORAGE FOR HOUSE HEATING. Journal of Solar Energy, Vol. 12 p. 31 1968.

104. Duffie J.A. and Beckman W.A., SOLAR ENGINEERING OF THERMAL PROCESSES.
Published by Wiley, New York (1980).
105. Klein S.A., Cooper P.A., Beckman W.A. and Duffie J.A., TRNSYS -
A TRANSIENT SIMULATION PROGRAM, Madison, University of
Wisconsin, Engineering Expt. Station, Report no 38, 1974.
106. M. Schwartzburg PERFORMANCE ANALYSIS OF SATELLITE ELECTRIC POWER
SYSTEMS BY COMPUTER SIMULATION. Intersociety Energy Conversion
Engineering Conference, Washington D.C., TRW Systems Group,
23-26 September 1969.
107. Weiner W. and Weinstains POWER SUB-SYSTEM PERFORMANCE PREDICTION
(PSPP) COMPUTER PROGRAM. Seventh Intersociety Energy Conversion
Engineering Conference, Sandiago, California, 25-29 September,
1972.
108. Stember L.H. and W.R. Huss USERS GUIDE TO SOLREL - A SIMULATION
OF RELIABILITY AND AVAILABILITY OF PHOTOVOLTAIC SYSTEMS. S AND
82-7152. Battelle-Columbus Division, 505 Kings Avenue, Columbus,
OH 43201 USA, 1982.

APPENDIX A

Photovoltaic Terminology

The Photovoltaic terminology used in this thesis is based on 'A Glossary of Terms used in Solar Energy'. SOLAR ENERGY, Vol. 33 No. 1 (97-114) 1984.

The IEC-TC82 is compiling a set of Photovoltaic standards but these were not available when the thesis was written. This appendix contains the most ambiguous terms used in the text.

ALBEDO:	Refers to reflectance from the surroundings
AMBIENT TEMPERATURE:	Temperature of the surroundings
ANGLE OF INCIDENCE:	The angle between a ray and the normal to the plane on which it is incident
DECLINATION:	The angular position of the sun at solar noon with respect to the plane of the equator
HOURLY ANGLE:	Angular displacement of the sun east or west of the observers meridian due to the rotation of the earth on its axis at 15° per hour
INSOLATION:	Radiation received from the sun (kwh/m ²)
IRRADIANCE:	The rate at which radiant energy is incident on a unit surface (kw/m ²)

APPENDIX B

Hourly Recorded Data at the Fotavoltaic Project

The data is recorded in a format specified for the CEC Pilot Program

[9]. The following is an example of the recorded data for one hour.

% FOTA %

1, 0.28, 0.53, 0.086, 61, 1.6, 2.1, 1.7
2, 13., 32., 20., 5.0, 1.9, 14.0, 13.0, 14.0, 0.083
3, 0.00, 0.00, 0.00, 1.1,
4, 1.5, 1.6, 1.5, 1.5, 1.4, 1.7, 1.7, 1.5, 1.4, 1.6
5, 1.7, 1.5, 1.1, 34, 27., 33., 13., 13., 10., 2.1
6, 287, 0.0, 23., 17., 59., 277., 0.0, 20., 20, 34,
7, 0.43, 0.89, 0.4, 1.0, 0.0, 0.29, 16., 0.0, 38., 36.,
8, 1.7, 2.3, 1.8, 948, 948, 0.96, 0.92, 4.0, 2.6, 0.55

The significance of each value is described as follows

Line 1,

1. Horizontal Insolation	0-1 kwh/m ²
2. Planar Insolation	0-1 kwh/m ²
3. Wind Speed	0-25 ms ⁻¹
4. Wind Direction	0-360 Degrees
5. Wind Pressure 1	0-50 Pa
6. Wind Pressure 2	0-50 Pa
7. Wind Pressure 3	0-50 Pa

Line 2,

1. Ambient Temperature	-10 -100°C
2. Module Temperature	-10 -100°C
3. PV Array Output Energy	0-50 kwh
4. Converter Output Energy	0- not used
5. Battery Input Energy	0-30 kwh



6. Battery Output Energy	0-50 kwh
7. Inverter Input Energy	0-50 kwh
8. Inverter Output Energy	0-50 kwh
9. Energy to the Utility Grid	0-50 kwh
10. Energy from the Utility Grid	0-50 kwh

Line 3,

1. PV Energy to Load 1	0-10 kwh
2. PV Energy to Load 2	0-10 kwh
3. PV Energy to Load 3	0-10 kwh
4. PV Energy to Loads from Minisemi	0-30 kwh

Line 4,

1. Sub-array 1 Energy	0-5 kwh
2. Sub-array 2 Energy	0-5 kwh
3. Sub-array 3 Energy	0-5 kwh
4. Sub-array 4 Energy	0-5 kwh
5. Sub-array 5 Energy	0-5 kwh
6. Sub-array 6 Energy	0-5 kwh
7. Sub-array 7 Energy	0-5 kwh
8. Sub-array 8 Energy	0-5 kwh
9. Sub-array 9 Energy	0-5 kwh
10. Sub-array 10 Energy	0-5 kwh

Line 5,

1. Sub-array 11 Energy	0-5kwh
2. Sub-array 12 Energy	0-5 kwh
3. Sub-array 13 Energy	0-5 kwh
4. Module Temperature 1	0-50°C
5. Module Temperature 2	0-50°C
6. Module Temperature 3	0-50°C

7. Voc * Isp (mean)	0-30kwh
8. Module Temperature 2 (mean)	0-50°C
9. Reference Module Voltage (mean)	0-12V
10. Reference Module Current (mean)	0-3A

Line 6,

1. Battery 2 Voltage (mean)	0-400 kV
2. Battery 2 Current	0-100 A
3. Battery 2 Temperature -ve Terminal	0-50°C
4. Battery 2 Temperature +ve Terminal	0-50°C
5. Battery 2 Maximum Charging Current	0-100 A
6. Battery 1 Voltage (mean)	0-400 kV
7. Battery 1 Current	0-100 A
8. Battery 1 Temperature -ve Terminal	0-50°C
9. Battery 1 Temperature +ve Terminal	0-100A

Line 7,

1. Solarverter 1 DC energy	0-10 kwh
2. Solarverter 1 Maximum DC Power	0-10 kwh
3. Solarverter 2 DC Energy	0-10 kwh
4. Solarverter 2 Maximum DC Power	0-10 kwh
5. Solarverter 3 DC Energy	0-10 kwh
6. Solarverter 3 Maximum DC Power	0-10 kwh
7. Minisemi DC Energy to Utility Grid	0-50 kwh
8. Minisemi DC Energy from the Utility Grid	0-50 kwh
9. Maximum Minisemi DC Power	0-50 kw
10. Maximum PV Array Power	0-50 kw

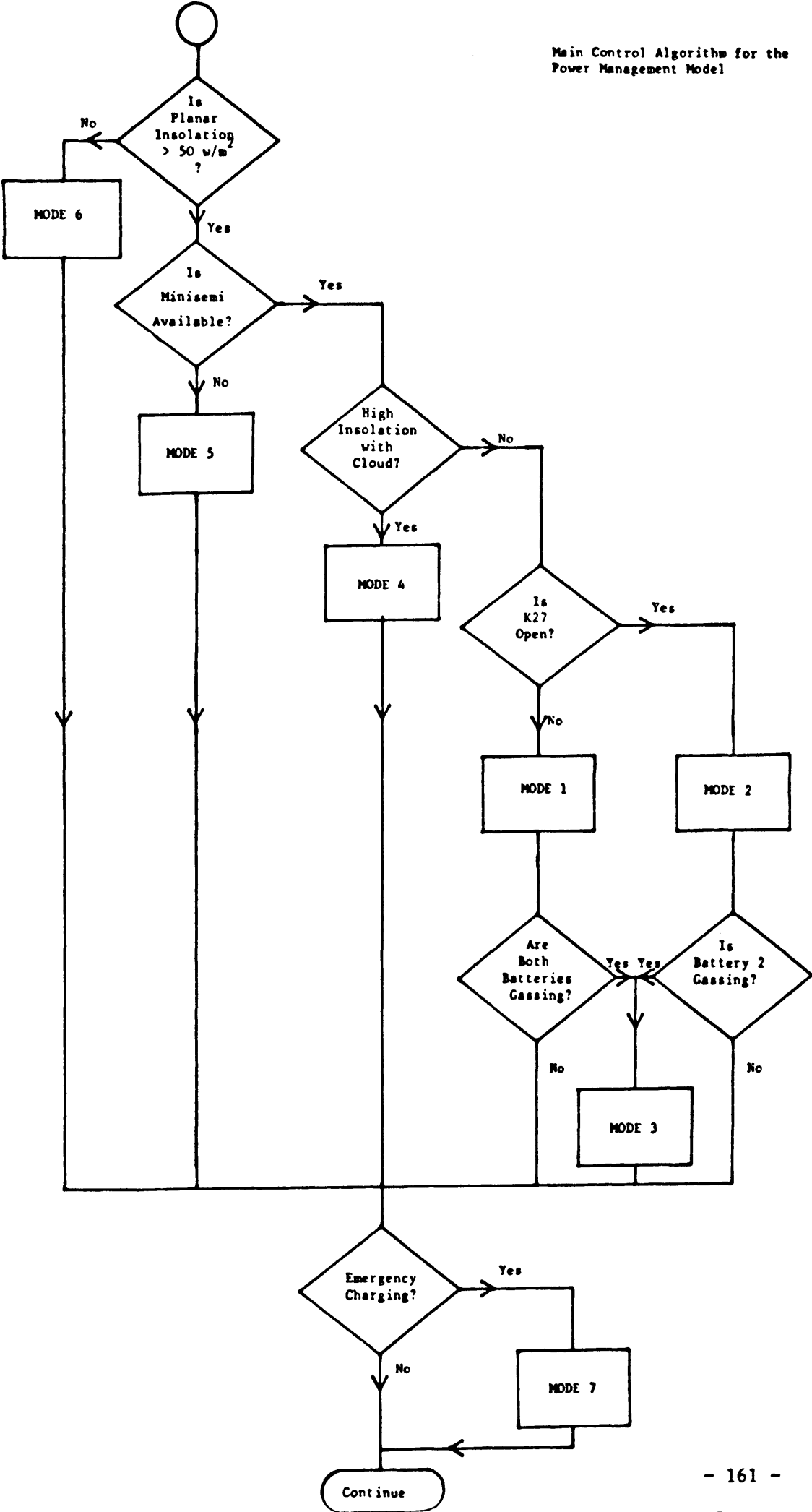
Line 8

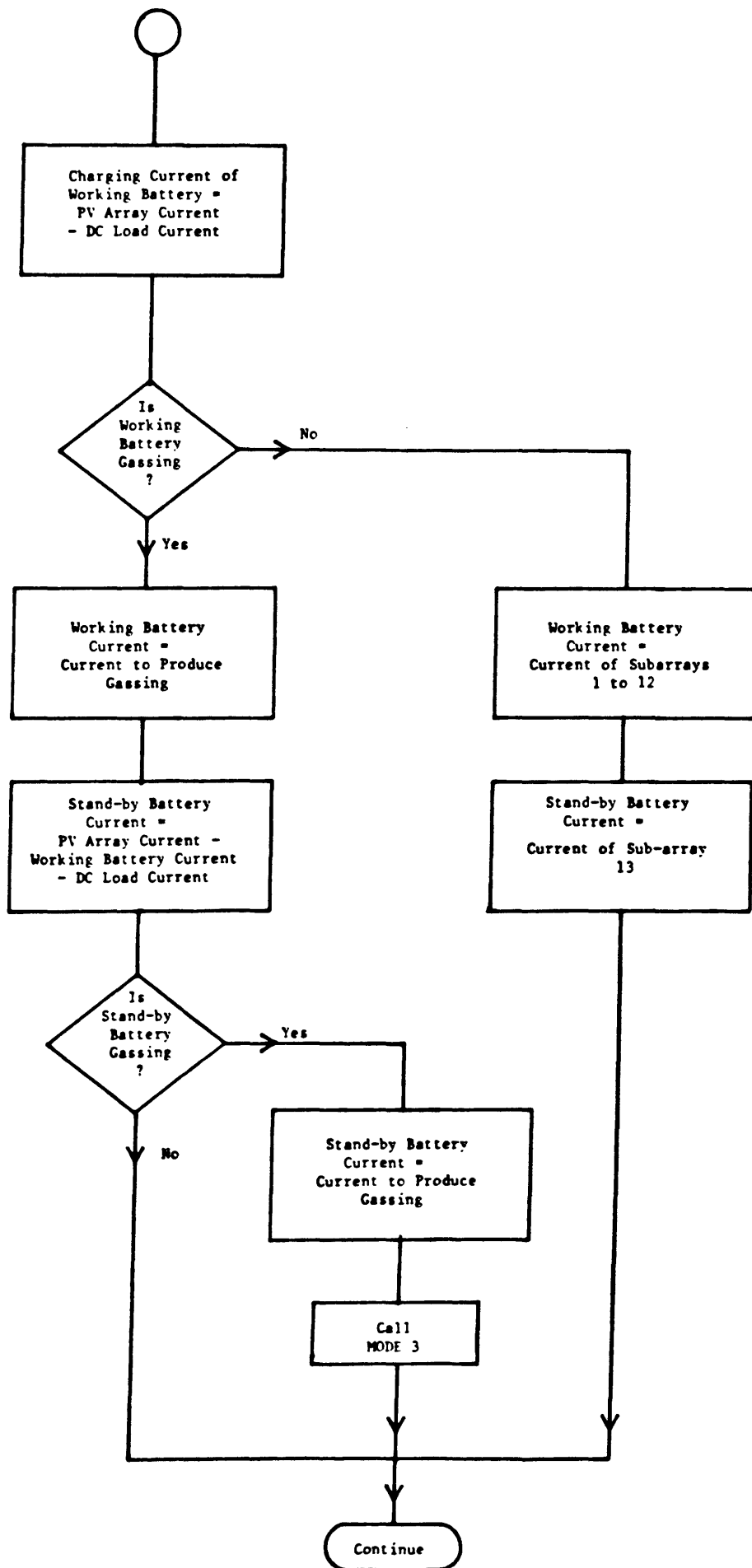
1. Wind Loading 1 (instantaneous)	0-50 Pa
2. Wind Loading 2 (instantaneous)	0-50 Pa
3. Wind Loading 3 (instantaneous)	0-50 Pa
4. Atmospheric Pressure (instantaneous)	
5. Atmospheric Pressure (mean)	
6. Maximum Wind Speed	0-25 ms ⁻⁷
7. Maximum Planar Insolation	0-1.5 kwh/m ²
8. Digital Event Recorder (test)	
9. Digital Event Recorder (test)	
10. Planar Insolation Calculated with 30 second samples	0-1 kwh/m ²

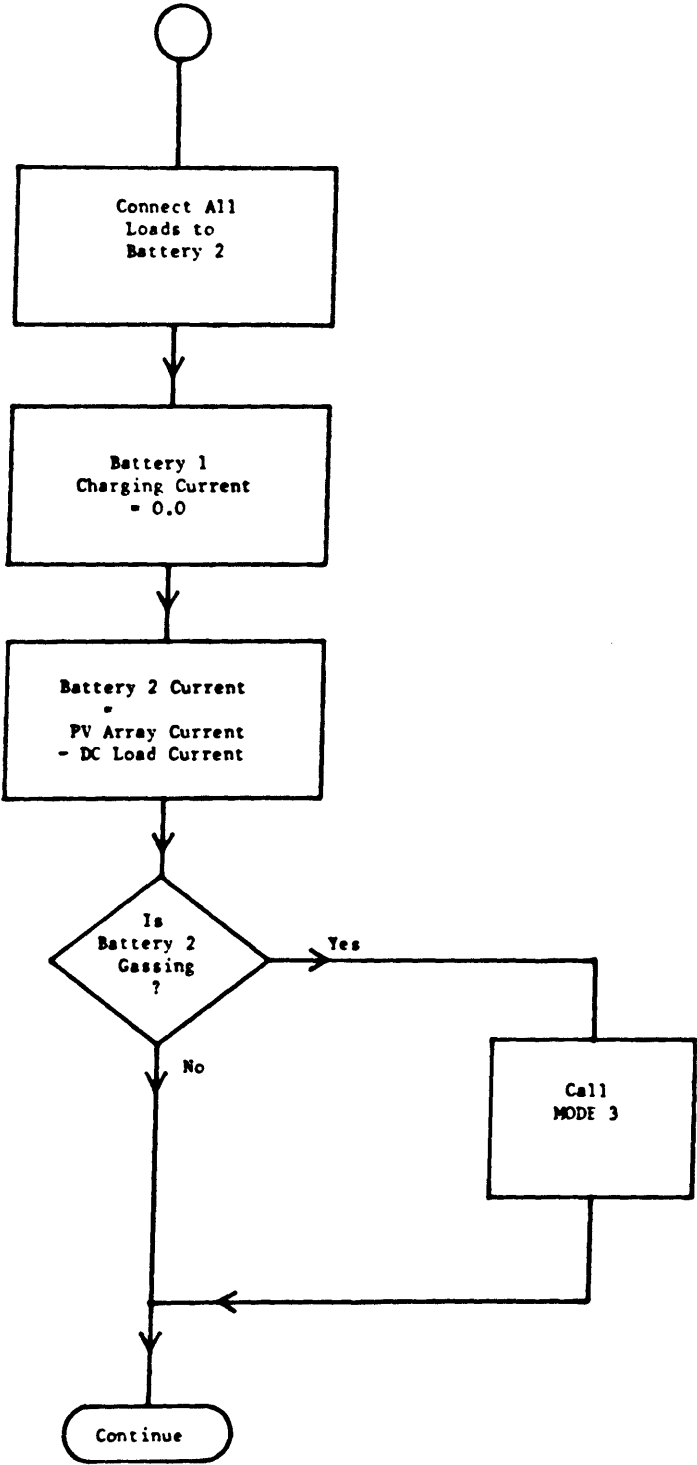
APPENDIX C

This appendix contains the algorithms which describe the power management of the Fotavoltaic System. The algorithms contained in the following pages are:

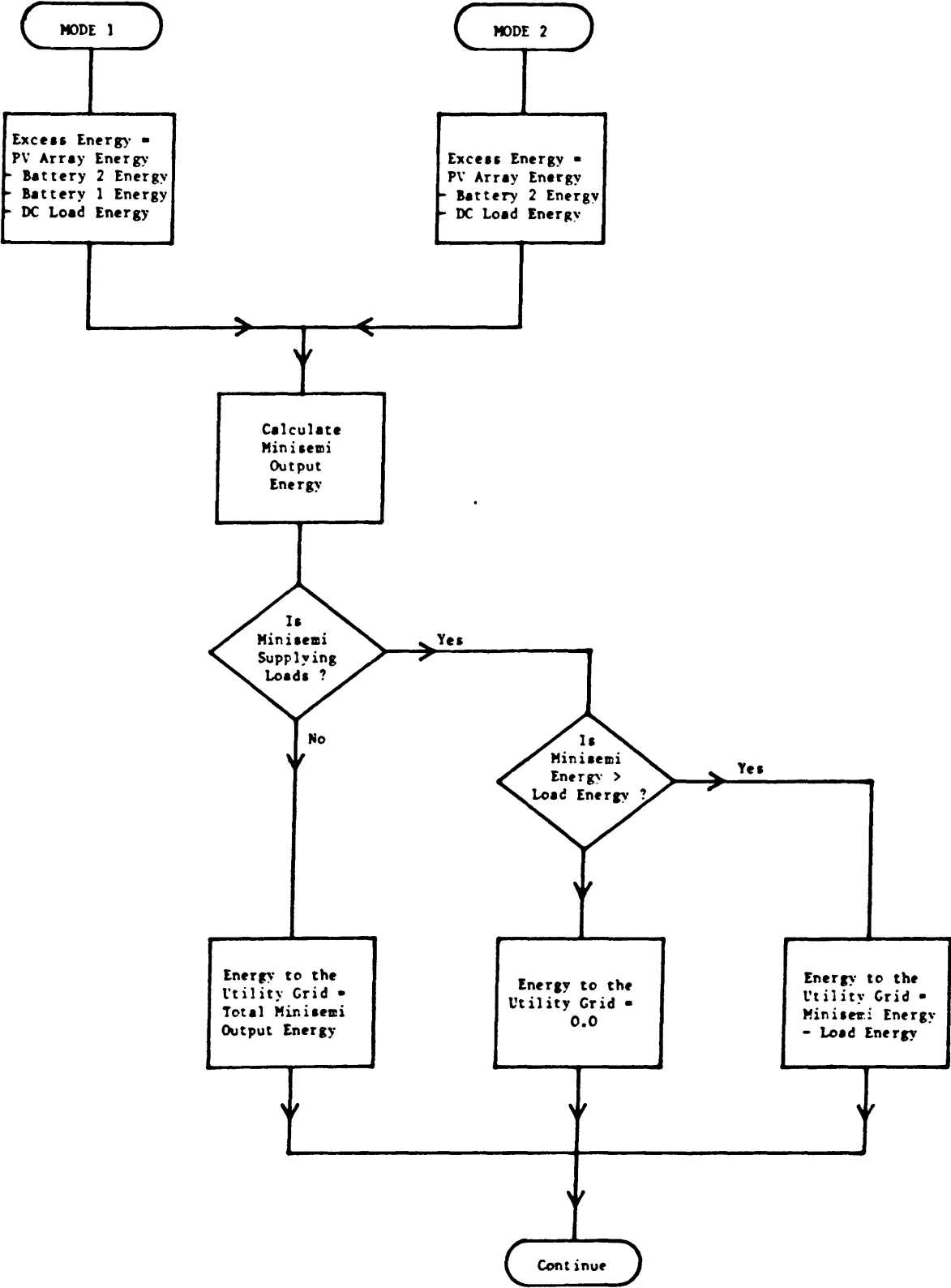
- a) Main control algorithm for the power management model
- b) MODE 1: Both batteries connected - K27 closed
- c) MODE 2: Battery 1 disconnected - K27 open
- d) MODE 3: Both batteries gassing - excess energy delivered to the utility grid.
- e) MODE 4: High insolation with varying cloud cover
- f) MODE 5: Minisemi disconnected
- g) MODE 6: Nighttime/low insolation operation
- h) MODE 7: Emergency charging of batteries from the utility grid
- i) LOAD MANAGEMENT MODEL



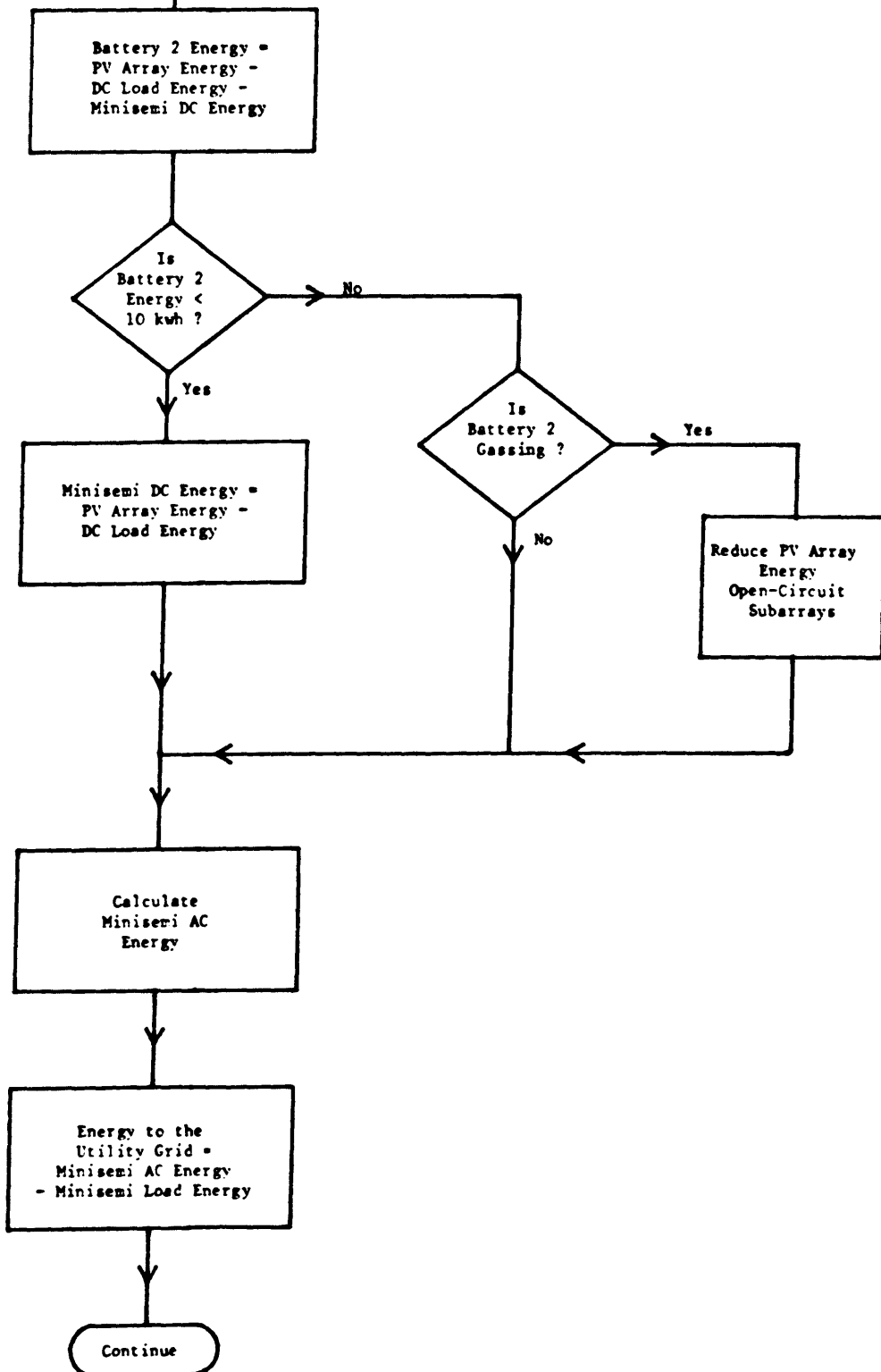


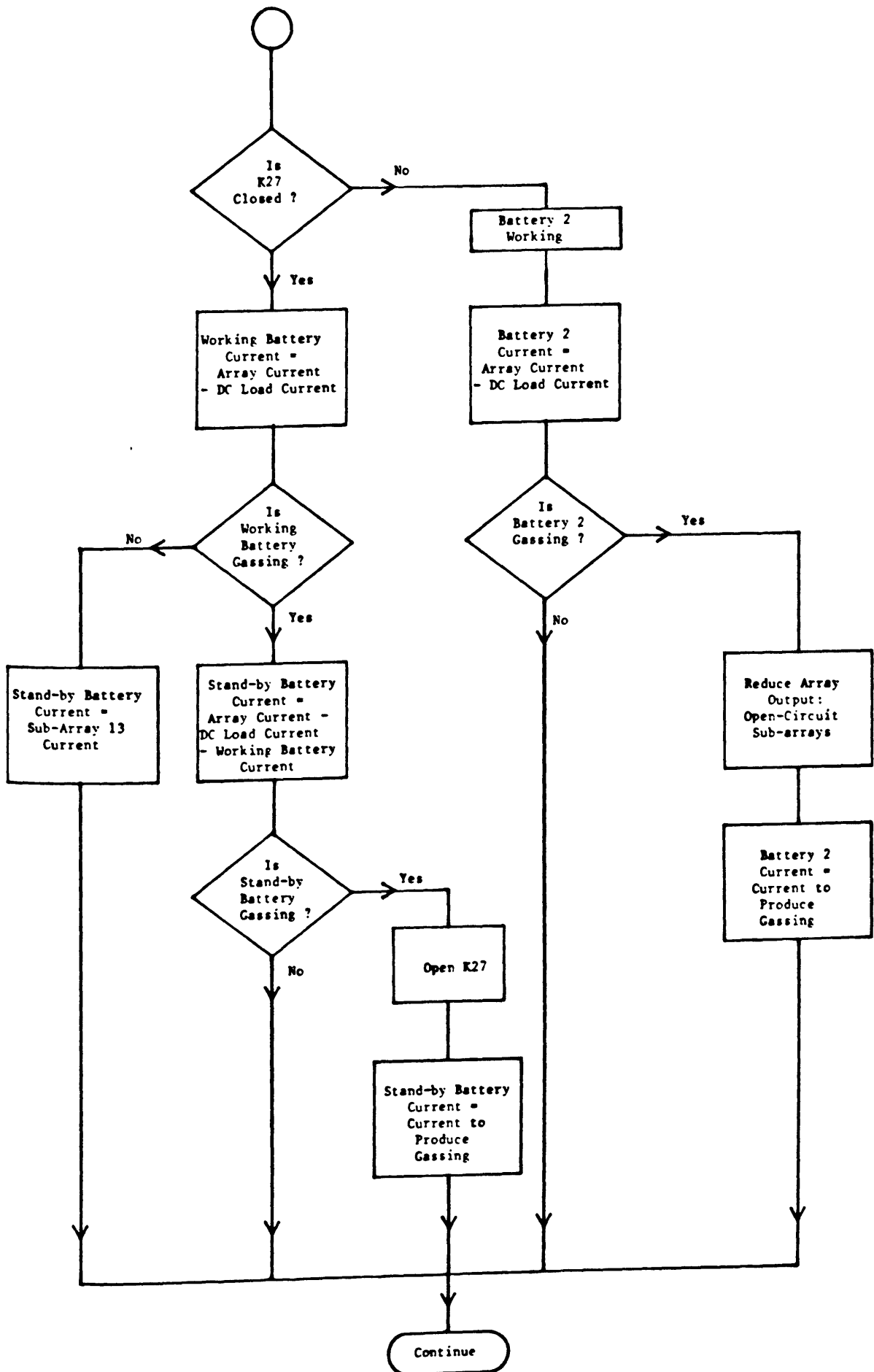


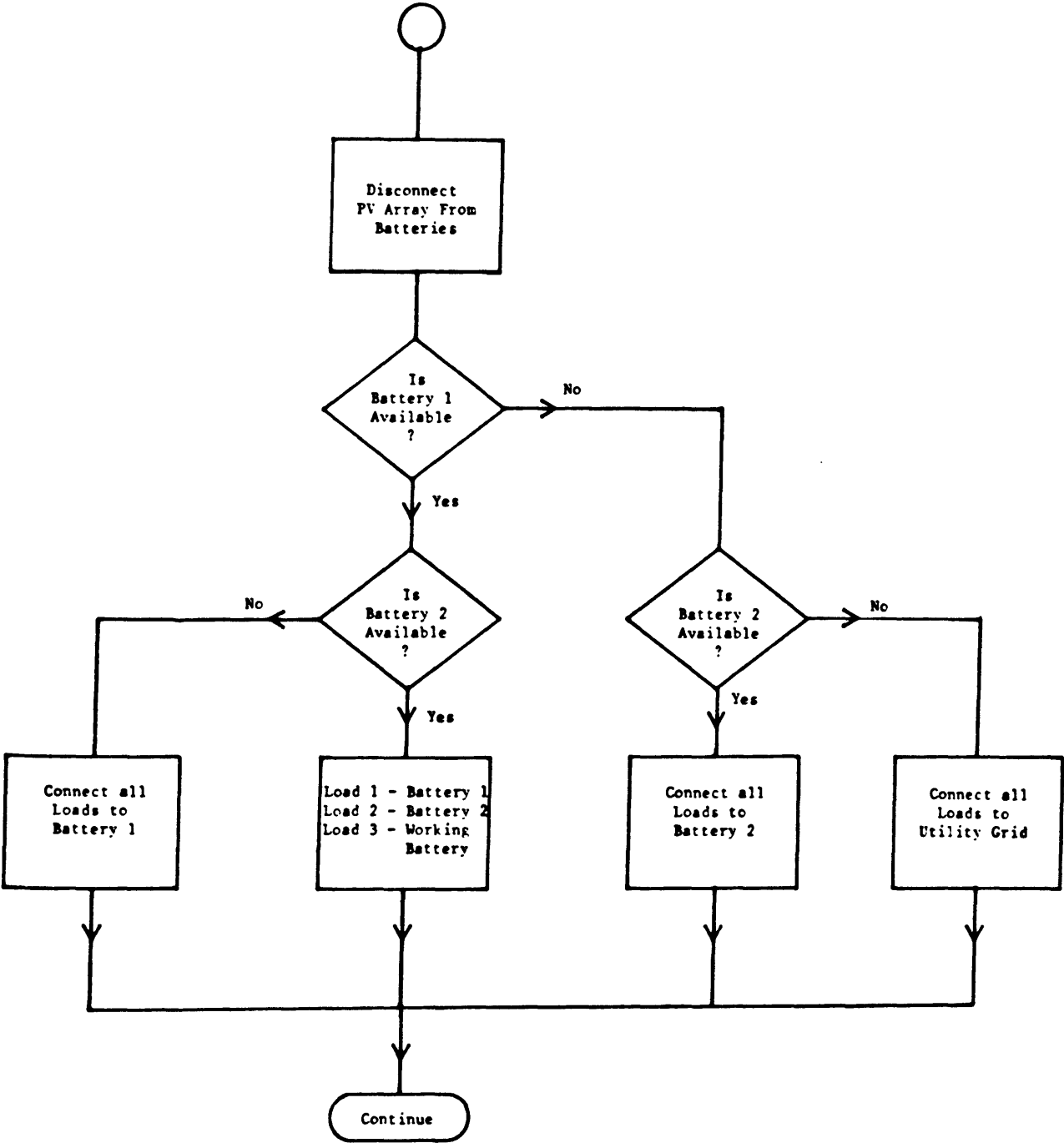
MODE 3: Both Batteries Gassing - Excess Energy Delivered to the Utility Grid

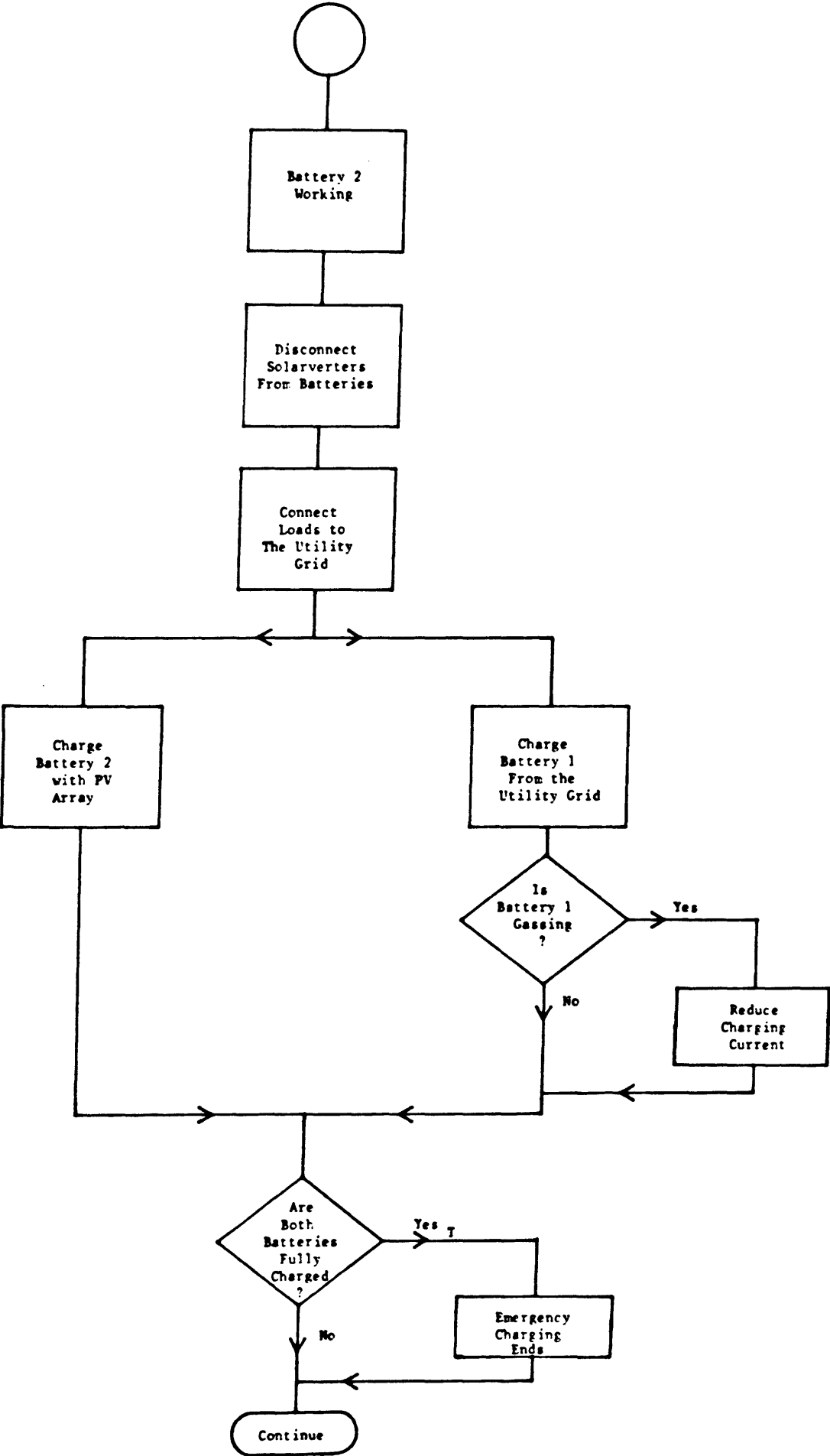


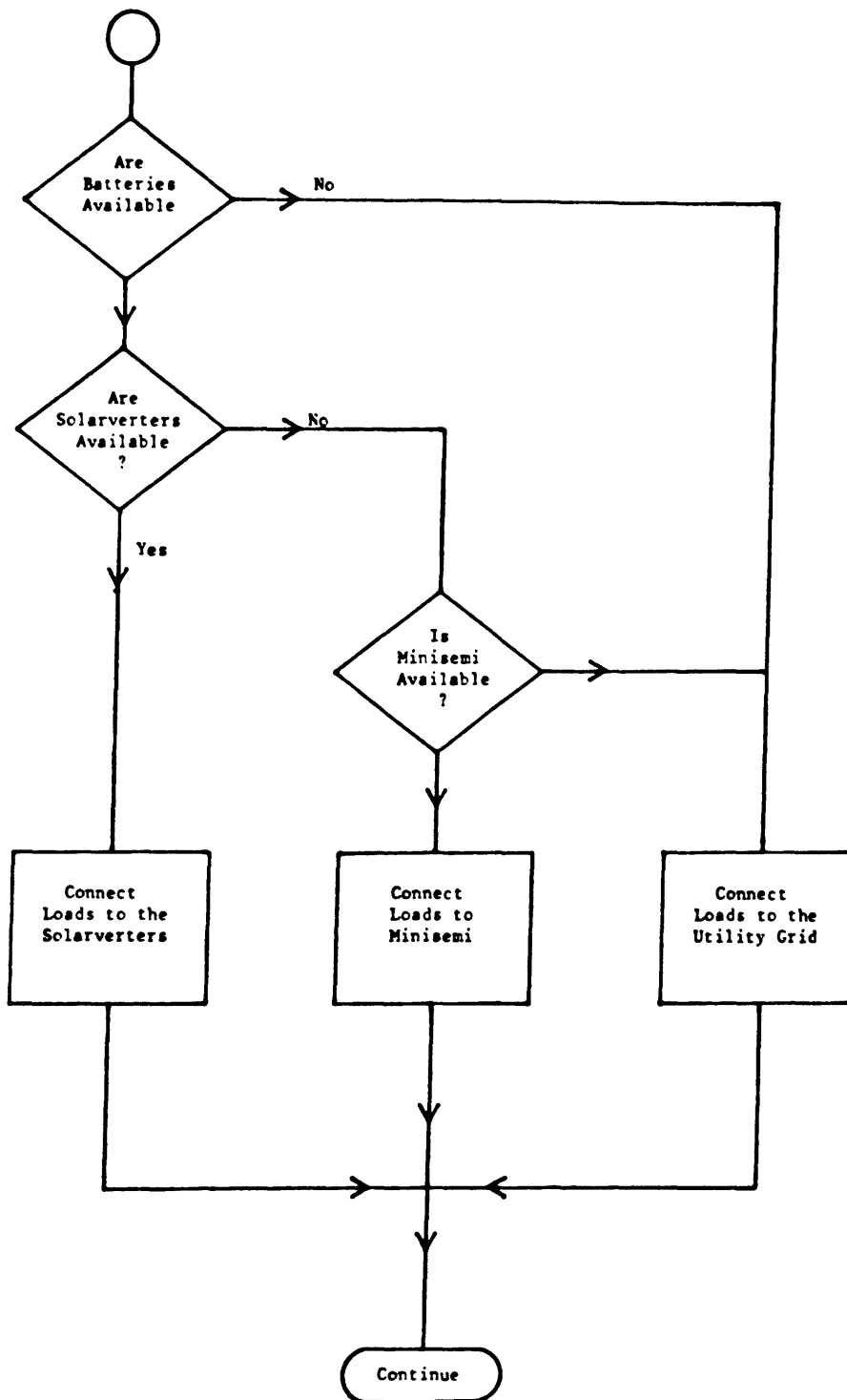
Planar Insolation > 0.6 kwh/m² - Minisemi DC Energy = 30 kwh
 Planar Insolation > 0.4 kwh/m² - Minisemi DC Energy = 23 kwh
 Planar Insolation > 0.2 kwh/m² - Minisemi DC Energy = 14 kwh











APPENDIX D

Variables and Logic used during each Hourly Simulation

The variables are stored in a dimensioned area VAR (60).

This list is a summary of the calculations which are performed during each hourly simulation.

1. No load voltage of stand-by battery.
2. No load voltage of working battery.
3. Ah of stand-by battery at the beginning of sampled hour.
4. Ah of working battery at the beginning of sampled hour.
5. Mean Ah of stand-by battery during sampled hour.
6. Mean Ah of working battery during sampled hour.
7. Ah of battery 1.
8. Ah of battery 2.
9. Voltage of stand-by battery.
10. Voltage of working battery.
11. Maximum charging current of stand-by battery.
12. Maximum charging current of working battery.
13. Maximum voltage of stand-by battery.
14. Maximum voltage of working battery.
15. Minisemi DC energy.
16. Solarverter 1 DC energy.
17. Solarverter 2 DC energy.
18. Solarverter 3 DC energy.
19. Auxillary power supply energy.
- 20.

21. Battery 1 energy. Input(+), output(-).
22. Battery 2 energy. Input(+), output(-).
23. Battery 1 current. Charge(+), discharge(-).
24. Battery 2 current. Charge(+), discharge(-).
25. DC Current of auxillary power supply.
26. DC Current from battery 2 to auxillary supply.
27. DC Current from battery 2 to auxillary supply.
28. Sub-array 1 DC Current.
29. Overcharge current for stand-by battery.
30. Overcharge current for working battery.
31. Number of subarrays connected to stand-by battery.
32. Number of subarrays connected to working battery.
33. Current produced by subarrays 1-12.
34. Current produced by subarrays 2-13.
35. Total current from PV array.
36. Maximum planar irradiance.
37. Load demand from stand-by battery.
38. Load demand from working battery.
39. PV array total energy.
40. Planar insolation (calculated) during sampled hour.
41. Planar insolation during previous hour.
42. Minisemi DC Current.
43. Minisemi AD energy.
44. PV array energy - inverter energy.
45. Battery energy required to begin gassing.
46. Minisemi DC Current during MINI4 operation.
47. Dummy variable in MINI3.
- 48.

49. Minisemi efficiency.
50. Solar module temeprature
51. Emergency charging current.
52. Planar insolation (test ony).
53. Total horizontal insolation.

The logic flags used during the simulations are stored in a dimensioned area LOGICAL cond (50). This list is a summary of the logical operations performed during each sampled hour. The conditions described in this list represent the .TRVE. condition.

1. Working battery. Battery 1 working =.TRUE.
2. Manual shutdown.
3. Emergency switch on farm (Jim's switch) pressed.
4. Minisemi tripped.
5. Solarverter 1 tripped.
6. Solarverter 2 tripped.
7. Solarverter 3 tripped.
8. Stand-by battery voltage is .lt. 250V.
9. Working battery voltage is .lt. 250V.
10. Both battery voltages are .lt. 250V.
11. Battery 1 is deep-discharged.
12. Battery 2 is deep-discharged.
13. Solarverter 1 is connected to battery 1.
14. Solarverter 2 is connected to battery 1.
15. Solarverter 3 is connected to battery 1.
16. Solarverter 1 is connected to battery 2.
17. Solarverter 2 is connected to battery 2.
18. Solarverter 3 is connected to battery 2.

19. Switch AlK14 (K27) is open.
20. Minisemi connected to battery 1.
21. Minisemi connected to battery 2.
22. Utility grid (ESB) not available.
23. Solarverter 1 not available.
24. Solarverter 2 not available.
25. Solarverter 3 not available.
26. PV array shutdown due to maintenance/computer failure.
27. Minisemi acting as backup to solarverters.
28. Planar insolation $>0.45 \text{ kWh/m}^2$, max. planar $> 0.7\text{kW/m}^2$
- 29.
30. Batteries have not gassed since array startup.
31. Battery 1 working (test)
32. Emergency charging requested.
33. Battery 1 is gassing.
34. Battery 2 is gassing.
35. Battery 1 and 2 voltages are .gt. 270V.
36. Solarverters are not available.
37. Battery 1 is not available for load supply.
38. Battery 2 is not available for load supply.
39. Both batteries are not available.
40. One battery is available.
41. MINI1 operation.
42. MINI2 operation.
43. MINI3 operation.
44. MINI4 operation.
45. MINI41 operation.
46. MODE7 operation.
47. Mid-day and one battery available.

APPENDIX E

Calculations for Ice Producing Unit

A detailed description of the ALFAGLACE milk cooling system is described on the following page. The following calculations are based on the maximum daily milk production and on the cooling capacity of the ice producing unit. (These figures and calculations were provided by the manufacturer)

Peak Daily Milk = 6,000 litres

Cooling Capacity Required to cool

6,000 litres from 35° to 4°C = 6000×31 kCals
= 186,000 kCals

The milk is first pre-cooled by water from 35° to 18°C i.e.
102,000 kCals.

This leaves 84,000 kCals to be removed by the ice producing unit.

The ALFAGLACE system has a cooling capacity of 85,000 kCal with a 5Hp motor running for 6.5 hours.

The ice builder could be linked with the milking machine motor so that when they are switched on the ice producer is switched off, and vice versa. In this way the ice builder is switched on every morning about 10 a.m. and is switched off again at 4.30 p.m. when afternoon milking restarts, thus having 6.5 hours running time.

As the milk cooling accounts for half the farm load during milking, its omission from the circuit at milking would very much reduce the peak demands.

ALFAGLACE

THE MOST ADVANCED MILK COOLING SYSTEM

ALFA-GLACE...WHY?

Studies have been conducted on quick cooling systems with milk storage at low temperature, namely:

- *Influence of the cooling speed and holding temperature in farm tanks on bacteria growth in raw milk*, by Messrs. MOURGUES, VASSAL and AUCLAIR (INRA).
 - *Study on instant cooling of milk*, carried out on 12 farms, from July 1980 to September 1981, by Messrs. QUINQUE, ROSSEL and DEVOITINNE (LABO-CILFA - 59 DOUAI, France). ALFA-LAVAL participated to this study by the erection and adjustment of some installations.
- These studies emphasized the interest of instant cooling and holding at low temperature, both on:
- bacteria growth at temperature close to 0°C (Messrs. MOURGUES, VASSAL and AUCLAIR), and on,
 - psychrotrophas germs, lipolysis and proteolysis indices (CILFA).

UNIQUE PERFORMANCES

ALFA-GLACE is an instant cooling system, particularly performant thanks to its original cooling energy storage system.

In fact, in traditional ice-bank systems, the Ice/Warmed water heat transfer surface area decreases as the ice-bank melts. This results in a significant reduction of the performances, especially by the end of the milking when the ice tends to disappear.

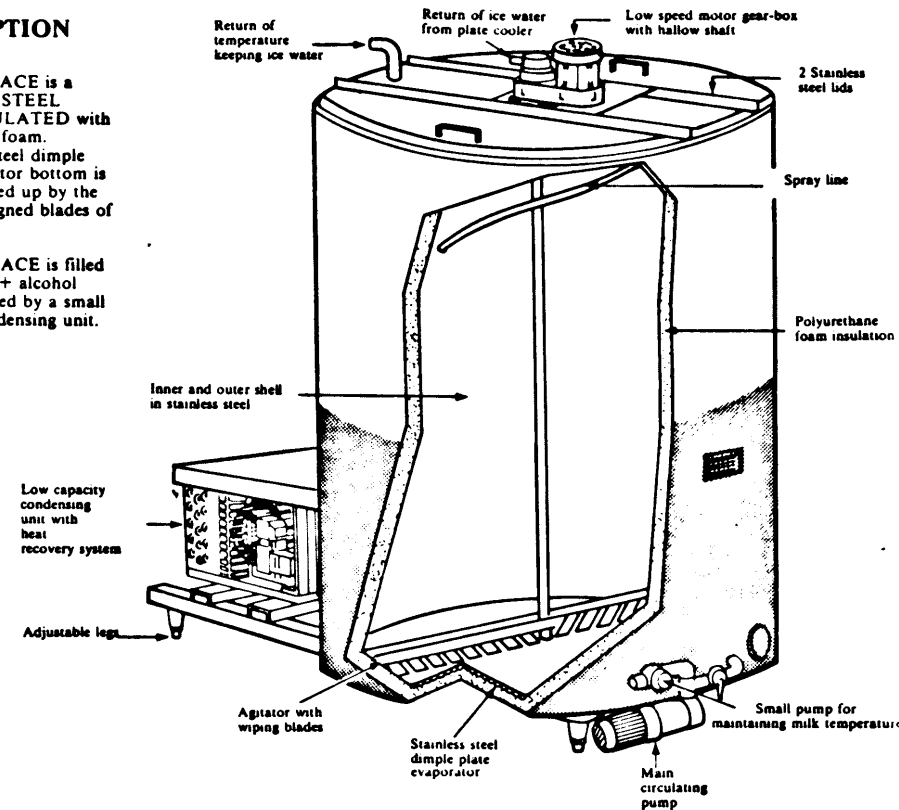
In the ALFA-GLACE system, the building-up of cooling energy is realized by a great number of small Soft Ice crystals which heat transfer surface area is considerable, much higher than in classical systems.

This advantage enables to obtain a very low milk temperature during milking and to maintain it low, with no risk of the cooling medium being warmed up before the end of the milking.

DESCRIPTION

● ALFA-GLACE is a **STAINLESS STEEL TANK**, insulated with polyurethane foam. Its stainless steel dimple plate evaporator bottom is regularly wiped up by the specially designed blades of the agitator.

● ALFA-GLACE is filled with a water + alcohol mixture, cooled by a small standard condensing unit.



RUNNING PRINCIPLE

(Patent N° 80-21147 ALFA-LAVAL & Cie)

- The water, when freezing on the evaporator, dissociates from the alcohol. Soft Ice crystals are formed which are regularly removed from the bottom by the agitator copper blades.
- The Soft Ice crystals go up to the surface and are surrounded by a film of alcohol which prevents them to stick together and make a bank.
- When the ALFA-GLACE is full of Soft Ice, a thermostat cuts off the condensing unit.
- During milking, the cooling medium, water + alcohol mixture at 0°C/-1°C, is pumped through the plate cooler where milk is instantly cooled.
- The water + alcohol mixture, warmed up by the milk, returns to the ALFA-GLACE as water spray and is immediately converted back to Soft Ice.
- The cold milk is stored in an insulated holding tank in which its temperature is maintained by circulating the mixture through the tank double-bottom by a small pump.

